KINEMATICS, PARTITIONING AND THE RELATIONSHIP BETWEEN VELOCITY AND STRAIN IN SHEAR ZONES

By

JUSTIN JAMES MURPHY

A dissertation submitted in partial fulfillment of
the requirements for the degree of

DOCTOR OF PHILOSOPHY

WASHINGTON STATE UNIVERSITY
School of Earth & Environmental Sciences

AUGUST 2007

To the faculty of Washington State University:

The members of the committee appointed to examine the dissertation of JUSTIN JAMES MURPHY find it satisfactory and recommend that it be accepted.

_____

Chair

_____

_____

ACKNOWLEDGMENTS

I would like to thank the faculty, staff and graduate students at the School of Earth and Environmental Sciences (SEES) for always being supportive. Dr. David Gaylord supported my unique graduate career and bravely navigated the bureaucracy of WSU. We would all be lost without Karen Libey and Lorelei Sterling. Mike Pope gave me my first taste of field work in the Mackenzie Mountains. Thanks to my committee members, Dr. A. John Watkinson, Dr. John S. Oldow and Dr. John A. Wolff for their contributions to this dissertation. Financial support came from Sigma Xi Grants in Aid of Research, The Geological Society of America and SEES. Special thanks to Gregg Teasdale of Teasdale Environmental PLLC for aerial photography provided free of charge!

Discussions with Keith Brunstad, Paul Olin, Scott Boroughs, Rick Conrey, Charles Knaak and Jesse Jennings were fundamental to my understanding of geology. The excellent training, insightful discussions and personal attention from Dr. A. John Watkinson, Dr. John S. Oldow and Dr. William C. McClelland taught me everything I know about structural geology. Special thanks to Dr. Watkinson for giving me both philosophy and friendship, thanks John. I could not have completed this dissertation without the constant love and support from my wife, Natalie and my family. If not for a dug up yard in Newport, Wa, my sister Shannin, a leaf fossil (psilomelane!) and Natalie's encouragement after I withdrew from my freshman year classes…none of this would have happened.

KINEMATICS, PARTITIONING AND THE RELATIONSHIP BETWEEN VELOCITY AND STRAIN IN SHEAR ZONES

Abstract

By Justin James Murphy Ph.D.
Washington State University
August 2007

Chair: A. John Watkinson

Granite Point, southeast Washington State, captures older distributed deformation deflected by younger localized deformation. This history agrees with mathematical modeling completed by Watkinson and Patton (2005; *2007 in prep*). This model suggests that distributed strain occurs at a lower energy threshold than localized strain and predicts deformation histories similar to Granite Point.

Ductile shear zones at Granite Point define a zone of deformation where strain is partitioned and localized into at least ten sub parallel shear zones with sinistral, west side down shear sense. Can the relative movement of the boundaries of this partitioned system be reconstructed? Can partitioning be resolved from a distributed style of deformation?

The state of strain and kinematics of actively deforming zones was studied by relating the velocity field to strain. The Aleutian Arc, Alaska and central Walker Lane, Nevada were chosen because they have a wealth of geologic data and are recognized examples of obliquely deforming zones. The graphical construction developed by Declan

De Paor is ideally suited for this application because it provides a spatially referenced visualization of the relationship between velocity and strain.

The construction of De Paor reproduces the observed orientation of strain in the Aleutian Arc, however, the spatial distribution of GPS stations suggest a component of partitioning. Partitioning does not provide a unique solution and cannot be differentiated from a combination of partitioning and distributed strain. In the central Walker Lane, strain trajectories can be reproduced at the domain scale. Furthermore, the effect of anisotropy from Paleozoic through Cenozoic crustal structure, which breaks the regional strain field into pure shear and simple shear dominated transtension can be detected.

Without GPS velocities to document strictly coaxial strain, the strain orientation should not be taken as the velocity orientation. The strain recorded at Granite Point should not be used to reconstruct the relative movement of the boundaries because the strain direction may not be parallel to the velocity orientation. Kinematic reconstructions of obliquely deforming zones that assume a palaeo-velocity orientation equal to the measured orientation of finite strain may not accurately reflect the deviation between velocity and strain.

TABLE OF CONTENTS

INTRODUCTION

Four chapters are presented in this dissertation. Chapters 2, 3 and 4 are manuscripts. Each manuscript is presented as a separate work that reflects the style of both the target journal and audience. Chapter 2 is a manuscript prepared following the format for *The Journal of Structural Geology*, Elsevier Publishing. Chapter 3 consists of a manuscript that is in press for publication in a Geological Society of America Special Paper edited by Dr. John S. Oldow, University of Idaho and Dr. Pat Cashman, University of Nevada Las Vegas. Chapter 4 is a manuscript written following the formatting guidelines of *Tectonics*, American Geophysical Union. Manuscripts in chapters 2 and 4 are in preparation for submission. Final formatting of each manuscript in chapters 2, 3 and 4 has been adjusted to satisfy the requirements of the graduate school at Washington State University.

The manuscripts in chapters 2, 3 and 4 are co-authored by Dr. A. John Watkinson and Dr. John S. Oldow. I am the chief author on each manuscript. My co-authors provided insightful discussions, reviewed iterative drafts of each manuscript and actively participated in the development and problem solving associated with each manuscript. Data, published and unpublished, was made available by Dr. Oldow. Dr. McClelland guided me through the process of Zircon geochronology reported in Chapter 1 and analyzed the grains.

LIST OF FIGURES

Page

CHAPTER 2:

LIST OF TABLES

Page

CHAPTER ONE

DEFORMATION HISTORY AND AGE OF GRANITE POINT, SOUTHEAST WASHINGTON STATE: DISTRIBUTED VS. LOCALIZED STRAIN AND LIMITATIONS OF KINEMATIC RECONSTRUCTIONS

INTRODUCTION

Plate tectonic theory provides a conceptual framework to connect observations made in exhumed metamorphic tectonites to deformation beneath active tectonic zones. Field geology has documented two recurring styles of deformation within these exhumed tectonites, distributed and localized strain. Pervasive textures such as cleavage, schistosity and crenulations characterize a distributed style of deformation, while localized deformation can be characterized by narrow zones of high strain called shear zones (Ramsay & Graham, 1970), or more generally, high strain zones (Jiang & Williams, 1998). Hudleston (1999) has shown that shear zones may inosculate around low strain domains, creating 3D networks with a strain compatible geometry (see also Sorenson, 1983). Decades of detailed field work, combined with analogue and numerical modeling, has explored the geometry, kinematics and strain within shear zones but the process controlling strain localization remains a persistent topic of discussion.

Granite Point, southeastern Washington State preserves structures that reflect both distributed and localized deformation styles. The earliest tectonite shape fabric is pervasive and transposed by a system of ductile shear zones. The classification of distributed and localized strains can become scale dependant. Textures such as shear

bands may be considered discrete in thin section but distributed in outcrop scale (Horsman & Tikoff, 2005).

The observation that the earliest fabrics at Granite point record distributed strain and the latest record localized strain is consistent with predictions from a model energy map developed by Patton & Watkinson (2005). This model energy map is based on a thermo-mechanical conceptual framework that models the earth using a diharmonic partial differential equation characterizing a second order fluid rheology (Patton & Watkinson, 2005; *2007 in prep*). The fundamental prediction of this modeling suggests distributed deformation is more energetically favorable than localized deformation. Based on this prediction, a progression from distributed strain in early fabrics to localized strain in younger fabrics could be anticipated. Classic shear zone localities such as Castle Odair, Scotland (Ramsay & Graham, 1970) and the Laghetti Shear Zone in the Maggia Nappe, Switzerland (Simpson, 1982) both preserve older distributed fabrics transposed by young localized fabrics.

The kinematics of ductile shear zones at Granite Point can be reconstructed using microstructural analysis, however, determining the boundary motion is complicated by the non-uniqueness of finite strain (Ramsay & Graham, 1970; Tikoff & Fossen, 1995). Furthermore, strain recorded within ductile shear zones may not record the actual movement of the boundaries because of a complex relationship between finite strain recorded within a deforming zone, incremental strain, particle motion and the velocity field (Ghosh & Ramberg, 1976; Weijermars & Poliakov, 1991; Tikoff & Fossen; 1993; Fossen & Tikoff, 1995). Partitioning of either, or both, the velocity and strain field may result in strain recorded within shear zones that reflects only a component of the total

kinematics. This possibility is further complicated by the possibility of temporal partitioning (e.g. Clifton & Kattenhorn, 2006).

This paper addresses the deformation history and age of Granite Point, as well as some insights into the localization of strain in the context of mathematical modeling completed by Patton & Watkinson (2205; *2007 in prep*). The limitations of reconstructing relative boundary motion of ductile shear zones at Granite Point is explored and the relationship between velocity fields and strain fields in oblique deformation is continued in chapters 2, 3 and 4.

GEOLOGIC SETTING

Active subduction along the northwestern margin of North America at the latitude of Washington State, Oregon, and British Columbia has been occurring since the Mesozoic (Armstrong et al., 1977; Bateman, 1992). Propagation of the Sevier thrust fold belt into central North America resulted in translation of Paleozoic supracrustal rocks to the east, over younger rocks (Price, 1981). Displacement on the Sevier thrust fold belt reflects shortening associated with terrane accretion (Coney et al., 1980), pluton emplacement and lithospheric shortening (i.e. Orogenic Float model of Oldow et al., 1990) that accompanied the active Pacific margin. Farther to the south, throughout west-central and south-western USA, the Laramide thrust fold belt was coeval with the Sevier thrust fold belt until cessation of the Sevier thrust fold belt in the early Tertiary (Price, 1981).

Subduction related Cretaceous and Tertiary granite, granodiorite, monzonite and tonalite plutons exposed throughout eastern Washington State, Idaho and Montana collectively define the Idaho Batholith (Armstrong et al., 1977). Analyzing the spatial distribution where the $^{87}Sr/^{86}Sr$ ratio measured within these plutons falls between .704-.706 has inferred the contact between accreted terranes and cratonic North America (Armstrong et al., 1977). This isotopic boundary is associated with the crustal scale Western Idaho Shear Zone (WISZ) in Idaho, which was active throughout the Cretaceous (Criss & Fleck, 2004; McClelland & Oldow, 2004). Together, the WISZ and isotopic boundary trend approximately north south through west central Idaho until the latitude of Orofino, Idaho where the tectonite fabric of the WISZ and isotopic boundary are transposed westward by the Orofino Shear Zone (OFZ) (e.g. McClelland & Oldow, 2004). The OFZ has been suggested to accommodate strain compatibility between the Sevier and Laramide thrust fold belts (McClelland & Oldow, 2004).

Granite Point lies unconformably beneath the 18 Ma to 6 Ma old Columbia River Basalt Group (CRBG) that covers much of southeast Washington State, western Idaho and northern Oregon. Extension associated with propagation of the Basin and Range province into Idaho and Washington State disrupts the CRBG along normal and strike slip faults. In some cases the CRBG provides a palaeo-horizontal surface for restoration of fault block rotation. Giorgiss et al. (2005) suggests these faults capture reactivation of earlier WISZ fabrics. The CRBG immediately surrounding Granite Point dips shallowly to the west and does not appear to be involved in significant fault block rotation.

LITHOLOGIC DESCRIPTIONS

Granite Point (Fig. 1.1) is broken into four distinct lithologies: Granite, pegmatite veins, leucocratic enclaves and mafic enclaves. Lithologic field descriptions are presented in this paper; a petrologic description of Granite Point can be found in Hooper & Rosenberg (1970). The main outcrop at Granite Point is an approximately 100 by 300 meter exposure along the north side of the Snake River southwest of Pullman, Washington State (Fig. 1.2). Smaller exposures lie to the northwest, along the bank of the Snake River and in railroad cuts north of Wawawai Road. Larger outcrops are available on the south side of the Snake River (Fig. 1.2) but the exposure is poor and plagued by poisonous plants, rattlesnakes and hornets.

Crystals of orthoclase and microcline up to two centimeters in size make the granite phase at Granite Point very distinctive (Fig. 1.3). Smaller crystals of quartz, plagioclase, microcline and orthoclase surround the larger alkali feldspar crystals. Biotite and amphibole are pervasive throughout the exposure and although they constitute less than 10% of the modal mineralogy, they help define the tectonite fabrics. Granite modal mineralogy reported by Hooper & Rosenberg (1970) lists the dominant minerals as 49.7% quartz, 20.6% plagioclase, 18.6% microcline, 8.5% biotite, 1.2% hornblende, .2% apatite with the remaining mode consisting of trace titanite, zircon and opaque minerals on the north side of the Snake River. The modal mineralogy of the southern exposure is 30.9% quartz, 33.2% microcline, 27.9% plagioclase, 5.1% biotite, 2.2% hornblende .2% apatite and the remaining mode consisting of trace titanite, zircon and opaque minerals. The modal mineralogy for the southern exposure seems more representative of the total exposure.

The lack of peraluminous indicator minerals such as garnet, muscovite or cordierite suggest Granite Point is probably metaluminous. The prevalence of biotite and hornblende suggest the granite at Granite Point would fall under the I classification of Chappel & White (1974), which suggests melting of an igneous source rather than a sedimentary source.

Purely for the purpose of description, pegmatite veins are divided into two groups, (1) veins that record no visible strain exposed throughout Granite Point and (2) veins exposed within ductile shear zones that record high strains. Pegmatite veins exposed at Granite Point have a planar morphology with a relatively constant width along strike between one centimeter and ten centimeters, most being about five centimeters in width (Fig. 1.4). A pegmatite vein two feet thick was described by Treascher (1925) at Granite Point but is no longer exposed because of high water levels from installation of the Lower Granite Dam.

Vein terminations are rarely exposed but are pointed, sometimes joined by smaller vein splays. Pegmatite vein texture is dominated by subhedral to anhedral, one to four centimeter sized orthoclase crystals. Approximately equal amounts of centimeter sized anhedral plagioclase crystals, anhedral alkali feldspar crystals and centimeter sized clear quartz surround the larger alkali feldspar crystals. Biotite books up to one centimeter tall are pervasive throughout pegmatite veins but constitute a small percentage of the assemblage. The second type of pegmatite vein is exposed within ductile shear zones at Granite Point. These veins are compositionally similar to the pegmatite veins exposed throughout the outcrop but differ texturally, recording strain associated with the ductile

shear zones. These deformed veins are discussed later in the context of the ductile shear zones.

Felsic and mafic discontinuous bodies are exposed throughout Granite Point (Figs. 1.5 & 1.6 respectively). These enclaves range in size from centimeter thick discontinuous ribbons, meter sized approximately equant blocks and decimeter thick planar sheets. The boundaries can be either sharp, or diffuse. Compositionally, the mafic enclaves are dominated by amphibole and biotite and the felsic enclaves are dominated by quartz and feldspar. In the farthest northwest exposure, an enclave with both dark and light layering contains garnet within biotite rich layers. One particularly intriguing enclave is approximately 200 meters up slope on the south side of the Snake River. This enclave is distinctly green in color, composed of calcite, diopside and multiple orientations of quartz veins. This enclave probably represents a large block of country rock approximately 2-3 m^3, which has been incorporated into the granite.

AGE

Three samples were collected for dating. Sample GP1 was collected from the main granite phase, sample GP2 was collected from a pegmatite within a continuous ductile shear zone and GP3 was collected from a leucocratic enclave. Each rock type sampled was in continuity with the other rock types.

Analytical Methods

Zircon grains (Fig. 17A. and 17B.) were separated by standard gravimetric and magnetic techniques, hand picked under alcohol on the basis of clarity, lack of inclusions and integrity, mounted in 2.54 cm epoxy rounds, and polished to expose grain interiors. Zircon U-Pb analyses were completed using the SHRIMP-RG (sensitive high resolution ion microprobe-reverse geometry) at the United States Geological Survey - Stanford University Ion Probe Laboratory, Stanford, CA. CL and reflected/transmitted light images are used to characterize the zircons and select spot locations. The analytical routine follows Williams (1998) and Barth et al. (2001). Calibration concentrations of U and Th are based on analyses of zircon standard CZ3 (U=550 ppm). Isotopic compositions are calibrated by replicate analyses of zircon standard R33 (419 Ma; Black et al., 2004). Calibration error for the $^{206}Pb/^{238}U$ ratios of R33 for the analytical session was 0.57% (2 σ). Data reduction and plotting utilizes the programs of Ludwig (2001, 2003). The U-Pb data for each sample are plotted on Tera-Wasserburg diagrams (Fig. 1.20) and presented in Table 1.1. Uncertainties in the isotopic ratios are reported at the 1σ level. Ages are assigned based on the weighted mean of observed $^{206}Pb/^{238}U$ ages corrected using the ^{207}Pb correction method. Common Pb compositions were estimated from Stacey and Kramers (1975). Weighted mean age uncertainties are reported at the 95% confidence level.

U-Pb results

Zircons from sample GP1 are elongate euhedral grains with well developed oscillatory zoning. Analyses from both cores and rims give ages ranging from 81 to 102

Ma with no discernable distinction between zircon domains. Attributing the 7 oldest analyses to inheritance and youngest 2 to Pb-loss, the remaining analyses yield a weighted mean $^{206}Pb/^{238}U$ age of 93.6 ± 1.0 Ma (MSWD = 1.0; n = 11) (Fig. 1.16) which may be interpreted as the emplacement age for the main granite. Alternatively, the older zircon components which give an age of 99.0 ± 1.2 Ma (MSWD = 1.4; n = 7) (Fig. 1.16) may be interpreted to record the crystallization age of the granite. In this scenario, the younger age spread would be attributed to younger growth or Pb-loss during metamorphism and deformation. Since the granite is a composite body with at least 2 phases recognized that predate penetrative ductile deformation, distinction between these two scenarios is not possible at this time. Nevertheless, the protolith of the granitic orthogneiss was emplaced between 90 and 100 Ma.

Sample GP2 yielded elongate euhedral oscillatory zoned zircon with 207Pb-corrected $^{206}Pb/^{238}U$ ages ranging from 76 to 95 Ma. Attributing the two oldest analyses to inheritance from the adjacent granite and the two youngest to Pb-loss, the remaining analyses give a weighted mean $^{206}Pb/^{238}U$ age of 83.6 ± 0.7 Ma (MSWD = 1.3; n = 12)

DEFORMATION HISTORY

Granite Point records a long and complex strain history. Field mapping and observations on thin sections and polished slabs have distinguished fabrics at Granite Point that track an evolution through distributed deformation to localized deformation. An early LS tectonite fabric with local zones of high strain is deformed by multiple

ductile shear zones. These ductile shear zones are generally associated with pegmatite veins and could reflect partitioning in transtensional strain.

LS tectonite fabric

The most striking textural feature of Granite Point is the large alkali feldspar crystals. These crystals are sub-augen to augen shaped and display a clear alignment when observed in the field (Fig. 1.7A). This orientation is reinforced by elongate grains of quartz and biotite - amphibole aggregates oriented with long axes approximately parallel to the length of the feldspars. These constituents define a linear fabric, which plunges shallowly to the north (Fig. 1.8). This linear component is contained within a planar fabric defined by the grain boundaries of quartz, feldspar and biotite mica crystals, which define a north-northeast striking, moderately west dipping planar tectonite fabric (Fig. 1.7B) that is pervasive throughout the main granite phase and both the leucocratic and felsic enclaves. The expression of this foliation is largely a function of the mineralogy; biotite poor and fine grained felsic enclaves do not capture the foliation well. As noted by Hooper & Rosenberg (1970), some mafic sheets are parallel to the planar fabric attitude.

Polished slabs with faces cut in three mutually perpendicular orientations help characterize the LS tectonite fabric. Sections parallel to L and perpendicular to S show ribbon quartz and augen feldspar with some incipient ribbon feldspar. In thin section, the elongate quartz crystals show strong subgrain development, undulatory extinction and irregular boundaries, but are generally unfractured. Feldspar crystals are subhedral, sub-

augen and some approach ribbon shaped but are still fractured. Deformation lamellae and twin boundaries of the orthoclase and plagioclase feldspar crystals are often parallel to quartz ribbon long axes.

The expression of this LS tectonite fabric varies across the exposure in both intensity and the relative L > S, L = S and S > L character. Oldow (personal communication, 2007) has suggested the presence of two foliations, S_{1A} and $S_{1B,}$ that cannot be differentiated in the main exposure but can be seen in the farthest northwest exposure of granite. S_{1A} and S_{1B} have an intersection that is parallel to the linear shape fabric at Granite Point (Oldow personal communication, 2007).

Although the planar component of the LS fabric could consist of some composite of these two foliations, differentiation of these fabrics is not possible at Granite Point. Possible scenarios include (1) the planar component of the LS tectonite fabric is the dominant foliation at Granite Point and a second foliation is weakly developed in the low strain domains that reflects a progressive sequence of strain, or (2) separate foliations formed in distinct deformational events have been rotated into parallelism and are indistinguishable. Differentiating these possibilities is currently not possible because of the coarse grained texture, strain associated with the ductile shear zones and lack of continuous exposure connecting low and high strain domains. For the sake of description, the term LS tectonite fabric will be used to describe the planar shape fabric and linear shape fabric that are pervasive throughout Granite Point.

Discontinuous ductile shear zones

The LS tectonite fabric is deflected into a sigmoidal shape by meter long, cm wide zones of ductile shear. These narrow ductile shear zones are discontinuous along strike, dying out usually within one meter and are referred to as discontinuous ductile shear zones (Fig. 1.9). The deflection of the early fabrics results in a change in orientation without any noticeable reduction in grain size or grain shape. Some of these discontinuous shear zones have more felsic material within their center. Sense of shear is both dextral and sinistral. When in close proximity to a continuous ductile shear zone, the discontinuous ductile shear zones generally have the same sense of shear as the larger shear zone.

The greatest density of discontinuous ductile shear zones is at a roadcut along Wawawai Rd, immediately northwest of the parking lot (Fig. 1.2). The spacing between these discontinuous shear zones is generally a few decimeters, with some up to one meter apart. Discontinuous ductile shear zones are generally less than one meter in length and occur throughout Granite Point. Three-dimensional exposure of these discontinuous shear zones is not available, however, the individual displacement on each discontinuous shear zone is probably very small based on the style of deformation.

Continuous ductile shear zones

The LS tectonite fabric and both types of enclaves are deflected into a sigmoidal shape by continuous ductile shear zones at Granite Point (Fig. 1.10). The timing relationship between the discontinuous ductile shear zones and the continuous ductile

shear zones is equivocal. Unfortunately, no crosscutting relationship has been observed between these two sets of shear zones.

The continuous ductile shear zones are characterized by a northeast to east-northeast striking, subvertical foliation defined by aligned biotite mica and quartz-feldspar grain boundaries. A set of continuous ductile shear zones (Fig. 1.11) strike approximately 045^0 with spacing between 50cm and two meters in the northwest corner of Granite Point. This grouping of continuous ductile shear zones is exposed across the Snake River at locations consistent with an along strike projection, which suggests their orientation does not change at least over several hundred meters. Isolated continuous ductile shear zones are exposed northwest of the main granite body, the middle of the main granite body and north of the parking lot: striking 055^0, 060^0 and 070^0 respectively. Deflection of the earlier tectonite fabric and enclaves define the total width of the continuous ductile shear zones from the narrowest 2-3 cm wide zone to the widest 2 meter wide zone (Fig. 1.11). The center of each shear zone is marked by mylonitic fabric, which reflects the highest strain.

The texture of each continuous ductile shear zone is very similar, characterized by cm wide zones of mylonitic fabric and mm wide seams of ultramylonitic fabric. Feldspar porphyroclasts ranging in size from sub-millimeter to several centimeters in diameter, most commonly about one centimeter, have a morphology that generally is a function of the location within the continuous ductile shear zones, where those nearest the margins are subhedral to sub-augen and those within the continuous ductile shear zones are augen shaped (Fig. 1.12). The subhedral and augen feldspar porphyroclasts are fractured. A mineral lineation defined by quartz ribbons and aligned amphibole aggregates created

from the deflection of the earlier linear fabric plunges 45^0 to 60^0 towards the southwest in the plane of the continuous ductile shear zone foliation.

Pegmatite veins are exposed in most of the continuous ductile shear zone (Fig. 1.11). The width of the pegmatite veins range from a minimum of one centimeter to a maximum of ten centimeters with the most common thickness between three and five centimeters. The geometry of the pegmatite veins exposed within the continuous ductile shear zones are generally planar but can also be distinctly lozenge shaped (Fig. 1.13). The texture of the pegmatite veins exposed within the continuous ductile shear zones is characterized by zones of mylonitic to ultramylonitic fabric, commonly present at either the center or edge of the pegmatite veins (Fig. 1.14 & 1.15) that inosculate around quartz – feldspar – biotite ribbons and asymmetric feldspar porphyroclasts.

The monoclinic symmetry of the sigmoidal trace defined by deflected earlier tectonite fabrics and enclaves in the continuous ductile shear zones consistently suggests sinistral, tops to the southwest sense of shear with a west side down component. The geometry of recrystallized quartz - feldspar tails on augen feldspars suggest that the vast majority are sigma type rotated porphyroclasts (Passchier & Trouw, 1998) (Fig. 1.12) and indicate a tops down to the southwest sense of shear except for a few feldspar porphyroclasts that may have back-rotated, giving an opposite shear sense (Simpson & De Paor, 1993). SC fabric (Passchier & Trouw, 1998) visible within a few continuous ductile shear zones further support tops down to the southwest sense of shear (Fig. 1.10).

INTERPRETATIONS

An LS tectonite shape fabric is preserved within the main granite phase and both the leucocratic and mafic enclaves at Granite Point. Subgrain development, undulatory extinction and the ribbon shape of quartz crystals suggest temperatures in excess of 250^0C. Feldspar crystals are subaugen - augen shaped but fractured, suggesting a transition from brittle to ductile deformation. Feldspar responds to deformation by ductile flow when temperature exceeds 500^0C. The feldspar texture at Granite Point suggests temperature may have approached this value. The deformation style at Granite Point suggests a depth of approximately 20 km assuming a standard continental geothermal gradient of 25^0C / km. Brittle – ductile behavior would be expected at a depth of 20 km because this depth marks the base of the brittle-ductile transition. Geothermal gradients may have been significantly greater than 25^0C / km, which would suggest shallower emplacement depths.

The earlier tectonite fabrics and enclaves are transposed by east-northeast striking discontinuous ductile shear zones and northeast striking, subvertical continuous ductile shear zones. The continuous shear zones preserve microstructures that suggest sinistral, tops down to the southwest shear sense. Deflected leucocratic and mafic enclaves and a moderately plunging, southwest trending mineral lineation defined by deflection of the earliest LS tectonite fabric further supports tops down to the southwest sense of shear in the continuous ductile shear zones. Strain could have been localized, forming the continuous ductile shear zones following syntectonic emplacement of pegmatite veins. Strain free grains visible in thin section within the deformed pegmatite veins suggest static recrystalization. This suggests deformation had essentially ended while the pegmatite veins were still hot enough to partially recover strain accumulated from ductile

shearing. The closure age on hornblende reported by Fleck & Criss (2004) of 74 Ma suggests temperatures greater than 500^0C persisted for approximately 10 Ma after emplacement of the pegmatite veins. Alternatively, this closure age could have been reset by younger intrusives that supplied sufficient heat to reset the ^{40}Ar geochronometer in hornblende.

Based on field relationships and textural observations, the tectonite fabric observed at Granite Point post dates emplacement of the granite and enclaves because the mineral constituents are deformed. Had deformation taken place in the magmatic state (i.e. magmatic flow fabric) strain should have been accommodated preferentially within the interstitial liquid phase, leaving relatively undeformed feldspar porphyroclasts. An earlier history of magmatic flow may exist, however was either destroyed or superposed by the LS tectonite fabric. Furthermore, the sub-augen feldspar porphyroclasts within the main granite phase suggest solid state deformation.

The continuous ductile shear zones deflect the earlier tectonite fabrics and enclaves. Pegmatite intrusives both within and outside of the continuous ductile shear zones do not show textural evidence of the earlier strain history and are interpreted to post date these fabrics. The relative timing of the pegmatite veins and continuous ductile shear zones is more ambiguous, evidence of strain localization along the edge and within the margin of the continuous ductile shear zones can be seen, however, numerous lozenge shaped pegmatite veins suggest syntectonic emplacement. This interpretation is also supported by the observation that the pegmatite veins are often at a slight angle, ~10^0, from the orientation of the foliation within the continuous shear zones. It would follow

that this angle could have originally been greater but reduced from rotation of the pegmatite veins during shearing.

The absolute age of the main granite phase at Granite Point is interpreted to be between 90 ma and 100 ma from dating Zircon crystals using the SHRIMP method. This provides a maximum age for the tectonite fabric. Based on the texture preserved within the tectonite fabric, deformation is suggested to have occurred after crystallization of the granite. The age of the pegmatite vein only strictly constrains the age of the tectonite fabric because the tectonite fabric is not observed within pegmatite veins. This requires that the undeformed pegmatite veins are coeval with deformed pegmatite veins. This cannot be documented without further geochronologic analysis. Because the pegmatite veins have textures and morphologies that suggest syntectonic emplacement, the age of the pegmatite veins suggest the continuous ductile shear zones were active at this time.

The association of pegmatite veins and ductile shear zones at Granite Point requires consideration of the space problem, i.e. how intrusives are emplaced syntectonically within a ductile shear zone. Differing models including either strain softening or strain hardening provide possibilities, however, because the pegmatite veins are intimately associated with the ductile shear zones, a strain context provides a straightforward model. If the state of strain were transtensional, rather than strictly simple shear, dilation could provide space for emplacement of the veins. In this scenario, transtensional strain is partitioned into simple shear and pure shear domains (Fig. 1.19). Simple shear strain could initially localize along the margin of the emplaced pegmatite vein but the pegmatite vein itself could still be deformed, which agrees with field observations at Granite Point. This sequence of events agrees with field observations in

the Northumberland Basin, United Kingdom, described by De Paola et al. (2005). Here, simple shear strain is localized along the margins of intruded veins within a transtensional basin.

DISTRIBUTED VS. LOCALIZED DEFORMATION

The evolution of deformation at Granite Point records pervasive, distributed fabrics in the earliest history followed by localized, discrete structures. This is a strain history path followed at other geologic localities, for exampleat Castle Odair, Scotland (Ramsay & Graham, 1970) and the Laghetti Shear Zone in Switzerland (Simpson, 1982) where older distributed fabrics transposed by younger localized fabrics are preserved.

A unifying conceptual framework to explore deformation history is provided by the recent mathematical modeling of Patton & Watkinson (2005). This work utilizes a diharmonic partial differential equation to model a thermo-mechanical second order fluid rheology of the earth. The immediate benefit of the approach taken by Patton & Watkinson lies in the intrinsic behavior of their model, that is the ability to store energy until a failure point. Previous models cannot store energy or reflect a failure, which could be analogous to an earthquake. This modeling has provided an energy map for different styles of deformation. The energy map is well suited for understanding ductile deformation because the axes correspond to stored strain energy and the ratio between the thermal diffusion and the mechanical diffusion.

Energy is stored in deformed rocks in the form of entangled dislocations, subgrains and strained crystals. This modeling establishes the idea of mechanical, or

strain diffusion, which is similar to heat diffusion. Strain diffusion is analogous to strain that propagates through a deforming object a certain distance per time. This mechanical diffusion (χ) results in strain, while the thermal diffusion (κ) works to undo the strain. This competition is directly analogous to the competition between dynamic recrystalization and static recrystalization (recovery). The energy map (Fig. 1.18) shows the strain history path intrinsic to the model through solutions for the onset of distributed (or pure shear) and localized (or simple shear) deformation.

Reading the energy map as a narrative for deformation history suggests that until sufficient strain energy is stored in a rock, a distributed strain is the most energetically favorable style of deformation. This distributed deformation could manifest in many ways, spaced cleavages in a slate belt, long wavelength folding in thrust belts, LPOs and pervasive tectonite fabrics like at Granite Point. Once sufficient strain is accrued, a localized style of deformation can occur. There is no requirement that the accumulation of strain energy be from the same deformation event and multiple episodes of strain could reach the threshold for localization.

LIMITATIONS OF KINEMATIC RECONSTRUCTIONS

The set of continuous ductile shear zones in the northwestern corner of Granite Point define a deforming zone where strain is partitioned into high strain zones separated by domains of low strain. The kinematics of each ductile shear zone within this partitioned system can be determined by examining the microstructures preserved within the tectonite fabric of the shear zone. However, based on this data, can the relative

motion of the boundaries be determined? I would suggest the answer is no. Finite strain is non-unique (Ramsay, 1967; Tikoff & Fossen, 1995; Jiang & Williams, 1998) and the strain recorded within each ductile shear zone could have been created by any combination of deformation. Because ductile shear zones represent a partitioning of strain into high strain zones, each individual ductile shear zone may record only a component of the total kinematics. Furthermore, if the relative motion of the boundaries was oblique to the shear zones then a complex relationship exists between the orientation of strain and the velocity direction (Fossen & Tikoff, 1993; Tikoff & Fossen, 1995) where the orientation of strain and the velocity field deviate from parallelism. The implication of this to kinematic reconstructions based on finite strain data in exhumed tectonites is profound. If the velocity field measured in oblique active tectonics cannot be taken as the orientation of strain then it follows that the orientation of strain measured in exhumed tectonites cannot be taken as the orientation of the palaeo-velocity field within the deforming zone.

CONCLUSIONS

Granite Point records a strain history where older distributed fabrics are deformed by younger localized fabrics. This progression from a distributed to localized style of deformation agrees with field observations in other geologic localities and the mathematical modeling of Patton & Watkinson (2005), which has produced a model energy map for deformation suggesting that because distributed deformation occurs at a lower energy threshold than a localized deformation, an earlier history of distributed

strain is followed by a younger history of localized strain. The sequence predicted by this model is explained eloquently by the competition between the thermal and mechanical diffusion and the accumulation of stored strain energy (Patton & Watkinson, *2007 in prep*).

The ductile shear zones at Granite Point collectively define a system where strain is partitioned between two boundaries that are moving relative to one another. Instead of a homogeneous, or distributed strain between these moving boundaries, localized zones of high strain are separated by zones of much lower strain. Microstructural analysis allows the sense of shear to be determined for each shear zone, however, can this data be used to reconstruct the relative motion of the boundaries? Furthermore, if the ductile shear zones were not exposed and only the relative displacement of the boundaries was apparent, could the partitioning captured by the ductile shear zones be detected?

These questions are difficult to answer, especially at Granite Point where exposure is limited and markers sweeping in and out of the high strain zones are lacking. Actively deforming zones represent a unique opportunity to examine these problems because strain data can be combined with GPS velocities that record particle motion within the deforming zone. Because differentiating different strain states (i.e. simple shear, pure shear, transtension or transpression) is very difficult to determine in ancient zones, obliquely deforming active tectonic zones should be examined to represent the most general case. These are the problems explored in the remainder of this dissertation.

REFERENCES

Armstrong, R.L., Taubeneck, W.H., and Hales, P.O., 1977, Rb-Sr and K-Ar geochronometry of Mesozoic granitic rocks and their Sr isotopic composition: Oregon, Washington, and Idaho: Geological Society of America Bulletin, v. 88, p. 397–411.

Barth, A. P., Wooden, J. L., and Coleman, D. S., 2001, SHRIMP-RG U-Pb zircon geochronology of Mesoproterozoic metamorphism and plutonism in the southwestern United States: Journal of Geology, v. 109**,** p. 319-327.

Bateman, P.C., 1992, Plutonism in the central part of the Sierra Nevada batholith, California: U.S. Geological Survey Professional Paper 1483, p. 186.

Black, L. P., Kamo, S. L., Allen, C. M., Davis, D. W., Aleinikoff, J. N., Valley, J. W., Mundil, R., Campbell, I. H., Korsch, R. J., Williams, I. S., and Foudoulis, C., 2004, Improved $^{206}Pb/^{238}U$ microprobe geochronology by the monitoring of a trace-element related matrix effect; SHRIMP, ID-TIMS, ELA-ICP-MS and oxygen isotope documentation for a series of zircon standards: Chemical Geology, v. 205, p. 115–140.

Clifton, A.E., Kattenhorn, S., 2006. Structural architecture of a highly oblique divergent plate boundary segment. *Tectonophysics*. Vol. 419, 27-40.

Coney, P.J., Jones, D.L., Monger, W.H., 1980. Cordilleran suspect terranes. Nature 288, 329 – 333

Criss, R.E., Fleck, R.J., 1987. Petrogenesis, geochronology, and hydrothermal systems of the northern Idaho batholith and adjacent areas based on 18O/16O, D/H, 87Sr/86Sr, K–Ar and 40Ar/39Ar studies. In: Vallier, T.L., Brooks, H.C. (Eds.), Geology of the Blue Mountains region of Oregon, Idaho, and Washington: the

Idaho Batholith and its Border Zone. U.S. Geological Survey Professional Paper 1436, 95–138.

Criss, R.E., Fleck, R.J., 2004. Location, Age, and Tectonic Significance of the Western Idaho Suture Zone (WISZ). U.S. Geological Survey Open-File Report 2004-1039 48p.

Fossen, H., Tikoff, B., 1993. The deformation matrix for simultaneous simple shearing, pure shearing and volume change, and its application to transpression-transtension tectonics. Journal of Structural Geology 15, 413-422.

Giorgis, S., Tikoff, B., Kelso, P., Markley, M. 2006. The role of material anisotropy in the neotectonic extension of the western Idaho shear zone, McCall , Idaho : Geological Society of America Bulletin. Vol. 118 No. 3/4 p. 259–273.

Gosh, S.K., Ramberg, H., 1976. Reorientation of inclusions by combination of pure and simple-shear. Tectonophysics 34, 1-70.

Hooper, P. R.; Rosenberg, P. E., 1970. The petrology of Granite Point, southeastern Washington. Northwest Science, v. 44, no. 2, p. 131-142.

Horsman, E., Tikoff, B., 2005. Quantifying simultaneous discrete and distributed deformation. Journal of Structural Geology Vol. 27, p. 1168-1169.

Hudleston, P.J., 1999. Strain compatibility in shear zones; is there a problem? Journal of Structural Geology Vol. 21, p. 923-932.

Jiang, D., Williams, P.F., 1998. High-strain zones: a unified model. Journal of Structural Geology. Vol. 20, No. 8, 1105-1120.

Ludwig, K. R., 2001, Squid version 1.02: A user's manual: Berkeley Geochronology Center Special Publication, v. 2, p. 1-22.

Ludwig, K. R., 2003, User's manual for Isoplot 3.00: a geochronological toolkit for Microsoft Excel: Berkeley Geochronology Center Special Publication v. 4, p. 1-70.

McClelland, W.C., Oldow, J.S., 2004. Displacement transfer between thick- and thin-skinned decollement systems in the central North American Cordillera. Geological Society of London Special Publication. Vol. 227, p. 177-196.

Oldow, J.S., Bally, A.W., Avé Lallemant, H.G., 1990. Transpression, orogenic float, and lithospheric balance. Geology. Vol. 18, no. 10, pg. 991-994.

Patton, R.L., Watkinson, A.J., 2005. A viscoelastic strain energy principle expressed in fold – thrust belts and other compressional regimes. Journal of Structural Geology, Volume 27, Issue 7, pg. 1143-1154.

Price, R.A., 1981. The Cordilleran foreland thrust and fold belt in the southern Canadian Rocky Mountains. In: Thrust and Nappe Tectonics. The Geological Society of London. Pg. 427 – 448.

Ramsay, J.G., Graham, R.H., 1970. Strain variation in shear belts. Canadian Journal of Earth Science. Vol. 7, pg. 786-813.

Sorenson, K., 1983. Growth and dynamics of the Nordre Strømfjord shear zone. Journal of Geophysical Research, Volume 88, Issue B4, pg. 3419-3438.

Stacey J. S., and Kramers, J. D., 1975, Approximation of terrestrial lead isotope evolution by a two-stage model: Earth and Planetary Science Letters, v. 26, p. 207-221.

Tikoff, B., Fossen, H., 1995. Limitations of three-dimensional kinematic vorticity analyses. Journal of Structural Geology Vol. 17, 1771-1784.

Treascher, R.C., 1925. Geology of the Pullman quadrangle. Thesis (M.S. in **Geology**)--State College of Washington.

Weijermars, R., Poliakov, A., 1991. Stream functions and complex potentials: implications for development of rock fabric and the continuum assumption. *Tectonophysics*. Vol. 220, 33-50.

Williams, I. S., 1998, U-Pb by ion microprobe, *in* McKibben, M. A., Shanks, W. C. and Ridley, W. I., eds., Applications of microanalytical techniques to understanding mineralizing processes: Society of Economic Geologists, Reviews in Economic Geology, v. 7, p. 1-35.

Figure 1.1: Location map of Granite Point.

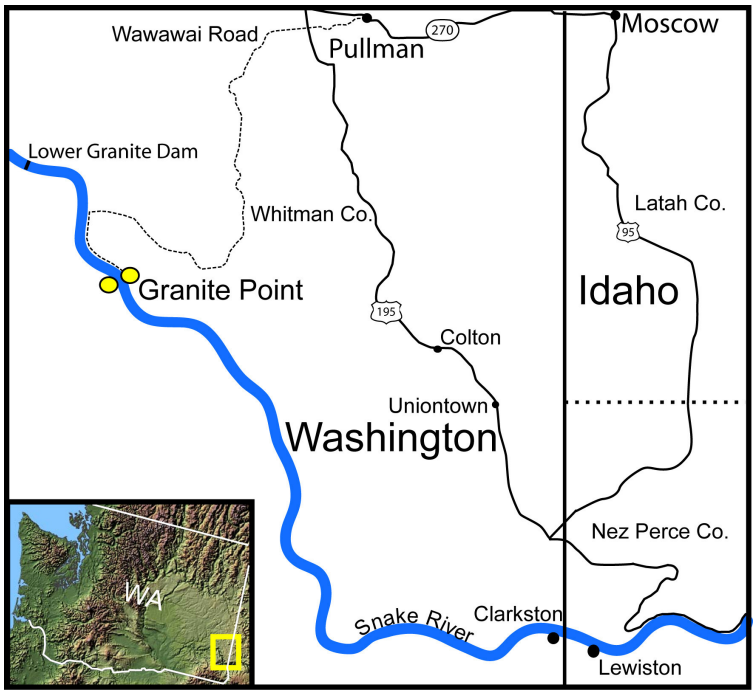

Figure 1.2: Natural color aerial image of Granite Point. Black outlines show extent of exposed granite. Localities referred to in text are indicated, with the exception of the Railroad exposure, which is outside the photograph. Ground pixel resolution is .25 m. Provided by Gregg Teasdale of Teasdale Environmental Associates pllc.

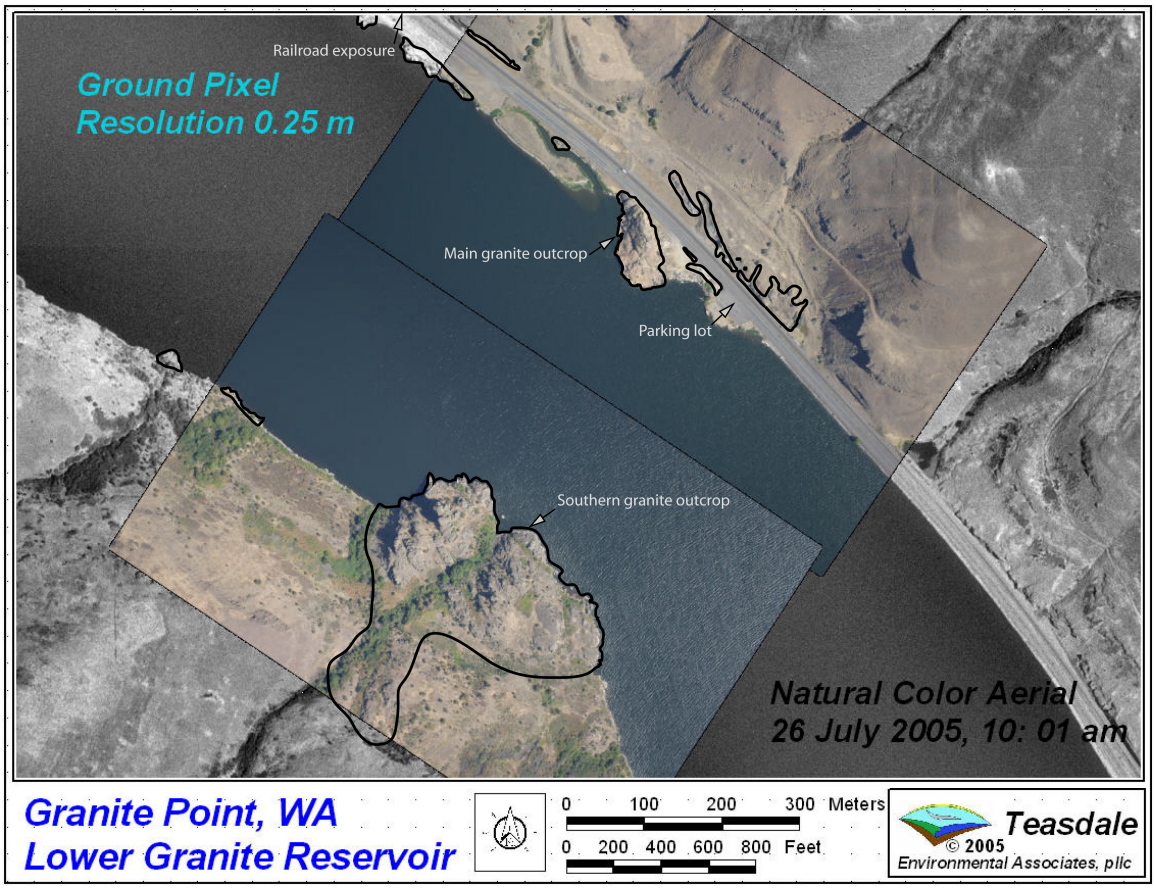

Figure 1.3: Photograph showing fresh profile exposure of granite at Granite Point. The large alkali feldspar crystals give Granite Point a distinct texture. Left of photograph is southeast.

Figure 1.4: Photograph of undeformed pegmatite vein in profile at railroad cut northwest of Granite Point. Left side of photograph is northwest.

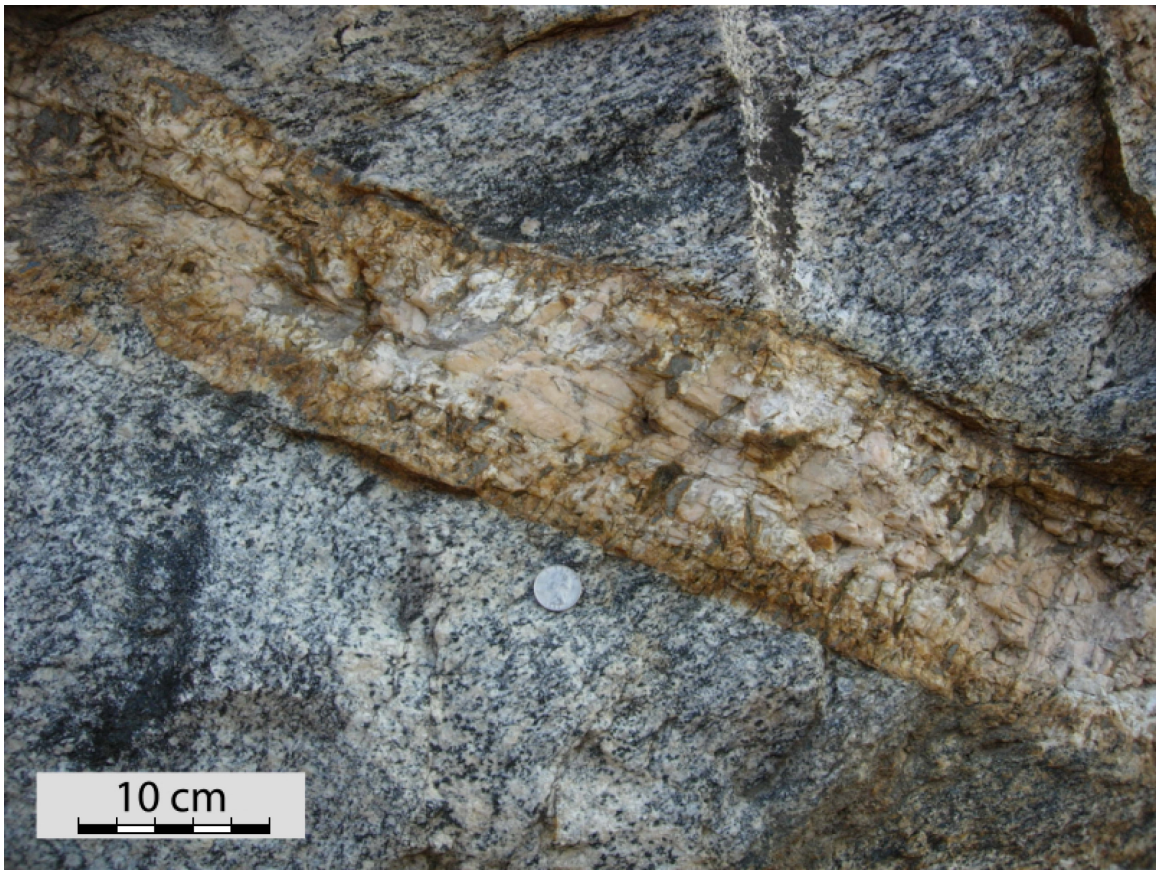

Figure 1.5: Profile view of leucocratic enclave, outlined in black, at Granite Point. Right side of photograph is southeast.

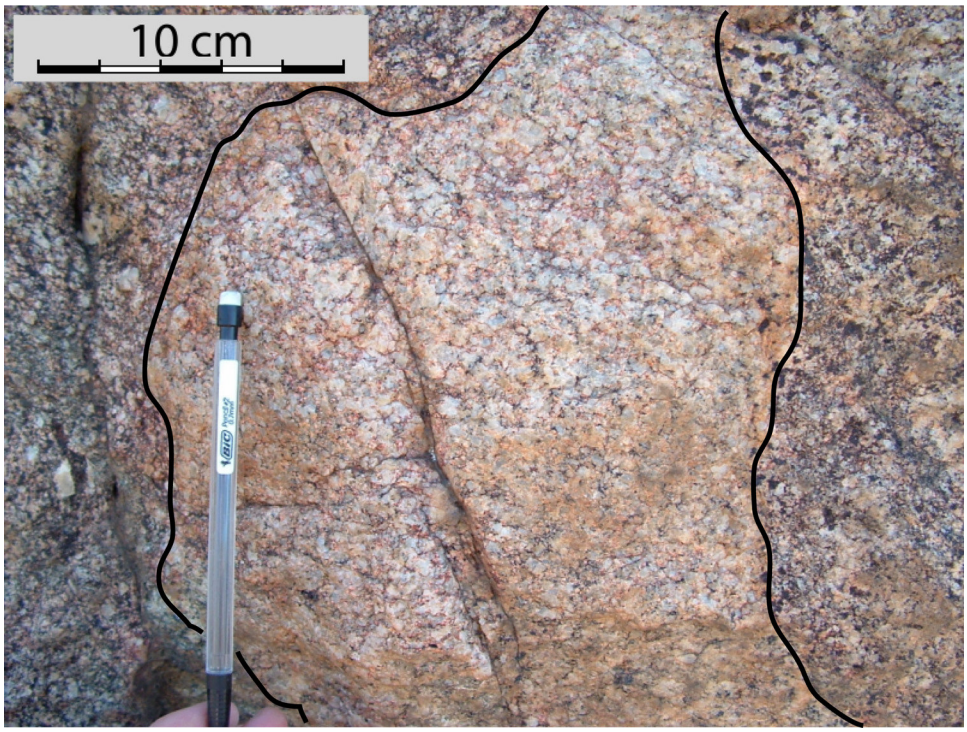

Figure 1.6: Photograph showing map view of a mafic enclave that has been deformed by discontinuous ductile shear zones. North is toward the top of the photograph.

Figure 1.7: Photographs showing variation in LS tectonite fabric strain. The elongate quartz and feldspar define a strongly linear fabric within the high strain domain in photograph A. The abundance of biotite within the high strain domain in photograph B. results in a strongly planar fabric. Photograph A. is taken looking perpendicular to the foliation surface showing the trace of the linear fabric. Photograph B. is taken parallel to foliation strike and perpendicular to the linear fabric.

A.

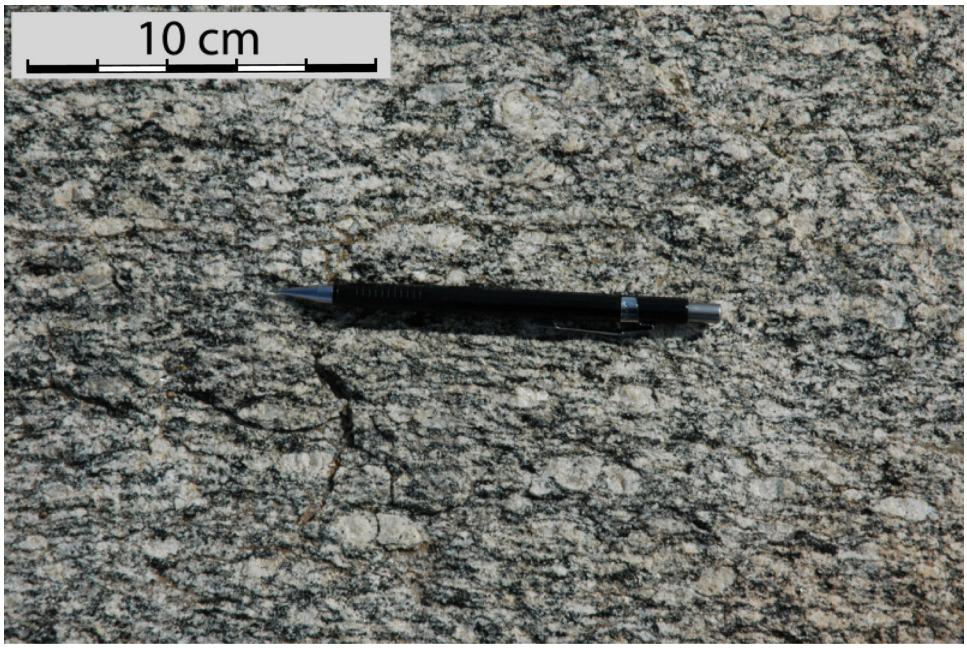

B.

Figure 1.8: Strike and dip measurements of LS tectonite fabric at Granite Point. Solid circles indicate measurements taken within the main outcrop (Fig. 1.2) and open circles represent measurements taken at the exposure bordering the northwest edge of the parking lot (Fig. 1.2). N_S and N_L correspond to number of measurements plotted for the planar (N_S) and linear (N_L) component respectively.

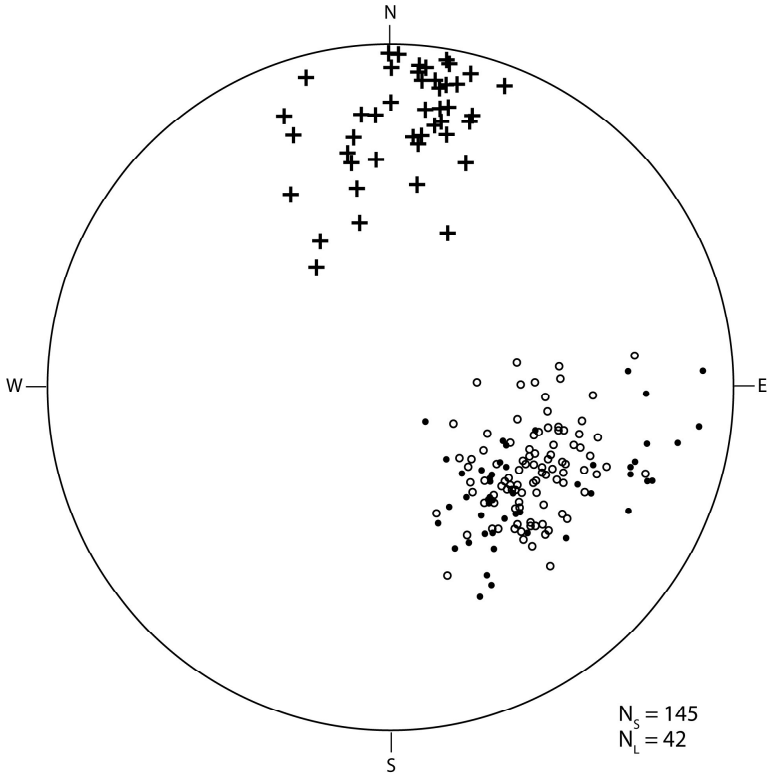

Figure 1.9: Photograph and line drawing of a discontinuous shear zone in profile view. The LS tectonite fabric is deflected without any noticeable reduction in grain size or change in grain shape. Sense of shear is right side down, northwest is right.

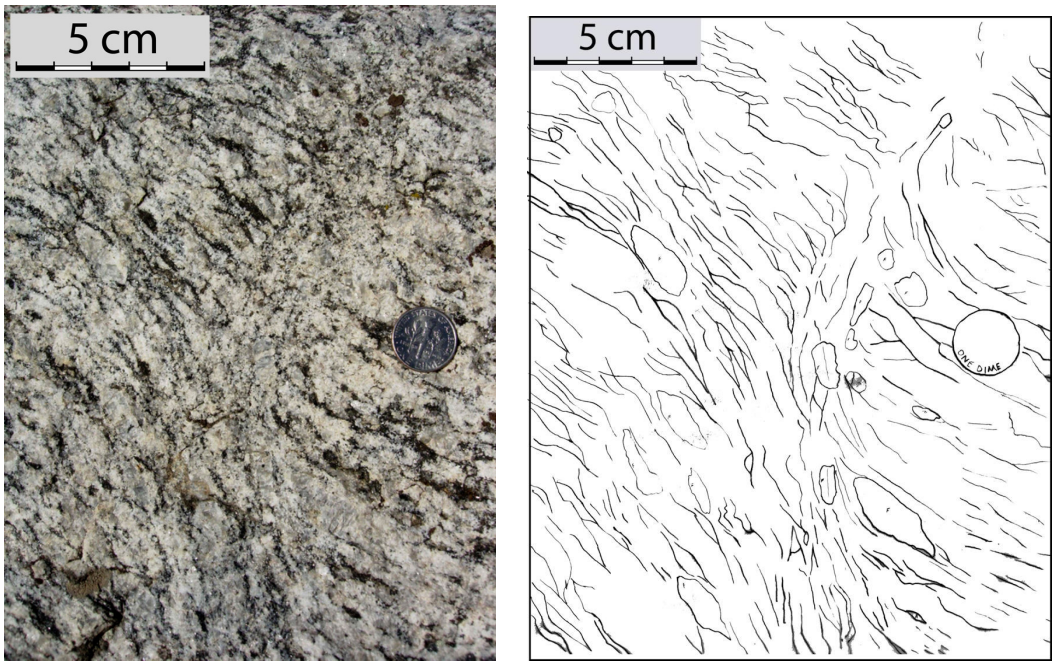

Figure 1.10: Profile photograph of SC fabric developed in a continuous ductile shear zone. The mylonitic fabric (dark band) on the right hand side of the outcrop marks the center of the shear zone. Deflection of LS tectonite fabric, asymmetric porphyroclast tails and SC fabric give left side down shear sense. Right side of photograph is southeast.

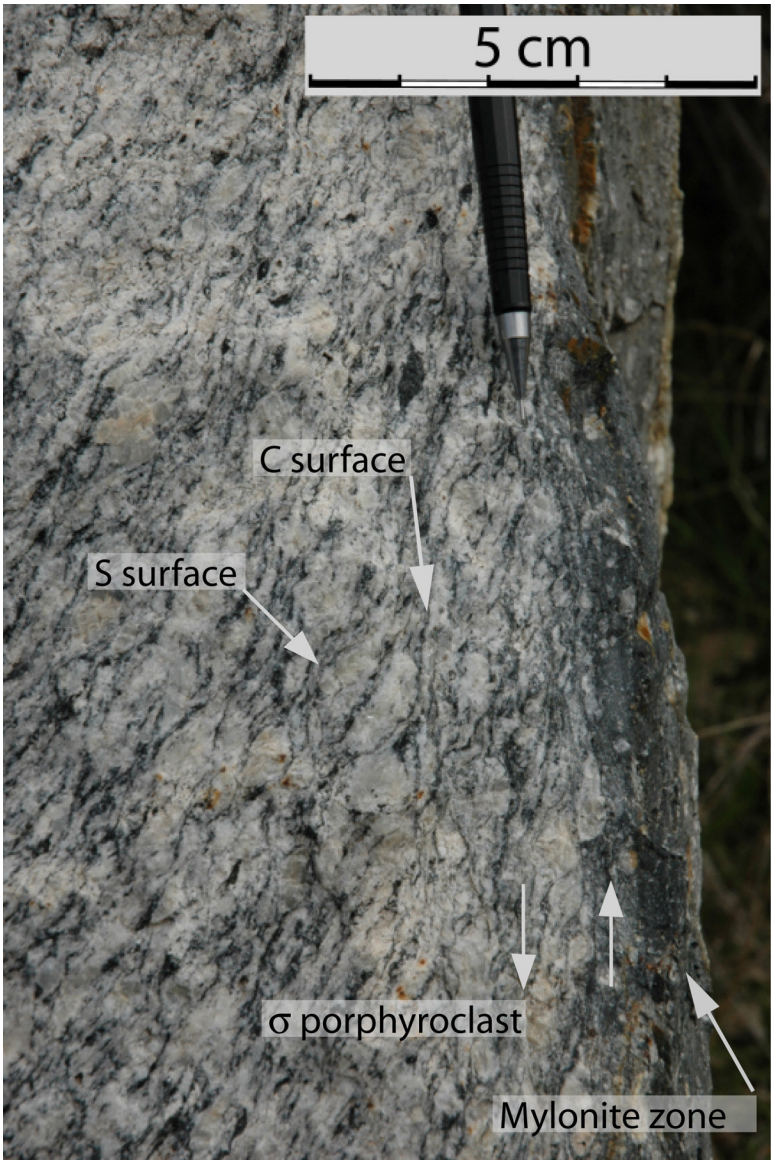

Figure 1.11: Composite image of roadcut exposed along Wawawai Road with line drawing that shows location of pegmatite veins and sheared enclaves. The left side of the photograph is southeast.

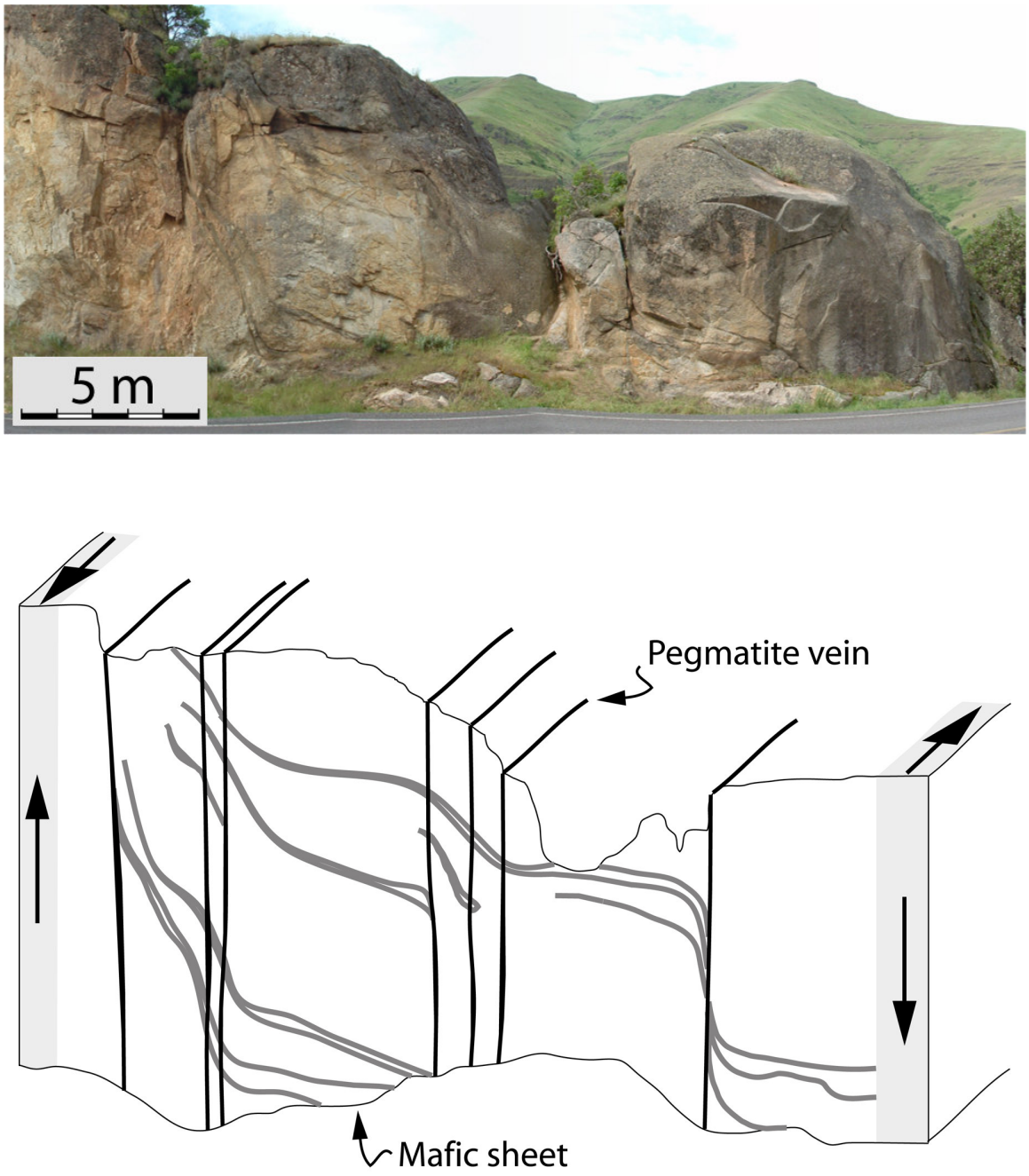

Figure 1.12: Map view photograph of Sigma type mantled feldspar porphyroclasts within a continuous ductile shear zone. Map view showing sinistral shear sense, which is a component of the tops down to the southwest shear expressed on a horizontal surface. Foliation strikes NE / SW, NE is to the left.

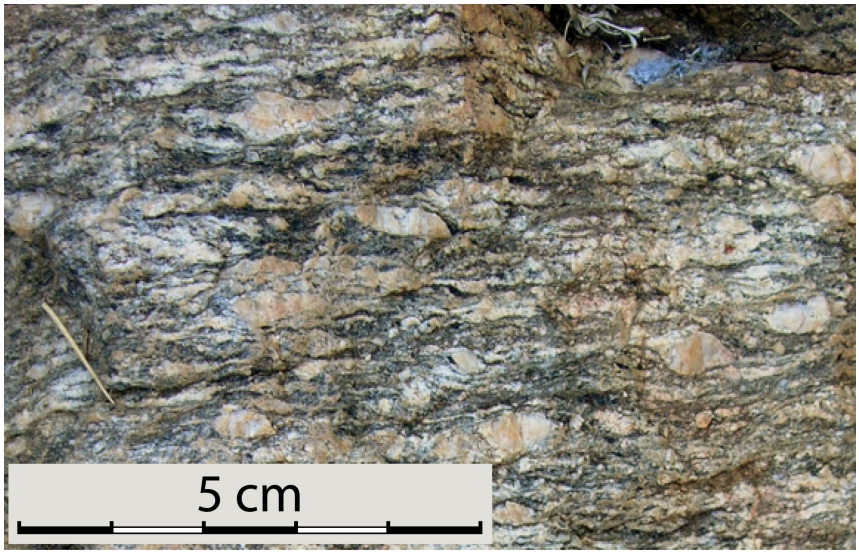

Figure 1.13. Map view photograph of lozenge shaped deformed pegmatite veins in a continuous ductile shear zone. Pencil points northeast.

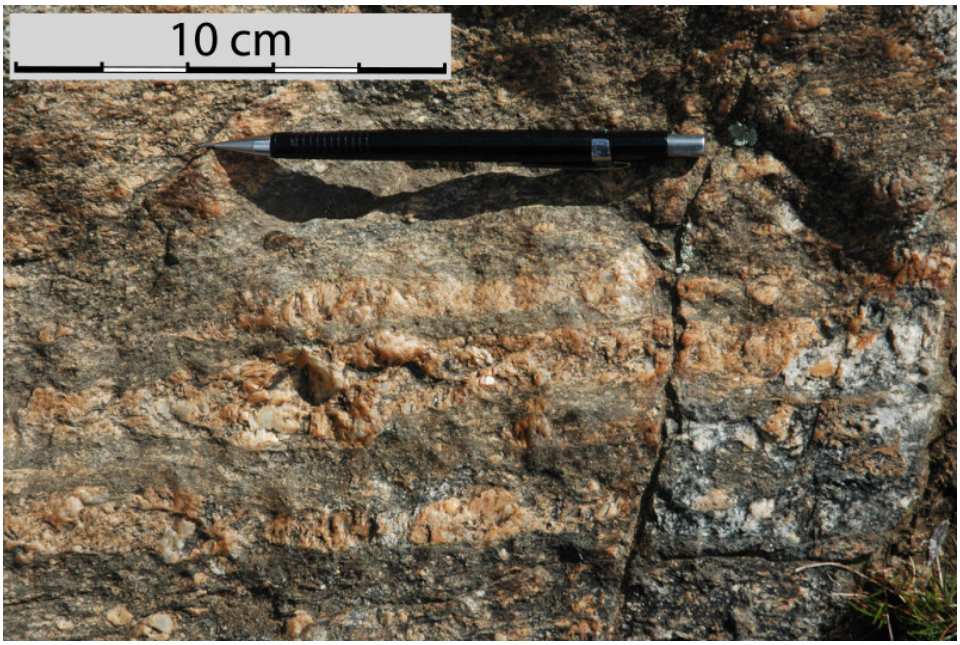

Figure 1.14. Photograph showing top surface of continuous ductile shear zone with deformed pegmatite vein. Note the localized seam of mylonitic fabric on the pegmatite margin. The sigmoidal deflection of the LS tectonite fabric gives sinistral shear. Pencil points southwest.

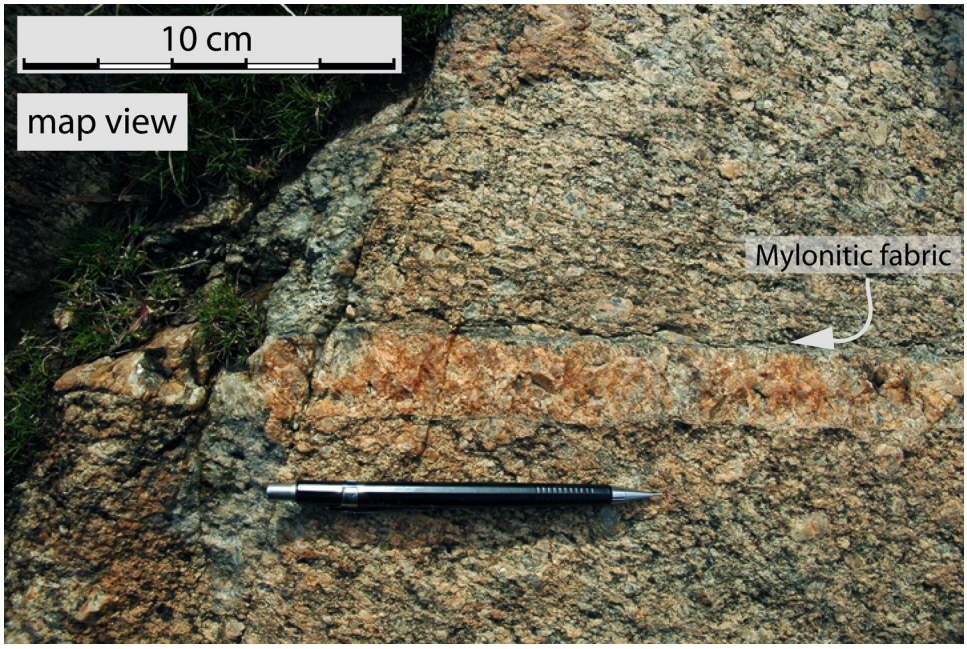

Figure 1.15. Profile photograph of deformed pegmatite vein in continuous ductile shear zone. The darker, fine grained seams are mylonitic fabric. Both pegmatite veins are within continuous ductile shear zones. Sense of shear is west side down and the right side of the photograph is northwest.

Figure 1.16. Tera-Wasserburg plots of sensitive high-resolution ion microprobe – reverse geometry (SHRIMP-RG) U-Pb data of zircon for samples (A) GP1 and (B) GP2. The data are presented as 1 σ error ellipses uncorrected for common Pb. MSWD = mean square of weighted deviates. Black ellipses correspond to analyses used in age calculation (Figure 22).

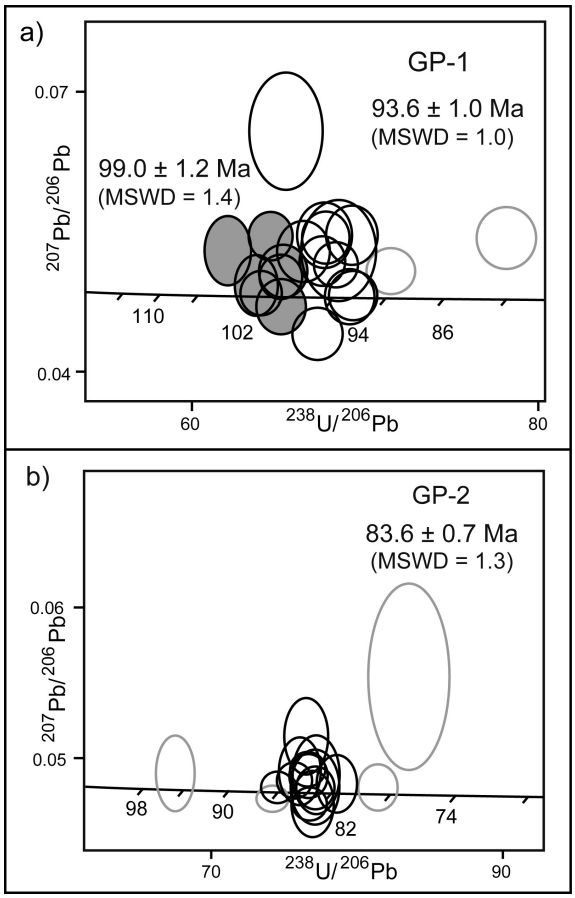

Figure 1.17. Photomicrographs of zircons in GP1 (A.) and GP2 (B.). Spot numbers correspond to data values presented in Table 1-1.

A.

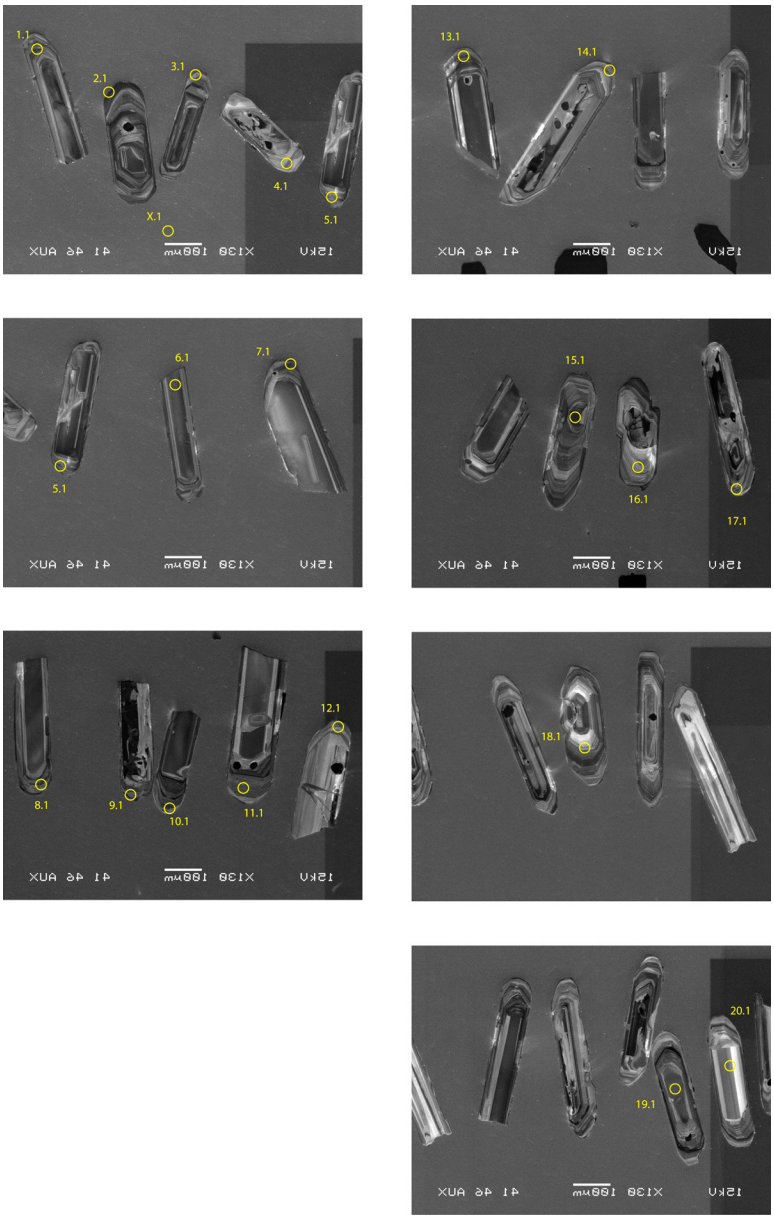

B.

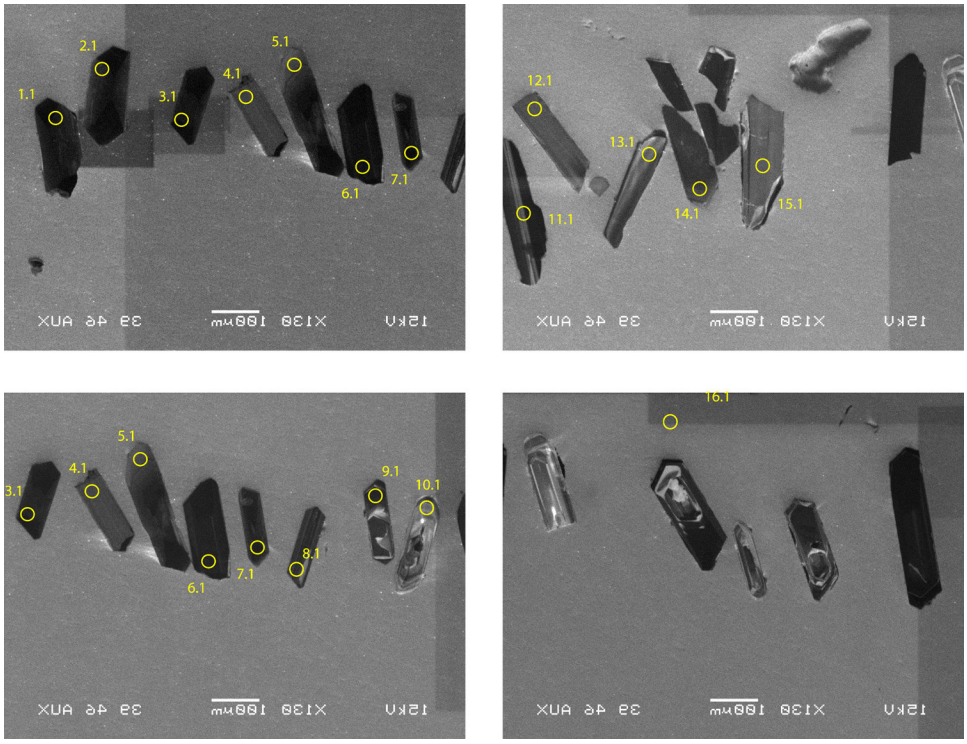

Table 1-1. U-Pb SHRIMP geochronologic data and apparent ages.

Spot		U[a] (ppm)	Th (ppm)	Th/U	$^{206}Pb^{*a}$ (ppm)	$f^{206}Pb_c$ [a]	$^{238}U/^{206}Pb$ [b]		$^{207}Pb/^{206}Pb$ [b]		$^{206}Pb/^{238}U$ [c] (Ma)	
Sample GP1												
1.1	R	419	144	0.4	5	0.8	67.728	(1.3)	0.05433	(3.3)	93.7	(1.3)
2.1	R	684	76	0.1	8	0.8	78.142	(1.4)	0.05430	(3.9)	*81.3*	*(1.2)*
3.1	R	300	42	0.1	4	0.6	62.068	(1.4)	0.05287	(4.6)	*102.4*	*(1.5)*
4.1	R	255	80	0.3	3	0.6	66.473	(1.5)	0.05286	(4.1)	95.7	(1.4)
5.1	R	281	89	0.3	4	----	65.156	(1.4)	0.04700	(4.1)	*98.3*	*(1.4)*
6.1	C	388	239	0.6	5	0.03	69.314	(1.3)	0.04812	(3.6)	92.3	(1.2)
7.1	R	459	156	0.4	6	0.2	63.759	(1.3)	0.04927	(4.4)	*100.2*	*(1.3)*
8.1	R	382	107	0.3	5	0.5	67.513	(1.3)	0.05181	(3.4)	94.3	(1.3)
9.1	R	479	91	0.2	6	0.4	68.316	(1.3)	0.05139	(3.1)	93.3	(1.2)
10.1	R	496	171	0.4	7	0.1	64.029	(1.3)	0.04845	(3.2)	*99.8*	*(1.3)*
11.1	R	415	141	0.4	6	0.8	64.545	(1.3)	0.05450	(3.2)	*98.3*	*(1.3)*
12.1	R	306	48	0.2	4	0.0	69.180	(1.4)	0.04804	(4.0)	92.5	(1.3)
13.1	R	466	153	0.3	6	0.3	65.164	(1.3)	0.05017	(3.0)	*97.9*	*(1.2)*
14.1	R	313	65	0.2	4	----	67.237	(1.4)	0.04401	(4.2)	95.6	(1.4)
15.1	C	502	294	0.6	6	0.4	71.458	(1.3)	0.05072	(3.1)	*89.3*	*(1.1)*
16.1	R	235	97	0.4	3	0.8	67.695	(1.5)	0.05458	(4.2)	93.7	(1.5)
17.1	R	308	106	0.4	4	0.3	65.294	(1.4)	0.05075	(3.7)	97.6	(1.4)
18.1	C	111	42	0.4	1	0.6	68.491	(2.1)	0.05293	(6.7)	92.8	(2.0)
19.1	C	311	162	0.5	4	0.8	69.273	(1.4)	0.05458	(3.8)	91.6	(1.3)
20.1	C	90	53	0.6	1	2.2	65.456	(2.1)	0.06574	(6.3)	95.6	(2.1)

Sample GP2

1.1	R	2,027	161	0.1	23	0.2	76.579	(1.0)	0.04925	(1.6)	83.5	(0.9)
2.1	R	1,232	72	0.1	13	0.06	81.350	(1.1)	0.04803	(2.1)	*78.7*	*(0.9)*
3.1	R	2,001	144	0.1	23	0.1	75.674	(1.1)	0.04854	(1.6)	84.5	(0.9)
4.1	R	501	74	0.2	6	0.5	76.496	(1.3)	0.05144	(3.3)	83.3	(1.1)
5.1	R	618	24	0.04	7	0.2	76.037	(1.2)	0.04911	(3.0)	84.1	(1.0)
6.1	R	2,296	94	0.04	26	----	76.668	(1.0)	0.04696	(1.5)	83.6	(0.8)
7.1	R	3,792	348	0.1	44	----	74.133	(1.0)	0.04725	(1.2)	*86.4*	*(0.8)*
8.1	R	1,045	43	0.0	11	0.08	78.538	(1.2)	0.04828	(2.6)	81.5	(0.9)
9.1	R	1,418	257	0.2	16	0.04	77.103	(1.1)	0.04799	(2.0)	83.0	(0.9)
10.1	R	417	58	0.1	5	0.1	67.579	(1.3)	0.04903	(3.3)	*94.6*	*(1.2)*
11.1	C	2,743	131	0.05	32	0.04	74.526	(1.0)	0.04804	(1.4)	85.9	(0.9)
12.1	C	528	77	0.2	6	0.05	77.090	(1.4)	0.04803	(3.4)	83.0	(1.2)
13.1	C	545	30	0.1	6	----	76.880	(1.2)	0.04696	(3.1)	83.4	(1.0)
14.1	C	1,297	55	0.04	15	0.1	76.655	(1.1)	0.04882	(2.0)	83.4	(0.9)
15.1	C	477	67	0.1	5	0.2	77.137	(1.3)	0.04887	(3.5)	82.9	(1.1)
16.1	C	99	6	0.1	1	1.0	83.487	(2.3)	0.05539	(7.4)	*76.0*	*(1.8)*

Note: All analyses were performed on the SHRIMP-RG ion microprobe at the United States Geological Survey-Stanford Microanalytical Center at Stanford University. Calibration concentrations and isotopic compositions were based on replicate analyses of CZ3 and R33 (419 Ma; Black et al., 2004), respectively. Analytical routine followed Williams (1998) and Barth (2001). Data reduction utilized Ludwig (2003).

[a] Abbreviations: c = core; r = rim.

[a] Pb* denotes radiogenic Pb; Pb_c denotes common Pb; $f^{206}Pb_c = 100*(^{206}Pb_c/^{206}Pb_{total})$.

[b] Reported ratios are not corrected for common Pb. Errors are reported in parentheses as percent at the 1 σ level.

[c] The $^{206}Pb/^{238}U$ ages are calculated from ratios corrected for common Pb using the ^{207}Pb method. Uncertainties in millions of years reported as 1 σ. Ages in italics were excluded in calculation of weighted mean $^{206}Pb/^{238}U$ ages cited in text and figures.

Figure 1.18. Simplified energy map of Patton & Watkinson (2005). Stored energy increases on the Y axis as the ratio of the thermal diffusivity (κ) to the mechanical diffusivity (χ) increases on the X axis. Time moves to the right. The black 1/α line shows the model strain path that moves through a distributed (pure shear) deformation to a localized (simple shear) solution as the amount of stored strain energy increases.

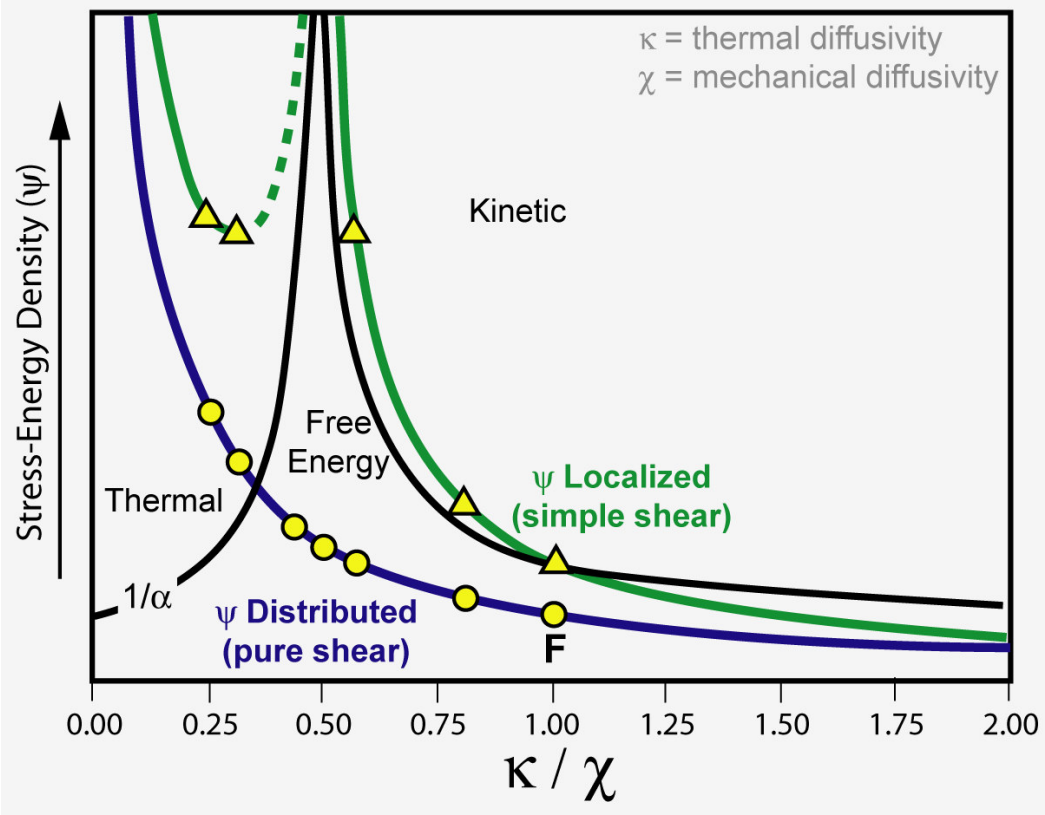

Figure 1.19. Block model diagram showing partitioned transtension with dilation (adapted from De Paola et al., 2005). Simple shear is localized within the deforming country rock because dilation from pegmatite vein injection accommodates extensional component of transtension.

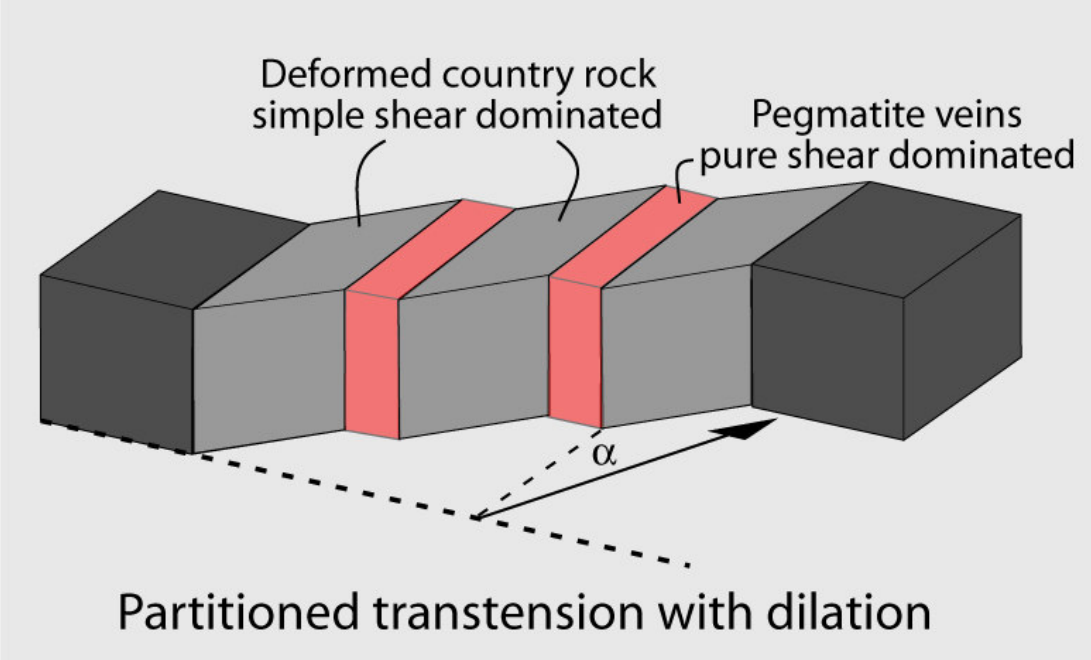

CHAPTER TWO

A GRAPHICAL VISUALIZATION OF THE RELATIONSHIP BETWEEN VELOCITY AND THE PRINCIPAL AXES OF STRAIN WITHIN OBLIQUELY DEFORMING TECTONIC ZONES

Justin J. Murphy[1*], A. John Watkinson[1], John S. Oldow[2]

[1] School of Earth and Environmental Sciences, Washington State University, Pullman, Washington 99164-2812

[2] Department of Geological Sciences, University of Idaho, Moscow, Idaho, 83844

Abstract

Relative plate motions are often oblique. This common boundary condition can result in simultaneous components of coaxial and non-coaxial strains within deforming tectonic zones. GPS technology allows the precise measurement of relative plate motion. However, relating these motions back to the state of strain is complex, especially with oblique relative motion, where the incremental and finite strain are in different orientations. While analytically based methods exist, a graphical construction originally developed for the analysis of strain in ductile shear zones allows the rapid determination of the orientation of the principal axes of strain within a zone that is generalized as homogeneously deforming. Furthermore, the method can estimate the finite rotation of differently oriented passive material lines. Two geologic examples have been chosen to illustrate the utility of this method: the Aleutian Arc, Alaska and the central Walker Lane, Nevada. The solutions obtained from the graphical method can be compared to available

strain orientations published for each geologic example: the orientation of upper plate earthquake P axes in the Aleutian Arc and strain trajectories constructed from fault slip inversion and earthquake focal mechanisms in the Walker Lane.

Keywords: Rotation, Graphical link, Vorticity, GPS Velocities, Strain Orientation

*murphywsu@hotmail.com

1. Introduction

Numerous publications on the expression of oblique relative plate motion at convergent boundaries have been published following the classic observations of Fitch (1972) at the Sunda arc. The Hikurangi trench, New Zealand (Walcott, 1978; Cashman, 1992) and the Aleutian Island Arc, Alaska (Spence, 1977; Ave Lallemant & Oldow, 2000) now have an impressive array of data including first motion studies, focal mechanism solutions, Global Positioning System (GPS) velocities, fault-slip inversion, structural analysis, paleomagnetics and refined relative plate motions such as NUVEL-1A (DeMets et al., 1994). The same is true of oblique divergent zones such as the Walker Lane, Nevada (Oldow, 2003; Unruh et. al., 2003) and the Reykjanes Peninsula, Iceland (Hreinsdottir et. al. 2001; Clifton & Kattenhorn, 2006).

One of the most distinctive features of deformation in oblique zones is the difference in orientation between the incremental strain and the finite strain, a predicted consequence of a non-coaxial strain component (Ramsay, 1967; Fossen & Tikoff, 1993; Teyssier & Tikoff, 1994; Jiang & Williams, 1998). Understanding the relationship between the incremental and finite strain directions is essential to the interpretation and

reconstruction of obliquely deforming zones because a common measurement in active tectonics is the velocity field, an orientation that will generally not be parallel to the strain field. Strain directions in ancient obliquely deformed zones should generally not be taken as the orientation of the palaeo-velocity within the deforming zone unless, for example, the manifestation of strain is strictly coaxial and/or strongly controlled by a crustal anisotropy.

Investigations that explore the link between velocity and strain include the work of Tikoff and Fossen (Fossen & Tikoff, 1993; Tikoff & Fossen, 1995), who employed tensor analysis to yield an incremental strain orientation and the McCoss (1986) construction that estimates the incremental strain orientation from inter-plate motion. This paper employs the graphical strain construction of De Paor (De Paor, 1981; Simpson & De Paor, 1993), which is well suited for linking velocity fields and strain fields in active tectonics because it provides a visual solution for finite and incremental strain that (1) captures the deviation from parallelism between the orientation of strain and the orientation of the velocity field, (2) the solution is translated back into the spatial reference frame of the geodetic data and (3) it captures the behavior of rotational strain (Murphy et al., 2006).

2. Construction modified for active tectonics

The De Paor construction (De Paor, 1981; Simpson & De Paor, 1993) was designed for the analysis of rotated porphyroclasts and passive material lines in ductile shear zones. Set in a polar coordinate reference system, the radius and polar angle of a line corresponds to the stretch and rotation, respectively, of a passive material line (Fig.

2.1). The circumference of a circle is created by the locus of points that describe the stretch and rotation of any line in any orientation (Simpson & De Paor, 1993). This plot can produce the orientation and value of the eigenvector(s), final and initial orientation of passive markers, maximum and minimum shear strain, two dimensional kinematic vorticity and the finite rotation of passive material lines.

Two integral pieces of data are needed to apply the graphical construction to tectonic problems: (1) The displacement rate components and orientation of the GPS velocity and/or NUVEL-1A plate motion (DeMets et al., 1994) to compute the velocity component parallel to the boundary, which captures the rotational strain and (2) the width of the deforming zone. In inter-plate regimes the width usually refers to the continental plate because exposure of the oceanic plate can be limited to Island Arcs. If partitioning has occurred within an arc, then the width of the transpressional terrane (Ave Lallemant & Oldow, 2000) defined by arc parallel strike-slip faults could be used to define the boundary. Additional data that aid in the construction are first motion and fault plane solutions, which give incremental strain directions that provide a powerful check on the graphical solution. Additionally, earthquake foci can delineate active fault planes, structural analysis gives the progressive superposition history and fault slip inversion techniques can give both the incremental strain axes and the vorticity provided the data are discriminating enough (e.g. Unruh et. al., 2003).

Certain assumptions must be made in order to apply this modified construction: (1) deformation across the zone is distributed, or can be generalized as a domain within a heterogeneous or partitioned system (Thatcher, 1995; Horsman & Tikoff, 2005), (2) non-coaxial strain is restricted to a horizontal section where the vorticity is perpendicular to

this plane and parallel to one axis of the finite strain ellipsoid and (3) elastic strain accumulation recorded within the velocity field cannot be resolved from permanent deformation.

Analyzing a kinematic cartoon allows a brief walkthrough of the method before analyzing real world tectonic settings. In a three-plate problem (Fig. 2.2) where plate A remains stationary relative to plate B, which is moving obliquely away from plate A at 23 mm/yr, the angle between the boundary and the plate motion vector is 30^0. Decomposing the plate motion vector yields a boundary parallel velocity of 20 mm/yr and a boundary normal velocity of 11.5 mm/yr with a 16 km wide deforming zone. The horizontal and vertical axes are scaled to the width of the zone.

The velocity field must be integrated over a period of time consistent with the available geologic data. For example, if the strain solutions from the graphical construction were to be compared with earthquake focal mechanism solutions then the velocity would need to be integrated over the earthquake recurrence interval within the deforming zone. The integrated velocity gives the distance that the Anchor Point is translated (Fig. 2.3 A.). One million years was chosen in this example, so the Anchor Point is moved 11.5 km perpendicular to the boundary and 20 km parallel to the boundary (Fig. 2.3 A.) from the height on the reference axis corresponding to the width of the deforming zone (Fig. 2.3 A.). Lines are drawn through the Anchor Point both in both the orientation of the velocity and parallel to zone boundary (Fig. 2.3 B.). This method uses the motion vector of plate B as the orientation of the oblique stable orientation of flow (Weijermars & Poliakov, 1991).

Three points are created: (1) The Anchor Point, (2) the intercept on the reference axis created by a line drawn from the Anchor Point to the reference axis in the orientation of the velocity field and (3) where a line drawn from the Anchor Point, parallel to the kinematic boundary, intersects the reference axis (Fig. 2.3 B.). A circle can be constructed passing through these three points (Fig. 2.3 C.). A line drawn from the origin through the center of the circle will produce two intercepts on the circumference of the circle, these are the points S_1 (greatest stretch) and S_2 (least stretch) (Fig. 2.3 C.).

Lines drawn from these two points back through the Anchor Point will produce the orientation of the principal strain axes with respect to the kinematic boundaries of the zone. Because the Anchor Point inverts the solution, the line drawn from S_2 through the Anchor Point yields the orientation of the long axis of the finite strain ellipse (Fig. 2.3 D.). The orientation of the principal strain axes can be plotted on the kinematic model. In this example, the long axis of strain is predicted to be 55^0 from the kinematic boundary and 25^0 from the velocity direction (Fig. 2.3 D).

3. Aleutian Arc, Alaska

The Aleutian Arc represents the tectonic boundary where the Pacific plate is subducting beneath the North American plate along an arcuate subduction zone. The affect of this boundary condition is a variation in the components of coaxial and non-coaxial strain along strike (Ave Lallemant & Oldow, 2000). The available data for the Aleutian Arc (Fig. 2.4) includes NUVEL-1A (De Mets et al., 1994) plate motion, GPS velocity vectors reported by Ave Lallemant & Oldow (2000) from 1996, 1998, 1999 and 2000 site occupations, extensive seismicity from the subduction slab (Apel et al. 2002)

and structural analysis (Avé Lallemant, 1996). Using parallel sided, linear segments from the discritized Aleutian Arc of Apel et al. (2002), the width of the deforming zone can be measured orthogonal to arc strike from the subduction trench and the northernmost boundary.

The graphical solution is integrated over a period of time consistent with the interseismic cycle in the Aleutian Arc, ninety years (Taber et al. 1991) because the P axis orientation reported by Apel et al. (2002) can be compared to the predicted strain orientation (Fig. 2.5). The strain solutions from the graphical construction are plotted along arc strike and compared to the orientation of the mean P axes (Fig. 2.6). The deviation between the predicted orientation of strain and the plate motion is small in the east and increases towards the west. The De Paor method places the long axis of strain 33^0, 30^0, 20^0 and 14^0 anticlockwise from the boundary at stations MRDR, SHEM, WHAL and AIRP, respectively. The solutions obtained using the method of Tikoff & Fossen (1995) yield estimates of 34^0, 29^0, 18^0 and 15^0 for each station from west to east, respectively.

Forward modeling is possible with the De Paor method. For example, if the graphical solution was integrated over a much longer period of time, one million years for example, the angle between the principal strain axes and the southern boundary of the arc for stations MRDR, SHEM, WHAL and AIRP are 26^0, 23^0, 18^0 and 14^0 respectively. The million year solutions for MRDR and SHEM are more clockwise than the previous estimates (Fig. 2.5). The solutions found after integrating over the interseismic cycle are within error of the incremental solutions from the method of Tikoff & Fossen (1995). However, integrating over a period of time more than four orders of magnitude larger

results in a finite solution that reflects the affect of the increased non-coaxial strain component in the western arc.

3.2 Central Walker Lane, Nevada

The central Walker Lane, Nevada acts to accommodate transform displacement at the boundary between the Pacific and North American plates, the northwesterly translation of the Sierra Nevada block and the actively extending central Great Basin (Unruh et al., 2003; Oldow, 2003). The Proterozoic through Cenozoic structural architecture within the central Walker Lane is strongly anisotropic (Oldow et. al., 1989; Oldow, 2003). Strain trajectories record the effect of this anisotropy, showing a counter clockwise rotation and deviation from the velocity direction as the Sierra Nevada is approached from the east (Fig. 2.7). This deviation is attributed to spatial partitioning of the regional strain field into domains of coaxially dominated oblique divergence directly east of the Sierra Nevada and non-coaxially dominated oblique divergence directly west of the central Great Basin (Oldow, 2003). The earthquake recurrence interval for a magnitude ≥ 7.0 is approximately 10,000 years, which is taken as the time scale to integrate the graphical solution.

The residual GPS velocity of the extension dominated domain was determined by subtracting the average GPS velocity of the wrench dominated domain from the average GPS velocity of the Sierra Nevada. The residual velocity is approximately 54^0 from the eastern kinematic boundary. The residual GPS velocity can be decomposed into its boundary parallel and perpendicular components, 5.7 mm/yr and 8 mm/yr respectively. The width of this domain is approximately 60km (Fig. 2.8).

Using this data, the elongation direction is predicted to be 71^0 anticlockwise from the eastern boundary, which is also 17^0 anticlockwise of the residual GPS velocity Fig. 2.9). This predicted elongation orientation can be compared to the orientation reported by Oldow (2003) that was constructed using fault slip inversion and earthquake focal mechanism solutions by plotting the solution on the map of the Walker Lane (Fig. 2.10). The orientation of elongation predicted using the method of Tikoff & Fossen (1995) is 73^0. The difference between the two solutions is less than the inherent error in the geologic data.

3.3 Reykjanes Peninsula, Iceland

The 16km wide Reykjanes Ridge in southwestern Iceland acts as a linkage in the Mid Atlantic Spreading Center (Clifton & Schlische, 2003). Plate motion on the Reykjanes Ridge has a predicted angle of 30^0 to the rift axis according to the NUVEL-1A model (DeMets et al., 1994) indicating sinistral oblique divergence with 8.5 mm/yr extension and 16.8 mm/yr of rift parallel shear (Fig. 2.11). Analyses of active deformation carried out using GPS velocities (Hreinsdottir et. al., 2001) only reported a boundary parallel velocity of 16.8mm/yr and no extensional component. This observation has been attributed to contemporaneous spatial and temporal partitioning of both the velocity and strain (Clifton & Kattenhorn, 2006).

Analogue clay modeling carried out by Clifton & Schlische (2003) addressed the effect of varying angles of divergent plate motion and produced fractures that are similar in structural style to those described on the Reykjanes Peninsula. From this modeling, Clifton & Schlische (2003) suggest the maximum extension direction is 59^0 from the rift

trend. If the available plate divergence velocity and geometry of the Reykjanes Ridge are used as inputs into the graphical construction, the orientation of the maximum direction of extension is predicted to be 60^0 from the rift trend (Fig. 2.11), which is also consistent with the prediction using the method of Tikoff & Fossen (1995). These estimates cannot take into account the spatial and temporal partitioning of strain that has been suggested by Clifton & Kattenhorn (2006) but agree with analogue modeling of the Reykjanes Ridge.

4. Rotation

If the orientation of a structure relative to the shear zone boundary, that can be idealized as passive and material, is known then a predicted amount of finite rotation can be determined for different states of strain (Fig. 2.12) following the steps outlined in Simpson & De Paor (1993) (Fig. 2.13). Modeling the rotation of passive material lines allows the angular relationship between rotating passive material lines and the orientation of finite strain to be evaluated. The rotation rate of the finite strain ellipse can be compared with the rate of rotation of different structures in different orientations so long as they can be idealized as passive and material. One possible end member of this behavior is a passive material line, where the rotation would be dictated by the vorticity and the orientation of the line (Ramsay, 1967). Another possibility is where a material line creates such an anisotropy in the deforming rock that the strain is controlled by that structure. The behavior of these active material lines (Watkinson, 1983; Markley & Tikoff, 2002) cannot be evaluated using this method, however plays an important role in the manifestation of strain within deforming rocks.

5. Discussion

The graphical construction of De Paor (De Paor, 1987; Simpson & De Paor, 1993) can be used to predict the orientation of the principal strain axes from a velocity field within a deforming zone. The strain orientation obtained using data from the Walker Lane, Aleutian Arc and Reykjanes Peninsula are consistent with published, independently determined orientations of strain and with the analytical method of Tikoff & Fossen (1995) for incremental strains.

In cases where a deforming zone is undergoing simultaneous simple and pure shear strains, there will be a difference in orientation between the observed structural expressions, joints, earthquakes, folds etc. and the orientation of the finite strain ellipse (Ellis & Watkinson, 1987). Furthermore, the incremental strain axes parallel the finite strain axes if the deformation is strictly coaxial, symmetrically orthorhombic. Contemporaneous coaxial and non-coaxial strain is a common style of deformation, suggesting the incremental strain directions should generally not coincide with the finite strain directions. The orientation of the velocity field should generally not be parallel to the strain direction in zones with a component of non-coaxial strain.

The graphical method of De Paor can be used to compare the finite rotation of passive material lines to the rotational behavior of the principal strain axes. This relationship is different for obliquely divergent and convergent zones. In oblique convergence, the coaxial component and non-coaxial component of deformation both act to cause rotation of passive material lines and the principal axes of strain toward the shear zone boundary. The effect of this can be seen in the solutions obtained for the Aleutian

Arc GPS stations MRDR and SHEM that were integrated over one million years. These plots predict an elongation direction closer to the kinematic boundary than the solutions obtained from integrating over the interseismic cycle. The stations in the east, WHAL and AIRP, are coaxially dominated while the stations in the west, MRDR and SHEM, are dominated by non-coaxial strain. The effect of the additional non-coaxial strain component in the west could be the rapid rotation of the principal strain axes. In oblique divergence, the rotation of passive material lines and the principal strain axes are slowed by the coaxial extension. This behavior results in rapid rotational strains in obliquely convergent environments compared to oblique divergence. The extension dominated domain of the Walker Lane is an example of this behavior, where the principal strain axes are predicted to rotate less than five degrees over three million years (Fig. 2.11).

6. Conclusions

A difference in orientation between the principal strain axes and the velocity direction in actively deforming tectonic zones agrees with the understanding of non-coaxial strain in simple shear, transtension and transpression. This deviation has direct implications on reconstructing the kinematics of ancient deformed zones. The graphical method of De Paor is a tool capable of relating the velocity field to the orientation of strain in active tectonics. This graphical construction is ideal because it provides a visualization of the relationship between velocity and strain that reflects the rotational effect of non-coaxial strain in a spatially referenced framework.

Because the velocity direction measured with geodesy is not predicted to coincide with the strain direction in a deforming zone with a component of non-coaxial strain, the

orientation of strain measured in ancient deformed zones cannot be used as the palaeo-velocity direction within that zone. Kinematic reconstructions that use a velocity direction that is parallel to the strain direction within an obliquely deforming zone may not take into account the relationship between the finite and incremental strain directions unless the control of a strong anisotropy can be documented.

11. Acknowledgements

This research was partially supported by National Science Foundation grants (EAR xxxxxxx and EAR xxxxxx) to J.S. Oldow.

12. References

Avé Lallemant, H.G., 1996. Displacement partitioning and arc parallel extension in the Aleutian volcanic island arc. Tectonophysics. 256, 279-293.

Avé Lallemant, H.G., Oldow, J.S., 2000. Active displacement partitioning and arc-parallel extension of the Aleutian volcanic arc based on Global Positioning System geodesy and kinematic analysis. Geology 28, 739-742.

Atwater, T., 1970. Implications of plate tectonics for the Cenozoic tectonic evolution of western North America. Geological Society of America bulletin. Vol 81, No. 12, 3513-3535.

Bobyarchick, A.R., 1986. The eigenvalues of steady flow in Mohr space. Tectonophysics Vol. 122, 35-51.

Clifton, A.E., Schlische, R.W., 2003. Fracture populations on the Reykjanes Peninsula, Iceland: comparison with experimental clay models of oblique rifting. Journal of Geophysical Research. 108.

Clifton, A.E., Kattenhorn, S., 2006. Structural architecture of a highly oblique divergent plate boundary segment. *Tectonophysics*. Vol. 419, 27-40.

Cashman, S.M., Kelsey, H.M., Erdman, C.F., Cutten, H.N.C., Berryman, K.R., 1992. Strain Partitioning between structural domains in the forearc of the Hikurangi subduction zone, New Zealand. Tectonics. 11, 242-257.

DeMets, C., Gordon, R. G., Argus, D. F., Stein, S. 1994. Effect of recent revisions to the geomagnetic reversal time scale on estimates of current plate motions. Geophysical Research Letterrs. Vol. 21, 2191–2194.

De Paor, D.G. 1981. Strain analysis using deformed line distributions. Tectonophysics 73: T9-T14

Ellis, M., Watkinson, A.J., 1987. Orogen parallel extension and oblique tectonics: The relation between stretching lineations and relative plate motions. Geology, Vol. 15, 1022-1026.

Fitch, T. J., 1972. Plate convergence, transcurrent faults and internal deformation adjacent to South-East Asia and the western Pacific. Journal of Geophysical Research. 77, 4432-4460.

Fossen, H., Tikoff, B., 1993. The deformation matrix for simultaneous simple shearing, pure shearing and volume change, and its application to transpression-transtension tectonics. Journal of Structural Geology 15, 413-422.

Fournier, M. & Petit, C., 2007. Oblique rifting at oceanic ridges: Relationship between spreading and stretching directions from earthquake focal mechanisms. Journal of Structural Geology 29, 201-208.

Horsman, E., Tikoff, B., 2005. Quantifying simultaneous discrete and distributed deformation. Journal of Structural Geology Vol. 27, p. 1168-1169.

Hreinsdottir, S., Einarsson, P., 2001. Crustal deformation at the oblique spreading Reykjanes Peninsula, SW Iceland: GPS measurements from 1993 to 1998. Journal of Geophysical Research, Vol. 106, No. B7. 13,803-13,916.

Jiang, D., Williams, P.F., 1998. High-strain zones: a unified model. Journal of Structural Geology. Vol. 20, No. 8, 1105-1120.

Markley, M.J., Tikoff, B., 2002. Matchsticks on parade: Vertical axis rotation in oblique divergence. Journal of Geophysical Research. Vol 107, No. B12, 2349.

McCoss, A.M. 1986. Simple constructions for deformation in transpression/ transtension zones. Journal of Structural Geology, 8, 715-718.

Miller, M.M., Johnson, D.J., Dixon, T., Dokka, R.K., 2001. Refined kinematics of the Eastern California shear zone from GPS observations, 1993-1998. Journal of Geophysical Research. 106, 2245-2264.

Murphy, J. J., Watkinson, A. J., Oldow, J. S., 2006. Graphical method that relates displacement fields and strain for the kinematic analysis of deforming tectonic zones: examples from the Walker Lane, western Great Basin and the Aleutian Island Arc, Alaska. Geological Society of America Abstracts with Programs. Vol. 38 No 7, p. 132.

Oldow, J.S., 2003. Active transtensional boundary zone between the western Great Basin and Sierra Nevada block, western U.S. Cordillera. Geology. 31, 1033–1036.

Oldow, J.S., Bally, A.W., Ave Lallemant, H.G., and Leeman, W.P., 1989, Phanerozoic evolution of the North American Cordillera (United States and Canada), in Bally, A.W., and Palmer, A.R., eds., The geology of North America: An overview: Boulder, Colorado, Geological Society of America, Geology of North America, Vol. A, 139–232.

Ramberg, H., 1975. Particle paths, displacement and progressive strain applicable to rocks. Tectonophysics Vol. 28, 1-37.

Ramsay, J. G., 1967. Folding and Fracturing of Rock. McGraw Hill, New York.

Simpson, C., De Paor, D.G., 1993. Deformation and Kinematics of High Strain Zones. Journal of Structural Geology. 15, 1-20.

Spence, W., 1977, The Aleutian arc: Tectonic blocks, episodic subduction, strain diffusion, and magma generation. Journal of Geophysical Research. 82, 213-230.

Taber, J.J., Billington, S., Engdahl, E.R., 1991. Seismicity of the Aleutian arc, in Slemmons, D.B., Engdahl, E.R., Zoback, M.D., Blackwell, D.D., eds., Neotectonics of North America. Boulder, Colorado, Geological Society of Amercia, Decade Map. 1, 29-46.

Teyssier, C., Tikoff, B., 1994. Strain modeling of displacement-field partitioning in transpressional orogens. Journal of Structural Geology. 16, 1575–1588.

Thatcher, W., 1995. Microplate versus continuum descriptions of active tectonic deformation. *J. Geophys. Res., 100,* 3885-3994.

Tikoff, B., Fossen, H., 1995. Limitations of three-dimensional kinematic vorticity analyses. Journal of Structural Geology Vol. 17, 1771-1784.

Twiss, R.J., Unruh, J.R., 1998. Analysis of fault slip inversions: Do they constrain stress or strain rate? Journal of Geophysical Research Vol. 103, No. B6. 12,205-12,222.

Unruh, J., Humphrey, J., Barron, A., 2003. Transtensional model for the Sierra Nevada frontal fault system, eastern California. Geology. 31, 327-330.

Watkinson, A.J., 1983. Patterns of folding and strain influenced by linearly anisotropic bands. Journal of structural geology. Vol. 5, No. 3-4, 449-454.

Walcott, R.I., 1978, Geodetic strains and large earthquakes in the axial tectonic belt of North Island, New Zealand. Journal Geophysical Research. 83, 4419-4469.

Weijermars, R., Poliakov, A., 1991. Stream functions and complex potentials: implications for development of rock fabric and the continuum assumption. *Tectonophysics*. Vol. 220, 33-50.

Figure 2.1. The graphical method of De Paor is based on a polar coordinate strain Mohr circle where the Mohr circle is created by the locus of points that describe the stretch and rotation of all orientations of passive material lines. Solutions obtained within Strain Space are translated through the Anchor Point into Geographical Space. The Reference Axis and Baseline Axis are scaled to the width of the deforming zone, the Reference Axis is perpendicular to the zone boundaries. Adapted from Simpson & De Paor (1993).

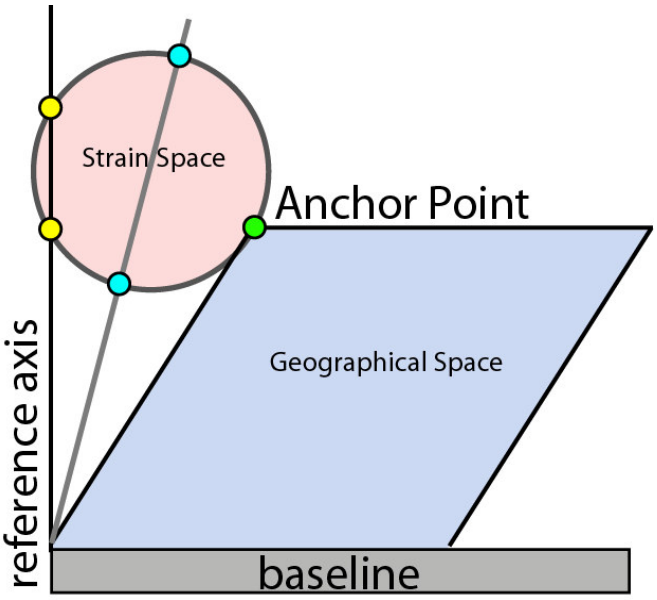

Figure 2.2. Three plate problem: plate B is fixed relative to plate A which is moving obliquely away from plate B. Deformation is accommodated within the deforming zone (white), which is 16 km wide. The graphical construction uses the width of the deforming zone (white), the angle between the plate motion vector of plate A and the boundary, 30^0, and the rate components of the plate motion vector.

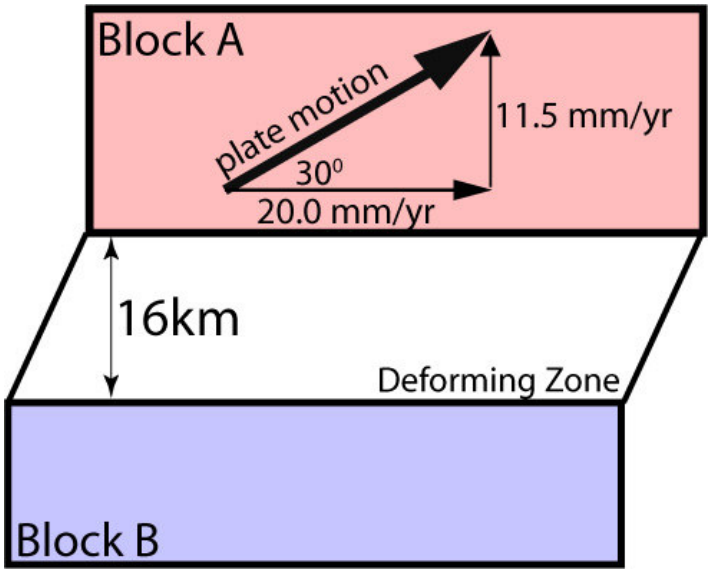

Fig. 2.3. Stepwise construction of the graphical method. (A) The reference axis (vertical) and baseline (horizontal) are scaled to the width of the deforming zone being analysed. The Anchor Point (yellow dot) is translated in the direction of the velocity field an amount equal to the velocity integrated over an amount of time consistent with the geologic data. In this example the Anchor Point is translated 11.5 km perpendicular and 20 km parallel to the zone, rates integrated over one million years. (B) A line is drawn in the orientation of the velocity field (blue arrow) and parallel to the zone, which creates three points. (C) The Mohr circle is constructed to pass through these three points (yellow dots). A line drawn from the origin through the center of the circle creates two intercepts, S_1 (upper intercept) and S_2 (lower intercept), which corresponding to the greatest stretch (S_1) and least stretch (S_2). (D) A line drawn from S_2 through the Anchor Point gives the orientation of the long axis of the strain ellipse. Note the solutions are inverted through the Anchor Point.

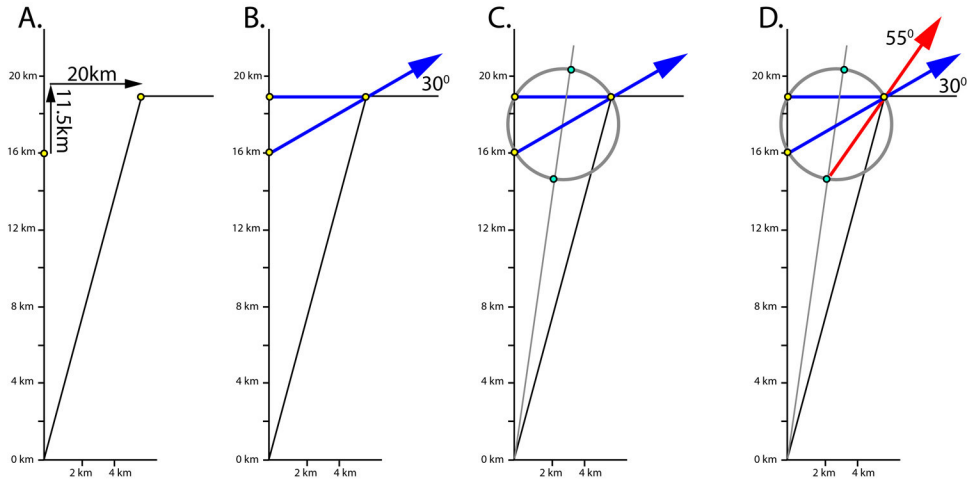

Figure 2.4. Diagram showing the Aleutian Arc discritized into the parallel segments of Apel et al. (2002). Pacific plate velocities are NUVEL-1A (De Mets et al., 1994). P axes compiled from seismicity within the interface between the subducting Pacific Plate and the North American plate by Apel et al. (2002). The blue bars correspond to the range of orientations represented by the mean P axis orientations. Variation from head on collision in the west to nearly parallel sliding in the east results in the characteristic refraction of the earthquake P axes from parallelism with the Pacific Plate motion.

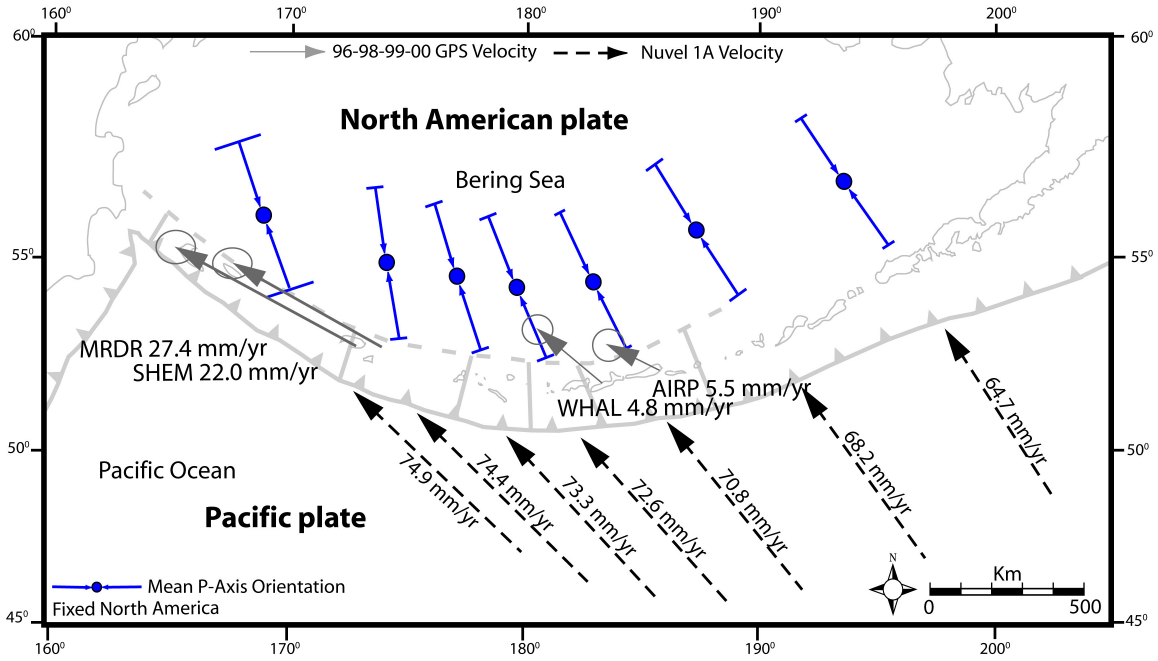

Figure 2.5. Completed plots for the GPS stations AIRP, WHAL, SHEM and MRDR, Aleutian Arc, Alaska: integrated over one million years (above) and one hundred thousand years (below). Grey arrows correspond to the plate motion vector of the Pacific Plate and dashed arrows give the predicted orientation of the maximum extension direction. Both the vertical and horizontal axes are scaled to the width of the deforming zone.

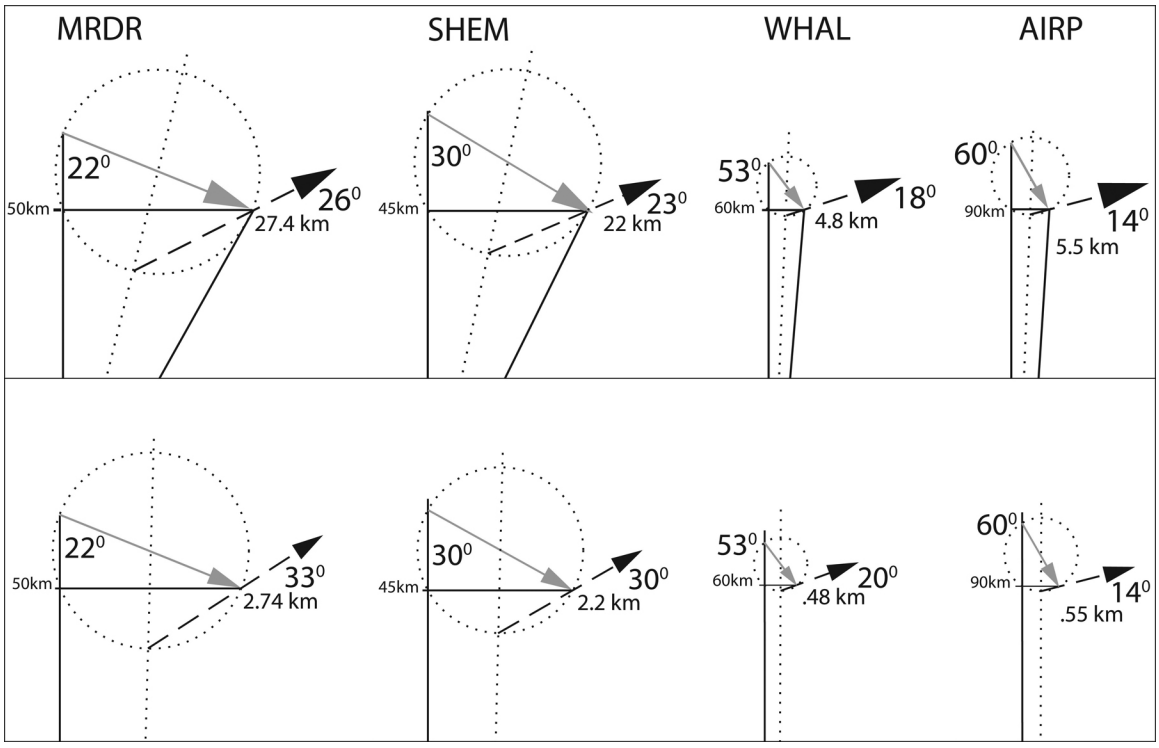

Figure 2.6. Orientation of the principal strain axes determined using the graphical method of De Paor (Simpson & De Paor, 1993) compared to the orientation of mean earthquake P-axes. Adapted from Apel et. al. (2002).

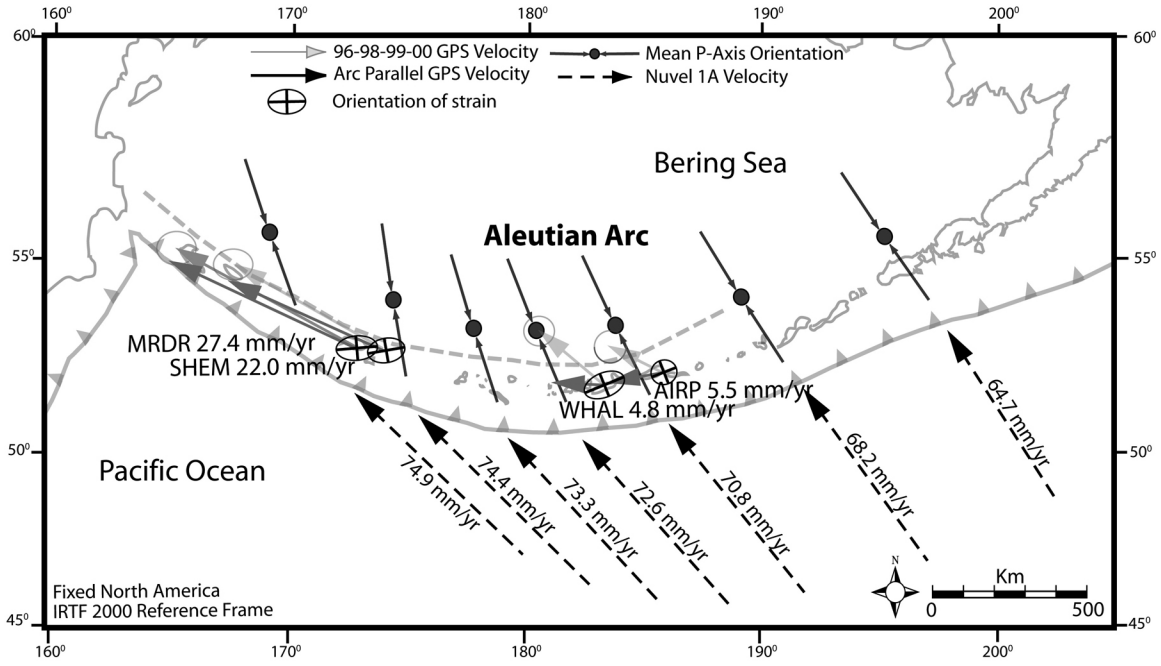

Figure 2.7. Strain trajectories from earthquake focal mechanism solutions and fault slip inversion (white lines) with velocity trajectories from GPS geodesy (red lines) in the Central Walker Lane, Nevada. After Oldow (2003).

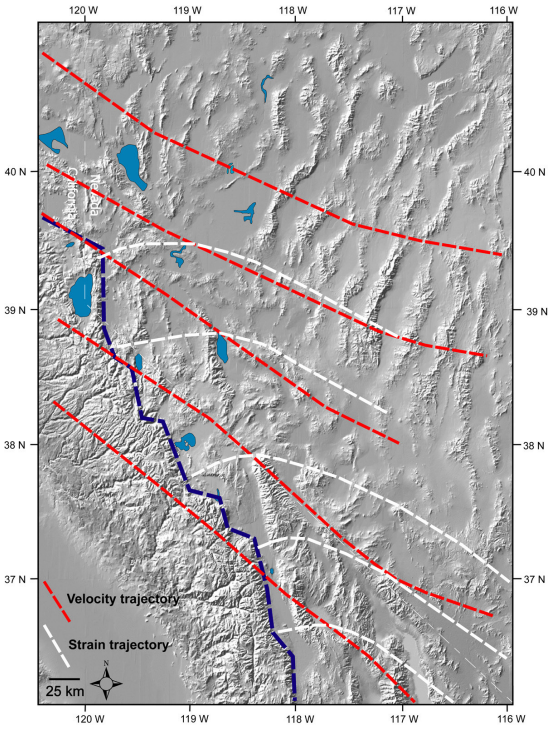

Figure 2.8. Differential velocity and strain domains within the Central Walker Lane, Nevada. Adapted from Oldow (2003).

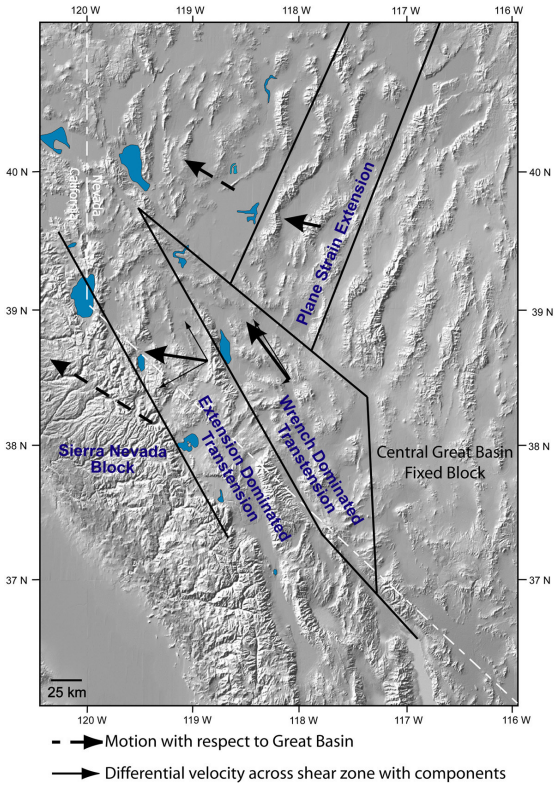

Figure 2.9. Enlarged view of the completed graphical construction for the extension (A) and wrench (B) dominated domains in the central Walker Lane (Oldow, 2003). Solid arrow is the residual GPS velocity and dashed arrow is the predicted maximum direction of elongation. The axes represent increasing distance from the deforming zone boundary.

A.

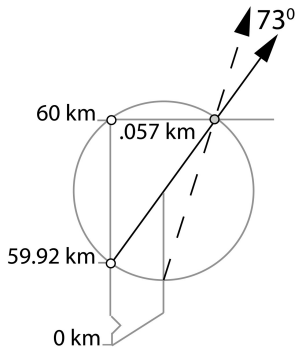

B.

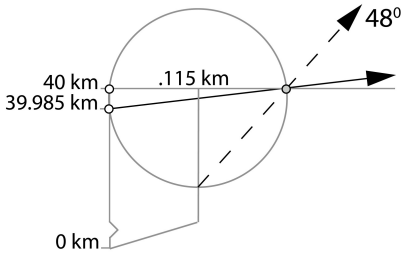

Figure 2.10. Predicted orientation of the principal axes of finite strain within the extension dominated domain of the Walker Lane, Nevada. Adapted from Oldow (2003).

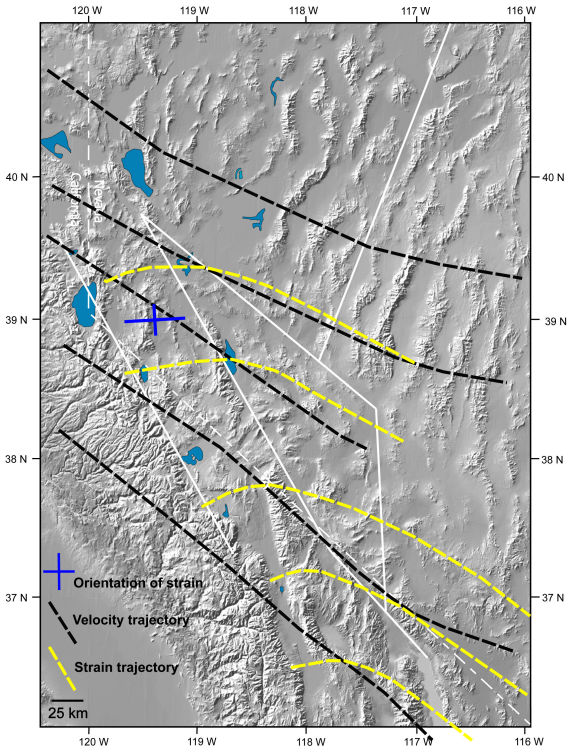

Figure 2.11. Geologic cartoon of the tectonic setting of the Reykjanes Peninsula, Iceland with the completed graphical construction. Adapted from Clifton & Schlische (2003).

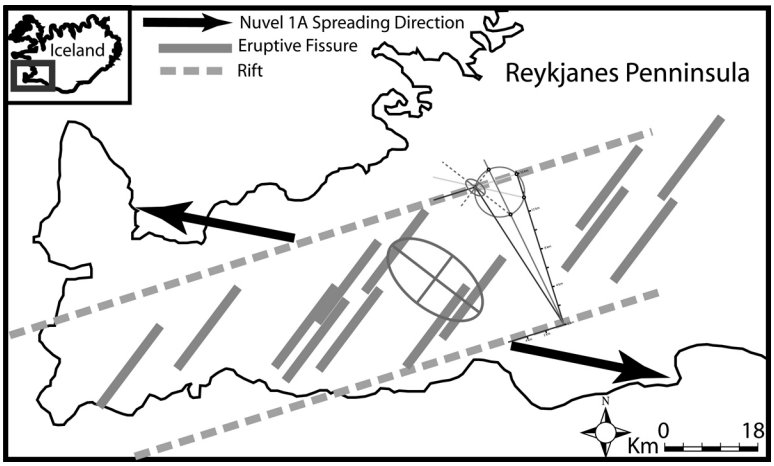

Figure 2.12. Rotation of the principal axes of strain in the extension dominated domain of the Central Walker Lane, Nevada for 1 (71^0), 2 ($<70^0$) and 3 (68^0) million years.

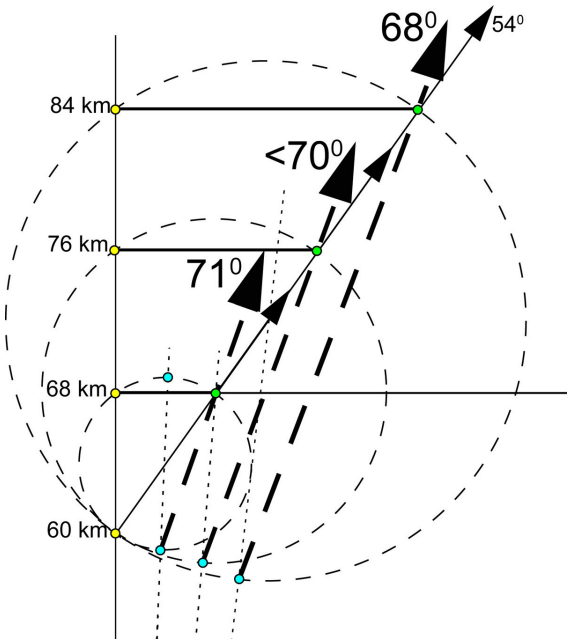

Figure 2.13. Construction for the finite rotation of passive material lines in a deforming zone. Adapted from Simpson & De Paor (1993).

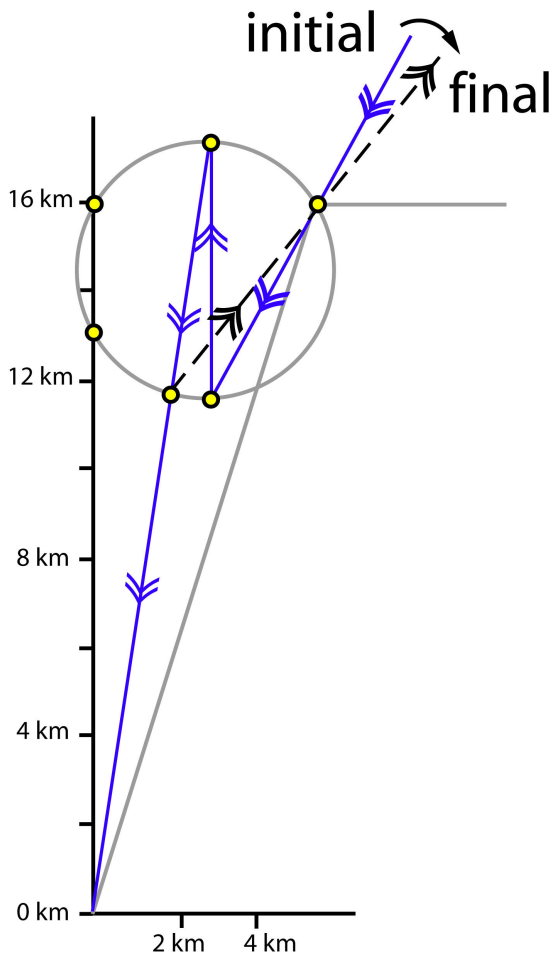

The kinematics of spatially partitioned transtension within the central Walker Lane, western Great Basin, western USA derived using a graphical method that links GPS velocity fields to the orientation of strain

Justin J. Murphy[1*], A. John Watkinson[1], John S. Oldow[2]

[1] Department of Geology, Washington State University, Pullman Washington, 99163

[2] Department of Geological Sciences, University of Idaho, Moscow, Idaho, 83844

*murphywsu@hotmail.com

Abstract

Deviation between velocity trajectories from GPS networks and strain trajectories from earthquake focal mechanisms and fault-slip inversion within the central Walker Lane are reconciled as the consequence of non-plane strain (constriction) within a transtensional zone separating the Sierra Nevada and central Great Basin. Dextral transtension within the central Walker Lane is produced by differential displacement of the Sierra Nevada away from the central Great Basin and is partitioned into domains exhibiting simple and pure shear dominated strain. From east to west across the central Walker Lane, velocities increase from 3 to 12-14 mm/yr. Along the same transect, the incremental elongation axis changes from west-northwest to west-southwest. The strain and velocity trajectories across the boundary zone deviate by 50^0 as the Sierra Nevada is approached from the east. This deviation in strain and velocity trajectories is consistent with theoretical models linking kinematic vorticity, particle velocity paths, and

incremental non-plane strain during transtensional deformation. The relation of strain to velocity fields requires analytical or numerical solutions for rigorous comparison. We use a 2D Mohr circle graphical solution for the rapid calculation and visualization of physical relations between velocity and strain. This construction is based on the stretch and rotation of passive lines and is well suited for tectonic-scale analysis providing a graphical link between surface velocities and the strain orientation. With input of the deformation zone(s) geometry and velocity field, the incremental strain orientation is calculated. Forward and inverse strain modeling is possible by integrating the graphical construction over different time intervals.

INTRODUCTION

The first-order correspondence between geodetic and tectonic displacement fields across plate boundaries (DeMets et al., 1994) is in good agreement with modeled velocity and strain-rate fields based on geologic, geodetic, and seismological observations in diffuse deformation zones such as the western US Cordillera (Shen-Tu et al., 1998, 1999; Holt et al., 2000; Thatcher, 2003). The general correspondence between strain and velocity field trajectories observed over large expanses of the US Cordillera reflects both the scale of observation and at least to some degree the general simplicity of the deformation field.

As the spatial resolution of Global Positioning System (GPS) networks has improved over the years, however, discrepancies between velocity field trajectories and active strain fields have become apparent, at least locally (Oldow, 2003; Unruh et al., 2003). In the discrete tectonic domain of the boundary zone between the Sierra Nevada

and central Great Basin (Fig. 3.1A.), non-plane strain deformation (Fig. 3.1B.) arising from the interaction of regional displacement fields and crustal anisotropy results in a deviation between the trajectories of the regional velocity field and strain field by as much as 50° (Fig. 3.1C.) (Oldow, 2003).

Based on the regional distribution of normal and strike-slip faults (Oldow, 1992) and the deviation between velocity and strain trajectories, an active transtensional deformation within the Walker Lane was interpreted by Oldow (2003) (Fig. 3.1C). The domain east of the Sierra Nevada is dominated by coaxial transtension while the domain farther to the east but west of the Great Basin is dominated by non-coaxial transtension (Fig. 3.1B) (Oldow, 2003). Although the observations are consistent with theoretical considerations, the transtensional source of the deviation between strain and velocity trajectories was not documented analytically.

A better understanding of the kinematics within actively deforming zones can be gained if displacement fields are related to the strain that is recorded in the earth's crust. This relationship has been explored analytically for incremental strains (McCoss, 1986; Withjack and Jamison, 1986; Wojtal, 1989; Jamison, 1991; Tron and Brun, 1991; Fossen and Tikoff, 1993; Horsman & Tikoff, 2005). In this paper, we expand on these earlier works by presenting a graphical tool, based on the polar coordinate Mohr circle for strain of De Paor (De Paor, 1981; Simpson and De Paor, 1993) to compare strain and velocity directly. The benefit of this graphical approach is that it can rapidly, even in the field, provide (1) a visual link between the GPS velocity and the strain, (2) solutions that are spatially referenced, (3) reflect both incremental and finite strains and (3) captures rotation from a non-coaxial strain component.

Based on the application of the graphical tool, the deviation between strain and velocity fields in the central Walker Lane is demonstrated to be the product of transtensional deformation. Differentiation between the plane and non-plane conditions of transtension cannot be resolved with the graphical construction, but the case for non-plane transtension is made based on regional strain compatibility.

GEOLOGIC SETTING

The northern part of the Eastern California Shear Zone (Dokka and Travis, 1990) and the central Walker Lane (Locke et al., 1940; Stewart, 1988; Oldow, 1992) form a narrow boundary zone that accommodates differential motion between the northwesterly migrating Sierra Nevada block and the central Great Basin (Fig. 3.1A). The physiographic expression reflects the structural style within the deforming zone.

The internal structure of the boundary zone is complex. In the region east of the southern Sierra Nevada, the Eastern California Shear Zone is underlain by the north-northwest trending Owens Valley and Panamint fault systems and the northwest trending Furnace Creek transcurrent fault system (Fig. 3.1A). The transcurrent faults are linked by a system of northeast trending extensional structures (Burchfiel et al., 1987, 1992) that together form a belt that narrows from 125 km in the south to about 75 km at the latitude of the central Sierra Nevada. Here, the deformation belt broadens to about 175 km along a system of east-northeast trending transtensional faults forming a structural stepover between the Owens Valley and Furnace Creek fault systems and northwest-trending transcurrent faults of the central Walker Lane (Oldow, 1992, 2003; Wesnousky, 2005).

Differential displacement across the boundary zone is accommodated on a complex array of normal and strike-slip faults (Stewart, 1988; Oldow, 1992) that are seismically active with normal and strike-slip focal mechanisms (Ryall and Priestly, 1975; Rogers et al., 1991). The earthquake recurrence interval constructed by Rogers & Harmsen (1991) is 10,000 years. GPS velocities increase from east to west across the boundary zone from 2-3 mm/yr in the central Great Basin to 12-14 mm/yr in the Sierra Nevada and are accompanied by a systematic clockwise change in orientation from west-northwest to northwest (Thatcher et al., 1999; Bennett et al., 1999, 2003; Dixon et al., 1995, 2000; Miller et al., 2001; Oldow et al., 2001; Oldow, 2003; Hammond and Thatcher, 2004). The orientation of incremental strain axes determined from fault slip inversion and earthquake focal mechanisms also vary systematically across the central Walker Lane (Oldow, 2003). The transitional zone between the central Great Basin and the central Walker Lane is marked by a change in the orientation of elongation from ~305° to ~280° and farther west the elongation axis changes from ~280° to ~255° as the Sierra Nevada is approached from the east (Oldow, 2003).

Comparison of the GPS velocity trajectories and strain trajectories (Fig. 3.1B) demonstrate an east to west deviation from parallelism toward the Sierra Nevada by as much as 50°. Major physiographic and strain boundaries within the central Walker Lane are defined using structures that are long-lived (Oldow et al., 1994) and the orientation of strain rate obtained using fault slip inversion is in agreement with strain rate directions from seismicity. This suggests the state of strain is also long lived and because the seismicity captures the strain rate that is over a similar time scale as the GPS velocities,

the deviation between velocity and strain rate observed in the central Walker Lane (Oldow, 2003) is presumably long lived and cannot be attributed to a transient effect.

The combination of active translation and pre-Tertiary crustal anisotropy results in a state of dextral transtension within the central Walker Lane. One character of transtension is that the elongation direction is not parallel to the velocity within the deforming zone (Tikoff & Fossen, 1995). The graphical construction produces an orientation of strain that agrees with the independently determined strain trajectories of Oldow (2003) from the velocity trajectories and so documents the effect of transtensional strain within the Walker Lane.

DISPLACEMENT AND STRAIN

When an object, such as a rock, consisting of a finite number of particles is moved through a reference frame, each particle will create a trace that records its path from an initial to a final position. The direction and length of these traces with respect to the reference frame give vectors describing the displacement of each particle. If this object moves along a straight line then each particle path vector will be parallel and the same length. Because each particle has moved the same amount, and in the same direction, the geometric properties of the object remain unchanged. This type of motion is considered a body translation (Ghosh & Ramberg, 1976; Ramsay and Huber, 1987). If one side of the object moves faster than the other, and volume is conserved, a velocity gradient will result in a strain, a change in length or angle from an original state (Ramsay, 1967).

If the previously described transformation was imposed on a square grid, strain could be recorded as changes in line lengths and angles. The grid is initially composed of squares geometrically identical to each other. Following a homogeneous deformation, every square will be deformed into identical parallelograms. If the displacement vectors had differed in orientation and magnitude, heterogeneous strain (Ramsay, 1967), the squares would no longer be identical everywhere. An exception to this case is rigid body rotation, where rotation about a single point results in vectors of different orientation and magnitude but the geometric properties of the object remain unchanged. If all particle motion is contained within a single plane then it is referred to as plane strain, while particle motion that cannot be fully described by a planar section is considered non-plane strain.

Pure shear and simple shear are end member forms of general shear deformation (Ramsay, 1967; Simpson & De Paor, 1993) with open ended particle paths. Directions of elongation and shortening that remain in a constant orientation during deformation characterize pure shear. Simple shear is distinctly different from pure shear because the orientations of elongation and shortening rotate with increasing strain. In pure shear, an orthogonal set of lines parallel to the instantaneous strain axes will remain in this orientation throughout the deformation. Pure shear is considered coaxial because the principal axes of finite strain will remain parallel to the instantaneous strain axes. During simple shear, the same orthogonal set of lines parallel to the instantaneous strain axes would rotate out of parallelism and orthogonality. Simple shear is non-coaxial because the finite strain axes will immediately rotate out of parallelism with the instantaneous strain axes during progressive deformation (Ramsay, 1967).

Only lines parallel to the shear zone boundary do not change their angular position during simple shear. Other passively rotating lines will asymptotically approach this orientation. In the case of 2D general shear, a second orientation is also stable. The orientation of this second stable direction with respect to the shear zone boundary is a function of the relative components of pure and simple shear, or more specifically, the vorticity (Fossen and Tikoff, 1993).

Particle displacement paths within a deforming body can create curved traces (Ghosh & Ramberg, 1976; Weijermars & Poliakov, 1991; Tikoff & Fossen, 1999) except for those in stable orientations, which record motion that is either directly toward, away or fixed with respect to the origin (Tikoff & Fossen, 1995). These linear traces are called eigenvectors, which represent a stable orientation throughout the deformational history. The eigenvectors within a velocity gradient field are known as the flow apophyses (Means et al., 1980; Bobyarchick, 1986; Fossen and Tikoff, 1993). In simple shear, there is only one flow apophysis and in the case of general shear there can be as many as three (Tikoff & Fossen, 1995).

An understanding of the relationship between particle displacement paths in different strain regimes can provide insight into the link between displacement fields and strain fields. Describing this relationship typically requires the use of quantitative tensor techniques, however can also be explored with the graphical method of De Paor (see appendix) (De Paor, 1981; De Paor, 1987; Simpson and De Paor, 1993), as used here for the analysis of deforming tectonic zones.

ANALYSIS OF THE CENTRAL WALKER LANE

Certain assumptions must be made in order to apply this modified construction: (1) deformation across the zone is distributed, or can be generalized as a domain within a heterogeneous or partitioned system (Thatcher, 1995; Horsman & Tikoff, 2005), (2) non-coaxial strain is restricted to a horizontal section where the vorticity is perpendicular to this plane and parallel to one axis of the finite strain ellipsoid and (3) elastic strain accumulation recorded within the velocity field cannot be resolved from permanent deformation.

The extension dominated domain adjacent to and east of the Sierra Nevada (Fig. 3.1C) is a good candidate for the graphical construction because it has approximately parallel boundaries striking ~ 332^0 with GPS velocities that record a marked deviation between displacement and strain trajectories (Fig. 3.1B). Residual velocities for each domain were constructed by (1) visually determining a best fit velocity within each domain (Fig. 3.2A) and (2) subtracting the relative velocity of the neighboring domains. The residual GPS velocity in the extension dominated domain trends ~ 276^0 and was determined by subtracting the average GPS velocity of the wrench dominated domain to the east from the average GPS velocity of the domain to the west (Fig. 3.2B). Decomposing the residual velocity into its boundary parallel and perpendicular components yields rates of 5.7 mm/yr and 8 mm/yr, respectively (Fig. 3.2B). The width of this domain, measured orthogonal to its boundary, is approximately 60 km. The seismic recurrence interval of 10,000 years determined by Rogers et al. (1991) is the period of time that the graphical construction is integrated for both the extension and wrench domains. This time period was chosen so the strain solution time scale matches the time scale of geologic strain data. The elongation direction is predicted to trend

approximately 73^0 (θ) anti-clockwise from the kinematic boundary, which is 16^0 more clockwise than the relative GPS velocity (Fig. 3.3A).

The wrench dominated domain to the east can be analyzed in a similar way. The width of the deforming zone is taken as the distance between the boundary with the extension dominated domain to the easternmost strike slip fault within the wrench dominated domain. The boundaries of this zone strike ~332^0 and the relative GPS velocity trends ~324^0 (Fig. 3.1C). Because the residual GPS velocity is nearly parallel to the boundary, this domain is predominantly dextral simple shear with a small component of pure shear elongation (i.e. wrench dominated transtension). The boundary parallel and perpendicular components are 11.4 mm/yr and 1.5 mm/yr respectively (Fig. 3.2B). The width is approximately 40 km. The maximum elongation direction is predicted to trend approximately 48^0 anti-clockwise from the kinematic boundary, which is 40^0 more anti-clockwise from the residual GPS velocity (Fig. 3.3B).

If these solutions are plotted on the map of the central Walker Lane (Fig. 3.4), they are consistent with the independently determined strain trajectories from first motion studies and fault slip inversion described by Oldow (2003). The θ values predicted by the graphical solution also agree with the analytical solutions obtained using the method of Tikoff and Fossen (1995) for strain, which predicted the maximum elongation direction in the extensional domain and the wrench dominated domain to be 73^0 and 50^0 from the kinematic boundary of each zone respectively.

DISCUSSION

When deforming zones undergo contemporaneous coaxial and non-coaxial strains, structures in non-stable orientations will rotate over time with rates that vary as a function of both their orientation and the relative components of coaxial and non-coaxial strain (Ramsay, 1967; Tikoff and Fossen, 1995). The rotation of passive markers is dictated by the rotation and ellipticity of the finite strain ellipse. Active markers may rotate at some different amount that is a function of either the relative competence contrast between the marker and the country rock or the degree of anisotropy created by the structure.

To investigate the rotation of the principal strain axes over time, we graphically solved the orientation in one million year increments (Fig. 3.5). The rotation of the finite strain ellipse within the extension dominated domain is slow (Fig. 3.5A) (Simpson & De Paor, 1997). The coaxial component of transtension appears to counteract the rotation resulting from the non-coaxial strain component. It would follow that the rotation of the finite strain ellipse was much faster in the wrench dominated domain (Fig. 3.5B) because the coaxial component is much smaller than the non-coaxial component, which causes the finite strain ellipse to rotate at a rate close, but not equal, to that of simple shear.

The orientations of strain obtained using the graphical method agree well with the strain trajectories derived from fault slip inversion and earthquake focal mechanism solutions (Oldow, 2003) within the central Walker Lane. Furthermore, the predicted strain orientation is consistent with results obtained using existing analytical solutions (e.g. Fossen and Tikoff, 1993; Tikoff & Fossen, 1995). However, the graphical method cannot distinguish between types of regional strain (i.e., plane strain, transtension, flattening plus shear, constriction plus shear or any combination ± a volume change).

Because 3D strain is generally non-unique (i.e. Tikoff and Fossen, 1995), the orientation of 2D strain can be reproduced by any deforming zone so long as the average velocity was in the same orientation and magnitude. We will look at what implications the two possible end-member states of strain, plane versus non-plane, have on the strain compatibility and physiography within the central Walker Lane. Velocities within each domain are integrated over 10^6 years to model strain compatibility over a time scale comparable to the inferred life of the strain field discussed above.

1. State of strain

Possible end-members are (1) the non-plane transtensional model (Sanderson and Marchini,1984; Fossen and Tikoff, 1993) and (2) plane strain, broadening sub simple (Simpson and De Paor, 1993) shear zones (referred to here as the plane strain model). The non-plane strain model has boundary conditions where the length of the shear zone boundary remains fixed. The plane strain boundary condition allows the shear zone boundary to shorten or elongate (Fig. 3.6). Vertical displacement components have to be estimated because data is currently unavailable, which could provide regional constraints.

The extension dominated zone is generalized as a deforming zone 500 km in length and 60 km in width. The thickness of the crust is taken as the depth to the Mohorovicic discontinuity, 32 km (Mooney and Braile, 1989). GPS velocity components are 8.0 mm/yr and 5.7 mm/yr perpendicular and parallel to the zone boundaries respectively. The eastern, wrench dominated domain has dimensions of approximately 500 km in length, 40 km in width and 30 km in thickness with displacement rate

components perpendicular and parallel to the deforming zone of 1.5 mm/yr and 11.4 mm/yr respectively.

Non-plane transtension (e.g. Sanderson and Marchini, 1984; Tikoff and Teyssier, 1994; Dewey, 1998) is characterized by a fixed shear zone boundary length and the movement of material in and out of the horizontal section. Strain components in this model consist of a non-coaxial strain in the horizontal plane and a vertically oriented coaxial shortening with an accompanying orthogonal coaxial elongation across the deforming zone (Fig. 3.7). The deforming zone progressively thins in order to accommodate elongation across its width but no change in the length of the shear zone boundary occurs. With these boundary conditions, transtensional deformation within the central Walker Lane would result in vertical shortening, no change in the north-northwesterly boundary length and west - northwesterly elongation. Using this data, the amount of vertical shortening and horizontal elongation can be computed, along with the shear strain and vorticity.

In the extension dominated domain, one million years worth of deformation in a non-plane transtensional setting would result in a change in domain width from 60 km to 68 km while thinning from 30 km to 27 km (Fig. 3.7). The geometry of the wrench dominated domain would change from 40 km wide to 41.5 km while thinning from 30 km to 28.9 km (Fig. 3.7). This model begins one million years ago, and assumes that volume is conserved.

The fundamental difference in the plane strain model is the changing length of the shear zone boundary. This results in elongation across the width of the zone and shortening along the boundary, with no change in the vertical thickness. Beginning with

the same dimensions and displacements described above, the width of the western boundary would lengthen from 60 km to 68 km as before. However, instead of vertically thinning, the length of the domain would shorten from 500 km to 437.5 km to accommodate the orthogonal stretch. Similarly, the eastern domain will lengthen from 40 km to 41.5 km across its width and shorten along its length from 500 km to just less than 499 km. The thickness of both domains remains constant throughout this deformation (Fig. 3.7).

The relative contributions from the non-coaxial and coaxial components to the overall strain can be expressed in terms of the vorticity number. This can be calculated using the value and orientation of the GPS rate components and the equation for the internal kinematic vorticity (Tikoff and Fossen, 1995).

The equation for elongation (Ramsay, 1967) gives the values of e_1, e_2 and e_3, the maximum, intermediate and minimum elongation respectively. Where l_1 is the current dimension of the deforming zone and l_0 the original.

$$e = \frac{l_1 - l_0}{l_0} \tag{1}$$

The principal values of stretch, S_1, S_2 and S_3 can be found by substituting the values of elongation determined from equation 1 into the equation for stretch.

$$S_n = 1 + e_n \tag{2}$$

The angular shear, Ψ, can be found by constructing a right triangle where the short side is equal to the time integrated parallel displacement and the intermediate side is equal to the length of the zone.

$$\gamma = \tan(\Psi) \tag{3}$$

The values of S_n and θ can be substituted into equation 4 to determine the internal kinematic vorticity (Tikoff and Fossen, 1995).

$$W k_i = \frac{\sqrt{(\gamma_{xy})^2 + (\gamma_{yz})^2 + (\gamma_{xz})^2}}{\sqrt{2\left[\ln(k_1)^2 + \ln(k_2)^2 + \ln(k_3)^2\right] + (\gamma_{xz})^2}} \qquad (4)$$

The calculated vorticity of the extension dominated domain is .379 in the non-plane transtension model and .352 using the plane strain model. In the wrench dominated domain, the calculated vorticity for the non-plane strain model is 0.966, while the plane strain model is 0.984. Both of these values indicate simple shear dominated transtension, near end member simple shear (Tikoff and Fossen, 1995). The graph of vorticity vs. Instantaneous Stretching Axis (ISA) orientation, Fig. 3.7 in Tikoff and Fossen (1995), predicts a θ of 71^0 using the non-plane strain model. This agrees with the θ value predicted from the graphical construction.

Some possible reasons why the non-plane transtension (Sanderson and Marchini, 1984) boundary conditions are the most likely option and the horizontal plane strain (e.g. broadening plane strain sub simple shear zones of Simpson and De Paor, 1993) case the less likely option are as follows:

(1) Plane strain would result in differential shortening across each domain within the Walker Lane to accommodate the spatial strain partitioning (Oldow, 2003). This would require a different finite length of each domain, and subsequently a different space accommodation around each domain.

(2) Geophysical data suggests a change in the depth to the base of the crust within the central Walker Lane. The depth shallows westerly from a maximum of 33 km toward the east, to 30 km near the Sierra Nevada (Mooney and Braile, 1989; Kaban and Mooney,

2001). This would be compatible in a non-plane strain setting because a wrench dominated domain would require very little vertical thinning to accommodate the small amount of horizontal stretch whereas an extension dominated zone would have to thin considerably more in order to supply material for the larger horizontal elongation. A difference in thickness could be accommodated by flow at depth or a contrast in crustal thinning within each domain.

(3) The consequences of the previous observation can be seen in the physiography within the central Walker Lane. Ranges developed within the wrench dominated domain are more subdued than ranges in the extension dominated domain. This observation could have resulted from greater extension and thus greater structural relief from normal faulting in the extensional domain compared to the wrench dominated domain. Strain could have been accommodated along strike slip faults in the wrench dominated domain.

(4) Having no strain parallel to the boundaries, as in the non-plane transtensional model, is an extremely compatible arrangement that ensures continuity across zones of different displacements and strains. Without this, domains would have shortened differentially along their lengths creating space problems.

(5) Flow lines created by particle velocity traces in non-plane transtension appear straight in map view, which qualitatively agrees with the morphology of the velocity field across the central Walker Lane (Tikoff & Fossen, 1998).

There may well be some intermediate configuration between the two end members, or indeed some other combination of general 3D strain and/or volume change (Robin & Cruden, 1994). However, to determine the actual type of strain would require reliable data including 3D strain markers, strain history and/or vertical GPS data.

CONCLUSIONS

Velocity trajectories and strain trajectories deviate from parallelism within the central Walker Lane by as much as 50^0 toward the eastern side of the Sierra Nevada. This deviation has been attributed to spatial strain partitioning into domains of non-coaxial and coaxially dominated transtension (Oldow, 2003). A better understanding of the kinematics within these zones can be gained if the GPS velocity field is related to the strain field. This relationship can be analyzed using a graphical solution (Simpson and De Paor, 1993) that estimates the orientation of the principal strain axes.

In the case of the central Walker Lane, the solutions of the graphical method agree with both the strain trajectories determined independently (Oldow, 2003) and solutions obtained from existing analytical tools (Fossen & Tikoff, 1993; Tikoff & Fossen, 1995). Together these tools illustrate that GPS velocities and strain trajectories should generally not be parallel within deforming zones that contain a non-coaxial strain component. Furthermore, structures behaving as passive material lines will rotate toward the oblique flow apophysis with increasing transtensional displacement.

The implications of different boundary conditions within the central Walker Lane suggest a state of strain characterized by non-plane strain transtension. A state of strain near this end member case would account for the westerly thinning of the crust towards the extension dominated domain, the contrast in the physiography and maintain strain compatibility across domains that have experienced differing strain amounts.

ACKNOWLEDGMENTS

The authors thank Declan De Paor and Basil Tikoff for reviewing this manuscript and inspirational research into the intricacies of vorticity and strain. This research was partially supported by National Science Foundation grants (EAR xxxxxxx and EAR xxxxxx) to J.S. Oldow.

REFERENCES

Bennett, R.A., Davis, J.L., and Wernicke, B.P., 1999. Present-day pattern of Cordillera deformation in the western United States. Geology, Vol. 27, p. 371–374.

Bobyarchick, A.R., 1986. The eigenvalues of steady flow in Mohr space. Tectonophysics Vol. 122, p. 35-51.

Burchfiel, B.C., Cowan, D.S., and Davis, G.A., 1992. Tectonic overview of the Cordilleran orogen in the western United States, *in* Burchfiel, B.C., et al., eds., The Cordilleran orogen: Conterminous U.S. Boulder, Colorado, Geological Society of America, Geology of North America, Vol. G-3, p. 407–479.

De Paor, D.G. 1981. Strain analysis using deformed line distributions. Tectonophysics 73: T9-T14

De Paor, D.G., 1987. Stretch in shear zones: implications for section balancing. Journal of Structural Geology Vol. 9, p. 893-895.

Dewey, J.F., Holdsworth, R.E., Strachan, R.A, 1998. Transpression and transtension zones. In: Holdsworth, R.E., Strachan, R.A., Dewey, J.F. (Eds.), Continental Transpressional and Transtensional Tectonics. Geological Society Special Publication, 135, pp. 1–14.

Fossen, H., Tikoff, B., 1993. The deformation matrix for simultaneous simple shearing, pure shearing and volume change, and its application to transpression-transtension tectonics. Journal of Structural Geology Vol. 15, p. 413-422.

Fossen, H., Tikoff., B., 1998. Extended models of transpression/transtension and application to tectonic settings. In: Holdsworth, R.E., Strachan, R.A., Dewey, J.F. (Eds.), Continental Transpressional and Transtensional Tectonics, Special Publications 135. Geological Society of London, pp. 15-33.

Fournier, M. & Petit, C., 2007. Oblique rifting at oceanic ridges: Relationship between spreading and stretching directions from earthquake focal mechanisms. Journal of Structural Geology 29, 201-208.

Gosh, S.K., Ramberg, H., 1976. Reorientation of inclusions by combination of pure and simple-shear. Tectonophysics 34, 1-70.

Horsman, E., Tikoff, B., 2005. Quantifying simultaneous discrete and distributed deformation. Journal of Structural Geology Vol. 27, p. 1168-1169.

Holt, W. E., Shen-Tu, B., Haines, A., Jackson, J., 2000. On the Determination of Self-Consistent Strain Rate Fields Within Zones of Distributed Continental Deformation. Geophysical Monograph – American Geophysical Union. Vol. 121, p. 113-142.

Jamison, W.R., 1991. Kinematics of compressional fold development in convergent wrench terranes. Tectonophysics Vol. 190, 209-232.

Kaban, M.K., Mooney, W.D., 2001. Density structure of the lithosphere in the southwestern United States and its tectonic significance. Journal of Geophysical Research. Vol. 106, 721-739.

Locke, A., Billingsley P. R., Mayo, E. B., 1940. Sierra Nevada tectonic patterns. *Geological Society of America Bulletin*. Vol. 51(4), p. 513-539.

McCoss, A.M. 1986. Simple constructions for deformation in transpression/ transtension zones. Journal of Structural Geology, 8, 715-718.

McKenzie, D.P., Jackson, J.A., 1983. The relationship between strain rates, crustal thickening, palaeomagnetism, finite strain and fault movements within a deforming zone. *Earth and Planetary Science Letters*, Vol. 65, 182-202

Means, W. D., Hobbs, B. E., Lister, B. E., Williams, P. F., 1980. Vorticity and non-coaxility in progressive deformations. Journal Structural Geology, Vol. 2, p. 371-378.

Miller, M.M., Johnson, D.J., Dixon, T., and Dokka, R.K., 2001. Refined kinematics of the Eastern California shear zone from GPS observations, 1993–1998. Journal of Geophysical Research. Vol. 106, p. 2245–2264.

Mooney, W. D., and Braile, L. W., 1989. The seismic structure of the continental crust and upper mantle of North America, in The Geology of North America, vol. A, Overview, edited by A. W. Bally and A. R. Palmer, pp. 39– 52, Geol. Soc. of Am., Boulder, Colo., 1989.

Murphy, J. J., Watkinson, A. J., Oldow, J. S., 2006. Graphical method that relates displacement fields and strain for the kinematic analysis of deforming tectonic zones: examples from the Walker Lane, western Great Basin and the Aleutian Island Arc, Alaska. Geological Society of America Abstracts with Programs. Vol. 38 No 7, p. 132.

Oldow, J.S., Bally, A.W., Ave Lallemant, H.G., and Leeman, W.P., 1989. Phanerozoic evolution of the North American Cordillera (United States and Canada), *in* Bally, A.W., and Palmer, A.R., eds., The geology of North America: An overview. Boulder, Colorado, Geological Society of America, Geology of North America, Vol. A, p. 139–232.

Oldow, J.S., 1992. Late Cenozoic displacement partitioning in the northwestern Great Basin, *in* Craig, S.D., ed., Structure, tectonics, and mineralization of the Walker Lane. Walker Lane Symposium Proceedings: Reno, Geological Society of Nevada, p. 17–52.

Oldow, J.S., Aiken, C.L.V., Ferguson, J.F., Hare, J.L., and Hardyman, R.F., 2001. Active displacement transfer and differential motion between tectonic blocks within the central Walker Lane, western Great Basin. Geology. Vol. 29, p. 19–22.

Oldow, J.S., 2003. Active transtensional boundary zone between the western Great Basin and Sierra Nevada block, western U.S. Cordillera. Geology Vol. 31, p. 1033–1036.

Ramsay, J. G., 1967. Folding and Fracturing of Rock. McGraw Hill, New York.

Ramsay, J. G., Huber, M. I., 1987. The techniques of modern structural geology Volume 1: Strain Analysis. Academic Press, London.

Robin, P.F., and Cruden, A.R., 1994. Strain and vorticity patterns in ideally ductile transpression zones. Journal Structural Geology, Vol. 16, p. 447-466.

Rogers, A.M., Harmsen, S.C., Corbett, E.J., Priestly, K., and de Polo, D., 1991, The seismicity of Nevada and some adjacent parts of the Great Basin, *in* Slemmons,

D.B., et al., eds., Neotectonics of North America: Boulder, Colorado, Geological Society of America, Decade Map Volume 1, p. 153–184.

Ryall, A.S., and Priestly, K., 1975. Seismicity, secular strain, and maximum magnitude in the Excelsior Mountains area, western Nevada and eastern California. Geological Society of America Bulletin. Vol. 86, p. 1585–1592.

Sanderson, D. J., Marchini, W. R. D., 1984. Transpression. Journal of Structural Geology. Vol. 6, p. 449-458.

Simpson, C., De Paor, D.G., 1993. Strain and kinematic analysis in general shear zones. Journal of Structural Geology. Vol. 15, p. 1-20.

Simpson, C., De Paor, D.G., 1997. Practical analysis of general shear zones using the porphyroclast hyperbolic distribution method: an example from the Scandinavian Caledonides. In: Sengupta, S. (Ed.), Evolution of Geological Structures in Micro to Macro scales. Chapman & Hall, London. p. 169-184.

Shen-Tu, B., Holt, W. E., Haines, A., 1998. Contemporary kinematics of the western United States determined from earthquake moment tensors, very long baseline interferometry, and GPS observations. Journal of Geophysical Research. Vol. 103 B8, p. 18087-18118.

Shen-Tu, B., Holt, W. E., Haines, A., 1999. Deformation kinematics in the western United States determined from Quaternary fault slip rates and recent geodetic data. Journal of Geophysical Research. Vol. 104 B12, p. 28927-28956.

Stewart, J.H., 1988. Tectonics of the Walker Lane belt, western Great Basin: Mesozoic and Cenozoic deformation in a shear zone, *in* Ernst, W.G., ed., Metamorphism

and crustal evolution of the western United States. Englewood Cliffs, New Jersey, Prentice-Hall, p. 681–713.

Thatcher, W., Foulger, G.R., Julian, B.R., Svarc, J., Quilty, E., and Bawden, G.W., 1999. Present day deformation across the Basin and Range province, western United States. Science, Vol. 283, p. 1714–1718.

Thatcher, W., 2003. GPS Constraints on the Kinematics of Continental Deformation. International Geology Review. Vol. 45, Part 3, p. 191-212.

Tikoff, B., Teyssier, C., 1994. Strain modeling of displacement-field partitioning in transpressional orogens. Journal of Structural Geology. Vol. 16, p. 1575–1588.

Tikoff, B., Fossen, H., 1995. The limitations of three dimensional kinematic vorticity analysis. Journal of Structural Geology. Vol. 17, p. 1771-1784.

Tron, V., Brun, J.-P., 1991. Experiments on oblique rifting in brittle-ductile systems. Tectonophysics Vol. 188, 71-84.

Wesnousky, S. G., Barron, A. D., Briggs, R. W., Caskey, S. J., Kumer, S., Owen, L., 2005. Paleoseismic transect across the northern Great Basin. Journal of Geophysical Research. Vol. 110, 5408.

Withjack, M.O., Jamison, W.R., 1986. Deformation produced byoblique rifting. Tectonophysics. Vol. 126, 99-124.

Wojtal, S., 1989. Measuring displacement gradients and strain in faulted rock. Journal of Structural Geology 11, 669-678.

Figure 3.1. (A) Regional tectonic setting of the western Great Basin. (B) Map of the central Walker Lane, Nevada showing the systematic change in orientation of the strain trajectories (white) and deviation from parallelism with the GPS velocity trajectories (black) toward the Sierra Nevada. (C) Regional transtension is spatially partitioned into strain domains dominated by non-coaxial strain in the east and coaxial strain in the west of the central Walker Lane. All figures after Oldow, 2003.

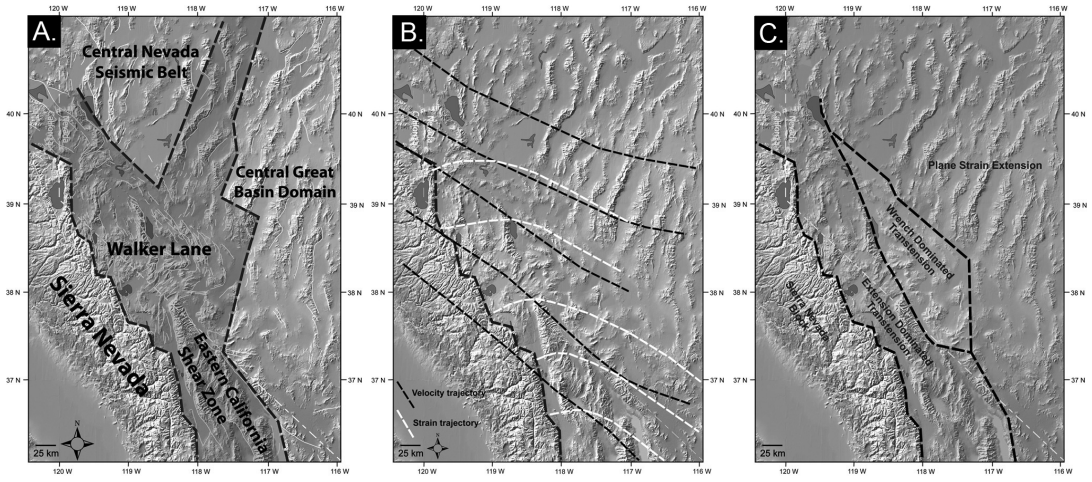

Figure 3.2. (A) Map of the central Walker Lane showing regional GPS velocities (white arrows) with error ellipses (white circles) in a North American reference frame. The black arrows correspond to a visually determined best-fit orientation of the velocity field within each domain. (B) Map of the central Walker Lane showing residual velocity of each domain with components (black arrows). The residual velocity of the wrench dominated domain (right) was determined by differencing the best fit velocity within the wrench dominated domain from the stable central Great Basin. The residual velocity within the extension dominated domain (left) was determined by differencing the best fit velocities of the wrench dominated domain and the motion of the Sierra Nevada. Adapted from Oldow (2003).

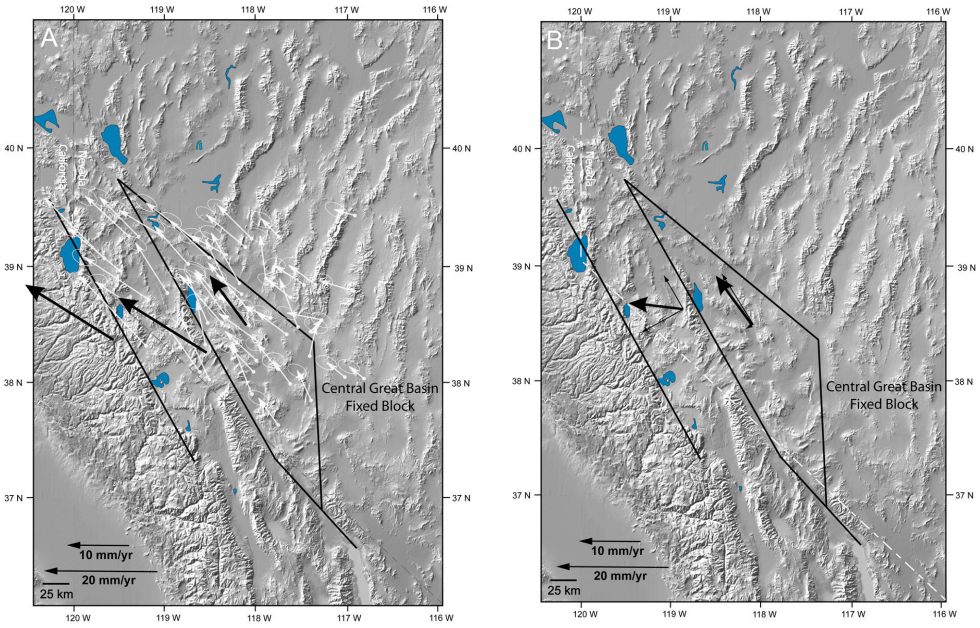

Figure 3.3. (A) Enlarged view of the completed graphical solution for the western, extension dominated domain. (B) Enlarged view of the completed graphical solution for the eastern, wrench dominated domain. Solid grey lines correspond to the vertical reference axis, horizontal baseline, the polar Mohr circle for strain (Simpson & De Paor, 1993) and the line projected from the center of the circle to the origin. The solid arrow corresponds to the orientation of the residual velocity, which is compared to the orientation of elongation shown by the solid black line. The vertical axis represents increasing distance perpendicular to the shear plane while the horizontal axis represents increasing distance parallel.

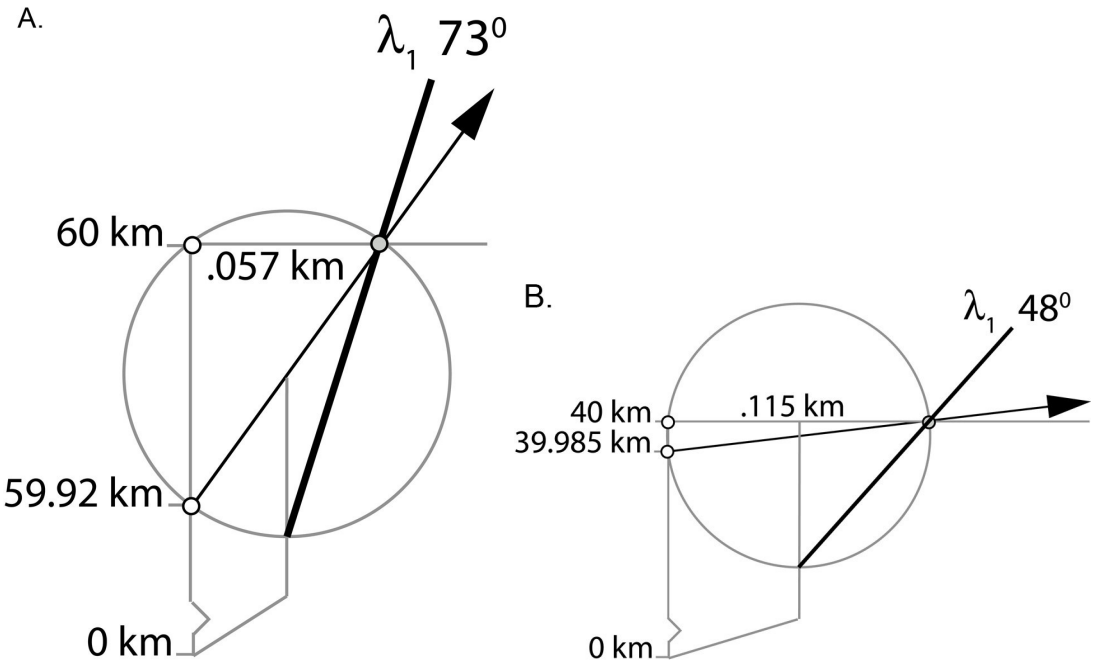

Figure 3.4. Map of the Walker Lane, Nevada showing GPS and strain trajectories with the predicted orientation of finite strain from the graphical method plotted in black. The dimensions of the strain axes do not correspond to the ratio of stretch, they indicate the long and short axes only. (Adapted from Oldow, 2003)

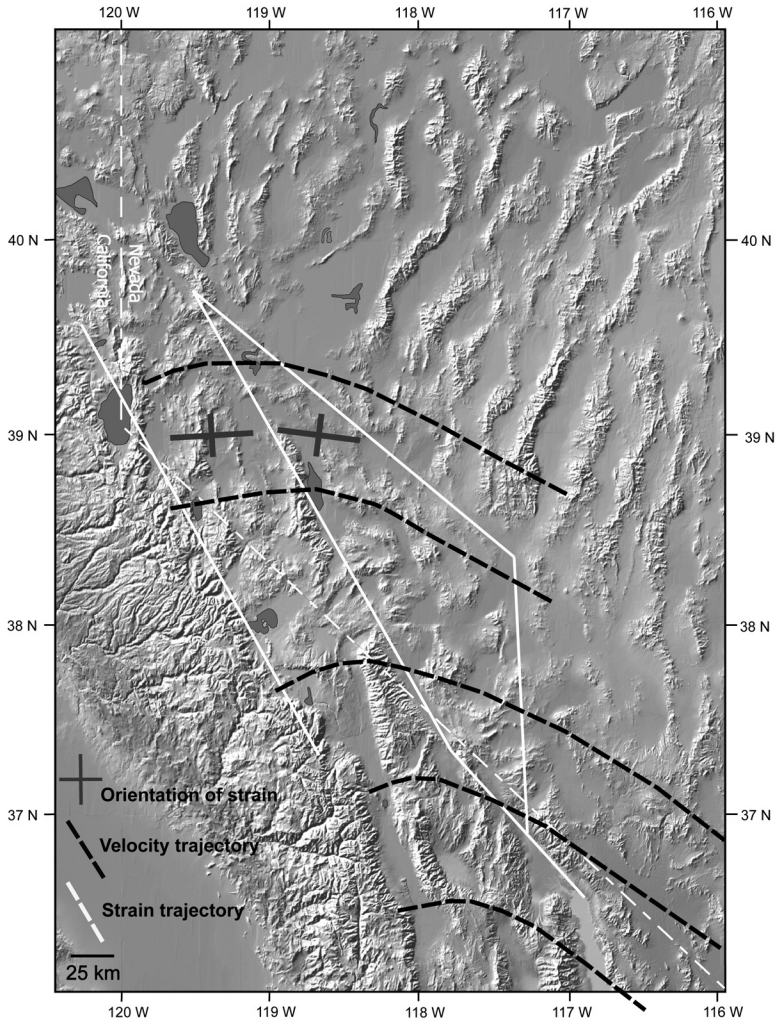

Figure 3.5. Rotation of the maximum elongation direction (solid line) integrated over one, two and three million years for both the wrench (A) and extension (B) dominated domains.

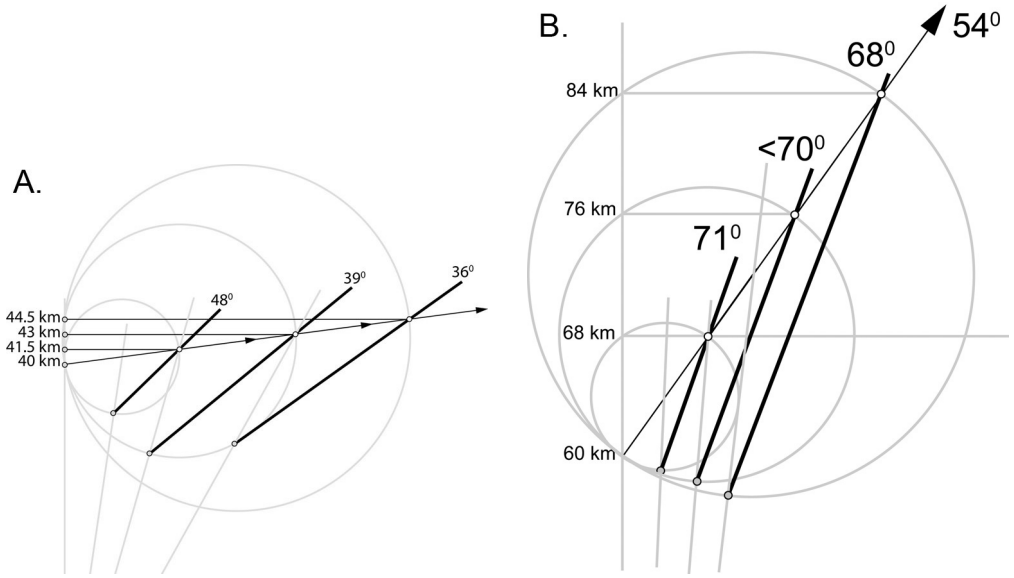

Figure 3.6. Cartoon of two end members of deformation: Non-plane strain transtension (above) has a fixed length shear plane. Material is supplied from the 3rd dimension to accommodate stretching. The length of the shear zone boundary in plane strain (below) changes, the deforming zone narrows to accommodate stretching and no change in thickness occurs. Adapted from Tikoff and Teyssier, (1994).

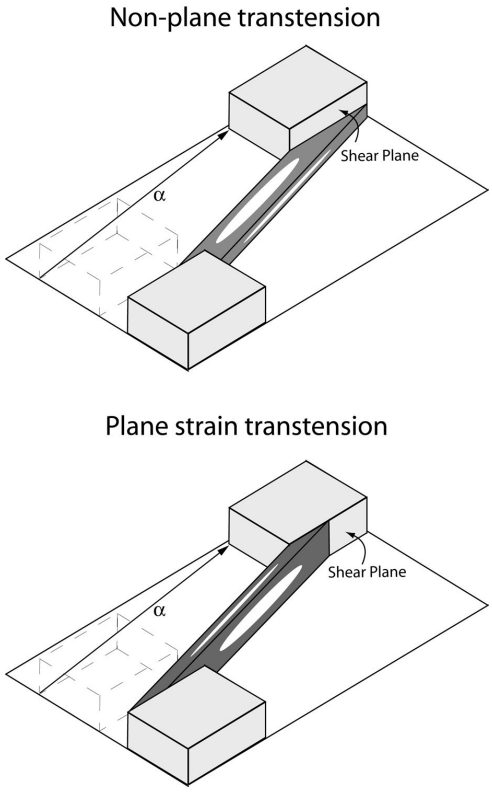

Figure 3.7. Cartoon illustrating the implications of each end member of strain. Non-plane strain (right) results in thinning of the crust while plane strain (left) requires shortening parallel to the length of the zone. The non-plane strain model illustrates a compatible style of deformation that results crustal thinning.

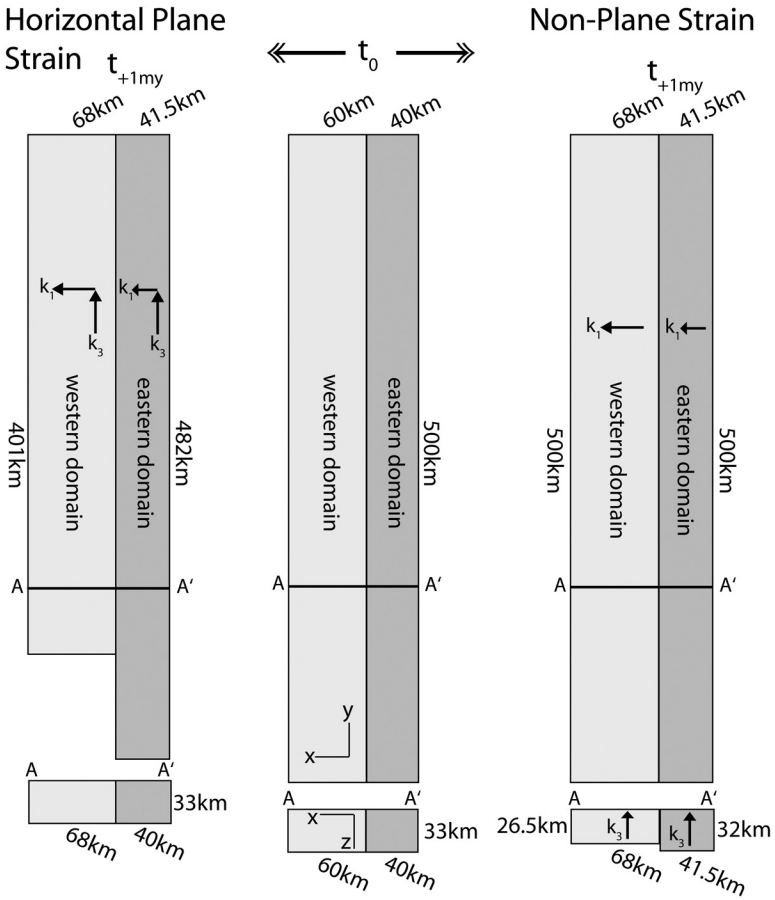

Appendix

The De Paor construction (De Paor, 1981; Simpson & De Paor, 1993) was designed for the analysis of rotated porphyroclasts and passive material lines in ductile shear zones. Set in a polar coordinate reference system, the radius and polar angle of a line corresponds to the stretch and rotation, respectively, of a passive material line (Fig. 3.8). The circumference of a circle is created by the locus of points that describe the stretch and rotation of any line in any orientation (Simpson & De Paor, 1993). This plot can produce the orientation and value of the eigenvector(s), final and initial orientation of passive markers, maximum and minimum shear strain, two dimensional kinematic vorticity and the finite rotation of passive material lines.

Two integral pieces of data are needed to apply the graphical construction to tectonic problems: (1) The displacement rate components and orientation of the GPS velocity and/or NUVEL-1A plate motion (DeMets et al., 1994) to compute the velocity component parallel to the boundary, which captures the rotational strain and (2) the width of the deforming zone. In inter-plate regimes the width usually refers to the continental plate because exposure of the oceanic plate can be limited to Island Arcs. If partitioning has occurred within an arc, then the width of the transpressional terrane (Ave Lallemant & Oldow, 2000) defined by arc parallel strike-slip faults could be used to define the boundary. Additional data that aid in the construction are first motion and fault plane solutions, which give incremental strain directions that provide a powerful check on the graphical solution. Additionally, earthquake foci can delineate active fault planes, structural analysis gives the progressive superposition history and fault slip inversion

techniques can give both the incremental strain axes and the vorticity provided the data are discriminating enough (e.g. Unruh et. al., 2003).

Certain assumptions must be made in order to apply this modified construction: (1) deformation across the zone is distributed, or can be generalized as a domain within a heterogeneous or partitioned system (Thatcher, 1995; Horsman & Tikoff, 2005), (2) non-coaxial strain is restricted to a horizontal section where the vorticity is perpendicular to this plane and parallel to one axis of the finite strain ellipsoid and (3) elastic strain accumulation recorded within the velocity field cannot be resolved from permanent deformation.

Analyzing a kinematic cartoon allows a brief walkthrough of the method before analyzing real world tectonic settings. In a three-plate problem (Fig. 3.9) where plate A remains stationary relative to plate B, which is moving obliquely away from plate A at 23 mm/yr, the angle between the boundary and the plate motion vector is 30^0. Decomposing the plate motion vector yields a boundary parallel velocity of 20 mm/yr and a boundary normal velocity of 11.5 mm/yr with a 16 km wide deforming zone. The horizontal and vertical axes are scaled to the width of the zone.

The velocity field must be integrated over a period of time consistent with the available geologic data. For example, if the strain solutions from the graphical construction were to be compared with earthquake focal mechanism solutions then the velocity would need to be integrated over the earthquake recurrence interval within the deforming zone. The integrated velocity gives the distance that the Anchor Point is translated (Fig. 3.10A.). One million years was chosen in this example, so the Anchor Point is moved 11.5 km perpendicular to the boundary and 20 km parallel to the

boundary (Fig. 3.10A.) from the height on the reference axis corresponding to the width of the deforming zone (Fig. 3.10A.). Lines are drawn through the Anchor Point both in both the orientation of the velocity and parallel to zone boundary (Fig. 3.10B.). This method uses the motion vector of plate B as the orientation of the oblique stable orientation of flow (Weijermars & Poliakov, 1991).

Three points are created: (1) The Anchor Point, (2) the intercept on the reference axis created by a line drawn from the Anchor Point to the reference axis in the orientation of the velocity field and (3) where a line drawn from the Anchor Point, parallel to the kinematic boundary, intersects the reference axis (Fig. 3.10B.). A circle can be constructed passing through these three points (Fig. 3.10C.). A line drawn from the origin through the center of the circle will produce two intercepts on the circumference of the circle, these are the points S_1 (greatest stretch) and S_2 (least stretch) (Fig. 3.10C.).

Lines drawn from these two points back through the Anchor Point will produce the orientation of the principal strain axes with respect to the kinematic boundaries of the zone. Because the Anchor Point inverts the solution, the line drawn from S_2 through the Anchor Point yields the orientation of the long axis of the finite strain ellipse (Fig. 3.10D.). The orientation of the principal strain axes can be plotted on the kinematic model. In this example, the long axis of strain is predicted to be 55^0 from the kinematic boundary and 25^0 from the velocity direction (Fig. 3.10D).

Figure 3.8. The graphical method of De Paor is based on a polar coordinate strain Mohr circle where the Mohr circle is created by the locus of points that describe the stretch and rotation of all orientations of passive material lines. Solutions obtained within Strain Space are translated through the Anchor Point into Geographical Space. The Reference Axis and Baseline Axis are scaled to the width of the deforming zone, the Reference Axis is perpendicular to the zone boundaries. Adapted from Simpson & De Paor (1993).

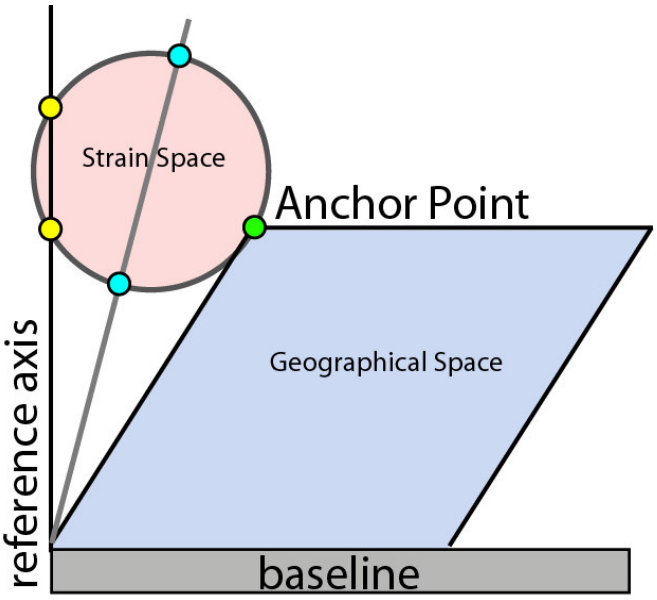

Figure 3.9. Three plate problem: plate B is fixed relative to plate A which is moving obliquely away from plate B. Deformation is accommodated within the deforming zone (white), which is 16 km wide. The graphical construction uses the width of the deforming zone (white), the angle between the plate motion vector of plate A and the boundary, 30^0, and the rate components of the plate motion vector.

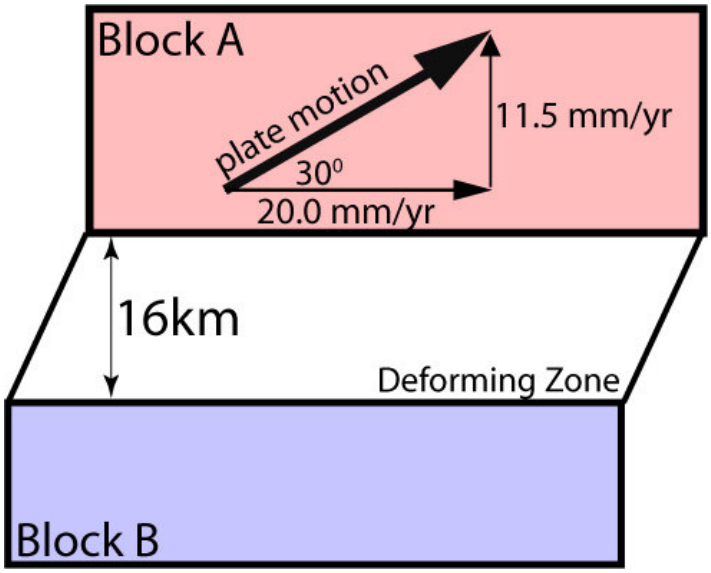

Fig. 3.10. Stepwise construction of the graphical method. (A) The reference axis (vertical) and baseline (horizontal) are scaled to the width of the deforming zone being analysed. The Anchor Point (yellow dot) is translated in the direction of the velocity field an amount equal to the velocity integrated over an amount of time consistent with the geologic data. In this example the Anchor Point is translated 11.5 km perpendicular and 20 km parallel to the zone, rates integrated over one million years. (B) A line is drawn in the orientation of the velocity field (blue arrow) and parallel to the zone, which creates three points. (C) The Mohr circle is constructed to pass through these three points (yellow dots). A line drawn from the origin through the center of the circle creates two intercepts, S_1 (upper intercept) and S_2 (lower intercept), which corresponding to the greatest stretch (S_1) and least stretch (S_2). (D) A line drawn from S_2 through the Anchor Point gives the orientation of the long axis of the strain ellipse. Note the solutions are inverted through the Anchor Point.

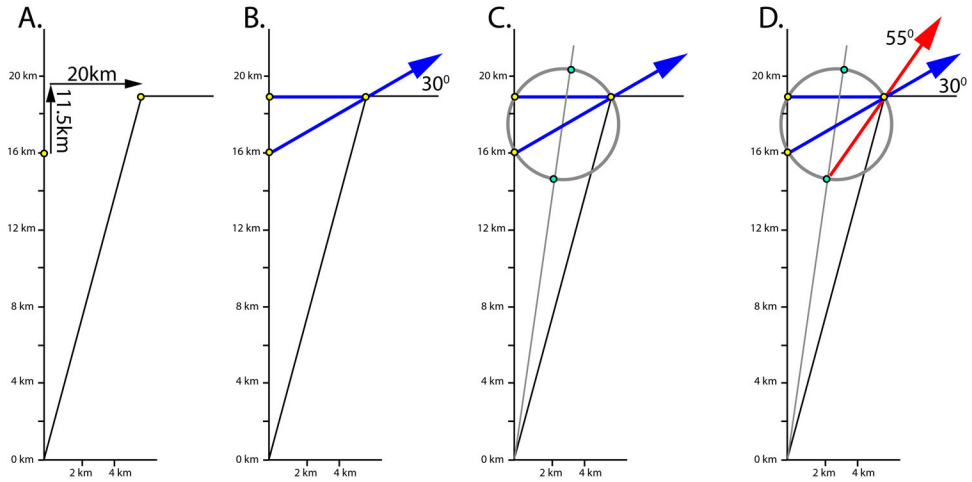

CHAPTER FOUR

DIFFERENTIATION PARTITIONING FROM DISTRIBUTED STRAIN IN OBLIQUELY DEFORMING TECTONIC ZONES USING A GRAPHICAL VISUALIZATION TO RELATE VELOCITY AND STRAIN FIELDS

Justin J. Murphy[1*], A. John Watkinson[1], John S. Oldow[2]

[1] School of Earth and Environmental Sciences, Washington State University, Pullman, Washington 99164-2812

[2] Department of Geological Sciences, University of Idaho, Moscow, Idaho, 83844

Abstract

Observations of obliquely deforming tectonic zones have shown the strain orientation within the deforming plate margin can be refracted from the converging plate velocity, which is a consistent relationship in transpression, transtension and simple shear. Alternatively, velocity field partitioning can result in a deviation between converging plate motion and strain orientation. Can partitioning be distinguished from the distributed strain model? Applying a graphical construction for strain tests the distributed model against geologic data. Partitioning can be detected if geologic data violate distributed strain model constraints. This technique allows the non-uniqueness of partitioned models, the relationship between velocity and strain and the rotational character of strain to be explored. Deformation in the Aleutian Arc, Alaska, appears distributed, the GPS velocity spatial distribution in the western arc suggests a component

of partitioning. In the central Walker Lane, Nevada, the principal strain axes deviate from a distributed strain model.

Keywords: Partitioning, Distributed strain, Velocity orientation, Strain orientation, Active tectonics

*murphywsu@hotmail.com

Introduction

Oblique relative plate motions can result in a refraction of the principal strain axes from parallelism with the plate motion vector of the converging plate. The classic observations made at the Sunda Arc, Indonesia (Fitch, 1972) have been reinforced with examples including the Hikurangi trench, New Zealand (Walcott, 1978; Cashman, 1992) and the Aleutian Arc, Alaska (Avé Lallemant & Oldow, 2000). A deviation between velocities measured using GPS and the orientation of strain can be seen in conservative tectonic environments such as the San Andreas fault in California (Tikoff & Teyssier, 1998) and oblique divergent regimes like the Walker Lane, Nevada (Oldow, 2003; Unruh et. al., 2003) and Reykjanes Peninsula, Iceland (Clifton & Schlische, 2000; Hreinsdottir et al. 2001; Clifton & Kattenhorn, 2006). Partitioning of either, or both, the velocity and strain field within obliquely deforming zones has been recognized as a fundamental style of deformation but quantifying the degree of partitioning can be difficult. The natural variation of geologic measurements combined with technological and logistical limitations in acquiring data, such as GPS velocities, limit the resolution available to detect partitioning. An alternative style of deformation where strain is distributed across

a deforming zone is possible (Horsman & Tikoff, 2005). Can partitioning within obliquely deforming tectonic zones be discerned from distributed strain without an acute method of detection?

Theoretical strain models predict a deviation between the orientation of the velocity field and strain field in zones deforming by transtension, transpression and simple shear (Fossen & Tikoff, 1993; Tikoff & Fossen, 1995). In the context of active tectonics (i.e. Teyssier & Tikoff, 1994), these states of deformation can result in a velocity field measured with GPS that is generally not parallel to the expression of strain: faults, folds, earthquakes etc. The relationship between the incremental and finite strain in different boundary conditions has been explored using strain theory (Ramsay, 1967; Jiang & Williams, 1998). These investigations document the rotational character of non-coaxial strain that can result in a difference in orientation and possibly an overprinting relationship between young geologic structures that have formed instantaneously and those that are either long lived or formed from accumulated finite strain.

To evaluate whether or not partitioning can be differentiated from distributed strain, a strain model is constructed by applying the graphical construction of De Paor (Simpson & De Paor, 1993), which is a method that can predict the finite and incremental orientation of strain within obliquely deforming zones (see also incremental strain methods of McCoss, 1986; Tikoff & Fossen, 1995). This distributed strain model assumes no partitioning of the velocity or strain fields, allowing the intrinsic constraints of the model to be tested against the available geologic data such as fault slip, GPS velocity fields, earthquake P axes and other data available in active tectonics. In this paper, geologic data available for the Aleutian Arc, Alaska and Walker Lane, Nevada

will be used to test whether or not partitioning can be differentiated from a distributed strain field. The benefit of the De Paor method lies (1) in its rapid construction, (2) graphical nature, which serves as a visualization of the relationship between velocity and strain, (3) spatially referenced solutions and (4) ability to capture the rotational character of non-coaxial strain.

Construction background

The motion of an object through a reference frame can be recorded by the path of the constitutive particles. If the object were to move in a straight line, each particle path will be parallel and the same length. The geometric properties remain unchanged because each particle has moved the same amount and direction. A velocity gradient would result if one side of the object were to move faster than the other, which could be accommodated by a change in shape, a strain. A homogeneous velocity gradient resolved onto a square grid results in identical parallelograms and homogeneous strain. Deformation would not be equal throughout the grid if displacement vectors had differed in orientation and magnitude and the strain would be heterogeneous (Ramsay, 1967). Particle motion contained within a single plane is plane strain, while particle motion not fully described by a planar section is non-plane strain.

Two end member forms of deformation are pure and simple shear. Pure shear is characterized by directions of elongation and shortening that do not rotate during deformation. Simple shear is different, the directions of elongation and shortening change orientation with increasing strain. Pure shear is coaxial because an orthogonal set of lines parallel to the instantaneous strain axes will not rotate during deformation,

meaning the finite strain axes remain parallel to the instantaneous strain axes. During simple shear, the same orthogonal set of lines parallel to the instantaneous strain axes would change orientation, out of parallelism and orthogonality, making simple shear non-coaxial because the finite strain axes will immediately rotate out of parallelism with the instantaneous strain axes (Ramsay, 1967) (Fig. 4.1).

The orientation of a shear zone boundary can act as a direction of stability in simple shear. Passive material lines asymptotically approach this orientation with increasing strain. In the case of general shear, transpression and transtension, a second orientation is also stable. Particles moving along a stable orientation create linear traces called eigenvectors. The maximum, minimum and intermediate eigenvectors within a velocity gradient field define the orientations of flow apophyses, which is a function of the relative contribution of pure and simple shear to the bulk strain (Ramberg, 1975; Means et. al., 1980; Bobyarchick, 1986; Fossen and Tikoff, 1993; Tikoff & Fossen, 1995). More complex states of three-dimensional strain are investigated by Jiang & Williams (1998) however are not discussed here because they violate the boundary constraints of the graphical construction.

Linking velocity and strain

This paper uses the graphical construction of De Paor (De Paor, 1981; Simpson & De Paor, 1993) to predict the orientation of strain from a velocity field measured within an actively deforming zone (Fig. 4.2). Results from the graphical method are compared to those found using the technique of Tikoff & Fossen (1995), which relates the velocity and deformation tensors to connect velocity and strain. The benefit of the De Paor

construction lies in its ability to (1) visualize the relationship between the orientation of the velocity field and the strain field in a deforming tectonic zone, (2) capture the rotational effect of non-coaxial strain, (3) integration over different periods of time is possible, allowing the behavior of passive material lines and the orientation of the principal strain axes to be forward or backward modeled, (4) the deviation between velocity and strain can be related to the width of the deforming zone and the translation of the Anchor Point, which records the angular shear strain in a spatially referenced framework (Simpson & De Paor, 1993) (Fig. 4.3).

Data needed to apply this construction to tectonic problems are (1) the orientation and magnitude of the NUVEL-1A (DeMets et al., 1994) relative plate motion for inter-plate deformation and / or the orientation and magnitude of the residual velocity field within a deforming intra-plate zone and (2) the width of the deforming zone. Assumptions are made when applying the construction to active tectonics. (1) Strain across the deforming zone is homogenous or can be generalized as a homogeneous domain within a heterogeneous or partitioned system (Horsman & Tikoff, 2005). (2) Non-coaxial strain is restricted to a horizontal section where the vorticity vector is perpendicular to this plane and parallel to one axis of the finite strain ellipsoid (Tikoff & Fossen, 1995). (3) The orientation of the plate motion velocity, or intra-plate velocity, is used as the oblique stable orientation of flow (Bobyarchick, 1986; Weijermars & Poliakov, 1991). (4) Elastic strain accumulation within a geodetic field may exist but cannot be resolved from permanent strain and is assumed to be parallel to the permanent strain.

Analysis of a kinematic cartoon

In a three-plate oblique divergence problem (Fig. 4.1), plate A remains stationary relative to plate B, which is moving away obliquely at 23 mm/yr. The angle between the plate boundary and the plate motion vector is 30^0. Decomposing the plate motion vector into its boundary parallel and perpendicular components yields a boundary parallel velocity of 20 mm/yr and a boundary normal velocity of 11.5 mm/yr.

The velocity field must be integrated over a period of time consistent with the available geologic data. For example, if the strain solutions from the graphical construction were to be compared with earthquake focal mechanism solutions then the velocity would need to be integrated over the earthquake recurrence interval within the deforming zone. The integrated velocity gives the distance that the Anchor Point is translated (Fig. 4.3 A.). One million years was chosen in this example, so the Anchor Point is moved 11.5 km perpendicular to the boundary and 20 km parallel to the boundary (Fig. 4.3 A.) from the height on the reference axis corresponding to the width of the deforming zone (Fig. 4.3 A.). Lines are drawn through the Anchor Point both in the orientation of the velocity and parallel to zone boundary (Fig. 4.3 B.). This method uses the motion vector of plate B as the orientation of the oblique stable orientation of flow (Weijermars & Poliakov, 1991).

Three points are created: (1) The Anchor Point, (2) the intercept on the reference axis created by a line drawn from the Anchor Point to the reference axis in the orientation of the velocity field and (3) where a line drawn from the Anchor Point, parallel to the kinematic boundary, intersects the reference axis (Fig. 4.3 B.). A circle can be constructed passing through these three points (Fig. 4.3 C.). A line drawn from the origin

through the center of the circle will produce two intercepts on the circumference of the circle, these are the points S_1 (greatest stretch) and S_2 (least stretch) (Fig. 4.3 C.).

Lines drawn from these two points back through the Anchor Point will produce the orientation of the principal strain axes with respect to the kinematic boundaries of the zone. Because the Anchor Point inverts the solution, the line drawn from S_2 through the Anchor Point yields the orientation of the long axis of the finite strain ellipse (Fig. 4.3 D.). The orientation of the principal strain axes can be plotted on the kinematic model. In this example, the long axis of strain is predicted to be 55^0 from the kinematic boundary and 25^0 from the velocity direction (Fig. 4.3 D).

The Aleutian Arc, Alaska

The Aleutian Arc represents the tectonic boundary where the Pacific plate is subducting beneath the North American plate. The arcuate nature of the boundary results in an along strike transition from nearly head on collision in the eastern arc to almost parallel strike slip motion in the western arc (Avé Lallemant & Oldow, 2000). Deformation within the North American plate margin is concentrated within a wedge shaped domain approximately 150 – 200 km wide, bounded to the south by the megathrust and to the north by a vertical zone of concentrated seismicity (Apel et al., 2002).

The average orientation of earthquake P axes measured within the subducting slab are parallel to the orientation of the Pacific plate motion (NUVEL-1A DeMets et al., 1994) in the Aleutian Arc east of Unalaska (Fig. 4.4.). West of Unalaska, the average P axis trend deviates from the orientation of the Pacific plate velocity, becoming

increasingly more clockwise along strike to the west. If the velocity field is partitioned within the Aleutian Arc, then a deviation between the Pacific Plate motion and the P axis orientation would be predicted because the P axes would reflect the effective, partitioned orientation of plate motion. McCaffrey (1992) estimates the degree of partitioning by determining the amount of plate velocity that would have to be removed through partitioning to rotate the effective plate motion into parallelism with the earthquake P axes.

The partitioning model of McCaffrey (1992) assumes the orientations of earthquake P axes are parallel to slip, however, P (or T in extension) axes and slip are expected to be collinear if the state of strain is strictly coaxial (Twiss & Unruh, 1998; Fournier & Petit, 2007). A general case where slip vectors are not parallel to the orientation of strain (P / T axes) occurs in transpression, transtension, and simple shear deformation (Fossen & Tikoff, 1993). The strain orientation would still be predicted to deviate from the partitioned Pacific plate motion found in the McCaffrey (1992) model because the orientation of the constructed velocity is oblique to the boundary. If the effective plate motion was orthogonal to the boundary then parallel velocity and strain fields would be expected. The partitioning model is not always unique because there are too many variables that can be changed, but not measured, such as the degree of coupling between the Pacific and North American plates and different seamless combinations of partitioning between the components of the Pacific plate velocity.

The observed deviation between the earthquake P axes and the Pacific Plate velocity is consistent with the conceptual relationship between velocity and strain in transpression (Teyssier & Tikoff, 1994; Tikoff & Fossen, 1995). A distributed strain

model constructed with the methods of De Paor and Tikoff & Fossen is constructed where 100% of the Pacific plate velocity is resolved onto the deforming arc and deformation of the arc is accommodated by distributed strain (Fig. 4.5 A.). The predicted orientation of strain found using this approach matches the average P axis trend along the Aleutian Arc (Fig. 4.6). Solutions for the orientation of strain from both the partitioning and distributed strain models cannot be differentiated relying only on the P axes.

Campaign GPS velocities at DTCH, AIRP, WHAL, SHEM and MRDR (Fig. 4.4) (Avé Lallemant & Oldow, 2000; Apel et al., 2002) can be used to test the distributed strain model because a prescribed velocity gradient is predicted that decreases from the parallel component of plate velocity at the southern boundary to zero at the northern boundary. The GPS measured within the arc should fit the homogeneous velocity profile if the velocity is not partitioned. In the eastern arc, up to Adak, the GPS velocities of DTCH, AIRP and WHAL are within error of a homogeneous velocity profile fit to the arc parallel component of the Pacific plate motion. West of Adak, around Attu, the GPS stations SHEM and MRDR record significantly higher rates near the northern boundary of the arc that far exceed a homogeneous velocity profile fit to the arc parallel component of the Pacific plate velocity. The spatial distribution of the GPS velocity suggests that partitioning is occurring. The nature of partitioning could be evaluated by examining the morphology of the velocity field, however is unlikely in the Aleutian Arc due to the lack of exposure.

The presence of a distributed strain is supported based on the style of deformation on Attu, Atka, Adak and Unalaska (Avé Lallemant, 1996; Avé Lallemant & Oldow, 2000) and the consistency in the orientation of the earthquake P axes across the width of

the arc. The excess velocity measured within the western arc could be explained if partitioning accompanied this distributed strain component. However, the components of partitioning and distributed strain cannot be rigorously quantified with this method because resolving very small strains with the graphical constructions is difficult and the error of the GPS data and the range in P axis orientation overwhelm the small strain solutions. Nevertheless, simultaneous distributed strain and partitioning can honor the orientation of the earthquake P axes, the deformation observed within the arc and the spatial distribution of the rates measured with GPS.

Volcanic centers are concentrated on the concave side of the arc, an observation consistent with many arcs worldwide. This trend of volcanic activity coincides with the locus of seismicity defining the northern boundary of the arc, possibly an anisotropic localization of deformation. The distributed nature of the pre-existing structural grain within the Aleutian arc could support a distributed style of strain. However, partitioning of the velocity field, where some component of the arc parallel velocity is taken up by translation of the forearc, honors the GPS velocities measured at stations MRDR and SHEM.

The Central Walker Lane, Nevada

The motion of the Sierra Nevada microblock relative to stable North America is essentially parallel to the San Andreas Fault (Unruh, 2003). However, the geometry of the eastern boundary of the Sierra Nevada results in transtension within the Walker Lane that accommodates motion between the Sierra Nevada and the Great Basin (Oldow, 2003) (Fig. 4.7). Multiple directions of anisotropy created by Proterozoic to Cenozoic

structures characterize the architecture of the central Walker Lane (Oldow et. al., 1989; Oldow, 2002; 2003). Strain trajectories constructed from fault slip inversion and earthquake focal mechanisms systematically change orientation from west-northwest to west-southwest as the back of the Sierra Nevada is approached from the east (Fig. 4.8). A relatively homogeneous velocity trajectory constructed with GPS velocities in a North American reference frame trends west-northwest and increases across the central Walker Lane from 2-3 mm/yr in the east, approaching the 12-14 mm/yr velocity of the Sierra Nevada to the west (Oldow, 2003) (Fig. 4.8).

Modeling the Central Walker Lane as a distributed zone of deformation following the same technique as in the Aleutian Arc with boundaries defined to the west by the eastern side of the Sierra Nevada and to the east by the western boundary of the Great Basin (Fig. 4.7) results in a predicted orientation of strain that does not capture the observed rotation of the strain trajectories (Oldow, 2003). In order to address the strain occurring within the central Walker Lane, (1) the graphical construction must be integrated over the 10,000 year earthquake recurrence interval (Rogers et al., 1991) and (2) residual velocities relative to the deforming domains are needed. The residual GPS velocity of the extension dominated domain was determined by subtracting the average GPS velocity of the wrench dominated domain from the average GPS velocity of the Sierra Nevada. The residual velocity in the extension domain is approximately 54^0 counterclockwise from the eastern boundary with the wrench domain. The residual GPS velocity in the extensional domain can be decomposed into its boundary parallel and perpendicular components, 5.7 mm/yr and 8 mm/yr respectively, with a width of approximately 60km (Fig. 4.9).

The wrench dominated domain to the east can be analyzed in a similar way. The width of the deforming zone is approximately 40 km. The angle between the easternmost strike slip fault defining the boundary with the Great Basin and the residual velocity within this domain is approximately 8^0. The boundary parallel and perpendicular components are 11.4 mm/yr and 1.5 mm/yr respectively. Because the residual GPS velocity is nearly parallel to the boundary, this domain is predominantly dextral simple shear with a small component of extensional pure shear, i.e. wrench dominated transtension.

Using the orientation and magnitude of the residual velocity within the extension and wrench domains as inputs into the strain constructions yields a predicted orientation of strain that captures the anticlockwise rotation of the observed strain trajectories from Oldow (2003) (Fig. 4.8). Despite the presence of strike slip and dip slip faults throughout each domain, no clear sub domains can be broken out at the scale of each domain, the strain is distributed at the domain scale of observation (Thatcher, 1995; Horseman & Tikoff, 2005). Although the GPS velocity field is remarkably homogeneous across the central Walker Lane, the effect of the crustal anisotropy is the partitioning of the strain field into at least two domains that appear to be deforming in a distributed manner at the scale of the Central Walker Lane (Oldow, 2003).

Discussion

Partitioning of either, or both, the velocity and strain field has been recognized as a mechanism operating in obliquely deforming tectonic zones. McCaffrey (1992) suggests the refraction of earthquake P axes from parallelism with the velocity orientation

of the Pacific plate in the Aleutian Arc can be explained by partitioning of the velocity field. This model fits the effective, partitioned velocity to the orientation of the P axes measured within the deforming arc. However, this scenario would be expected in coaxial, obliquity of zero, deformation. A more general case where the orientation of the velocity and strain deviate from parallelism is expected in transpression.

Deformation within the Aleutian Arc is complex. Multiple generations and orientations of faulting post date early megascopic folds (Avé Lallemant, 1996), yet the structural style and history of deformation is remarkably similar along the length of the arc (Avé Lallemant & Oldow, 2000). A distributed deformation model developed using the graphical constructions of De Paor (Simpson & De Paor, 1993) and Tikoff & Fossen (1995) can test whether or not partitioning can be differentiated from distributed strain. A distributed deformation results in a model that (1) is allowable based on the style of deformation observed within the arc (Avé Lallemant, 1996; Avé Lallemant & Oldow, 2000; Apel et al., 2002) and (2) predicts orientations of strain found using the constructions of De Paor (Simpson & De Paor, 1993) and Tikoff & Fossen (1995) that are parallel to the observed average P axis orientation. However, distributed deformation alone cannot account for the excess velocity measured within close proximity to the northern boundary of the arc by GPS stations MRDR and SHEM in the western Aleutian Arc. Instead, a unifying model could include a component of distributed strain and a partitioning of the velocity field. Velocities recorded at GPS stations in the eastern arc, WHAL, AIPR and DTCH, are allowable in either a partitioning model or a distributed strain model. In the case of partitioning below 50% of the velocity budget of the

converging plate, GPS measured east of Unalaska for example, it does not appear that partitioning can be differentiated from distributed strain.

The uncertainty and range in the geologic measurements, together with the insensitivity of the strain constructions to varying degrees of partitioning, does not permit the rigorous determination of the relative percentage of partitioning between the arc parallel and perpendicular components of the Pacific plate velocity and the strain occurring within the arc. Nevertheless, this model does make predictions that could be tested because a distributed strain gradient would have a prescribed velocity profile.

Despite the distributed character of faulting throughout the arc, resolving the velocity field from the Pacific plate onto the deforming zone results in a partitioning of the velocity field. One possible controlling feature of this behavior could be the effect of the anisotropy of the geologic boundaries, the northern chain of volcanism that localizes seismicity and the plate boundary megathrust, which define the wedge shaped deforming margin of the North American plate.

Modeling the transtensional central Walker Lane with a distributed strain between the Sierra Nevada and the western Great Basin fails to capture the observed anti-clockwise rotation of the principal strain axes (Oldow, 2003) towards the eastern boundary of the Sierra Nevada. This is despite the homogeneous nature of the velocity field that increases across the central Walker Lane to the northwest. Breaking the central Walker Lane into domains of coaxial and non-coaxial dominated transtension (Oldow, 2003) results in a predicted orientation of strain obtained using the constructions of De Paor (Simpson & De Paor, 1993) and Tikoff & Fossen (1995) that captures the observed rotation of the principal strain axes. The strain constructions illustrate the anisotropic

control of the crustal structure. Although the deforming central Walker Lane is bounded by the Sierra Nevada and the Great Basin, the crustal architecture promotes a partitioning of strain into simple and pure shear dominated domains.

Conclusions

A deviation between the orientation of the velocity field and the strain field in transpression, transtension and simple shear is consistent with the effect of non-coaxial strain in obliquely deforming zones. In inter-plate environments, this deviation could manifest as the refraction of the principal axes of strain from parallelism with the convergent plate velocity. Similarly, a deviation from parallelism between the velocity field and the orientation of strain can be observed in intra-plate zones such as the central Walker Lane, Nevada. The style of deformation and the nature of both the velocity field and strain field can be influenced by anisotropy that may control partitioning of the velocity field and/or the strain field.

Limits in the ability to measure deviations from homogeneity and the natural variability of geologic data affect the resolution to detect partitioning within deforming tectonic zones. Heterogeneous or partitioned domains may appear distributed at a large enough scale of observation. Using a distributed strain model can provide intrinsic predictions that are testable. The graphical construction of De Paor (De Paor, 1981; Simpson & De Paor, 1993) is well suited to connect GPS data to strain in active tectonics because it provides a visual solution that is both spatially referenced and captures the rotational behavior of non-coaxial strain. The morphology and spatial distribution of the velocity field can be compared to the requirements of the distributed strain model. With

this approach, partitioning can be been inferred based on the compatibility between the spatial distribution of velocities and the orientation of strain.

Acknowledgements

This research was partially supported by National Science Foundation grants (EAR xxxxxxx and EAR xxxxxx) to J.S. Oldow.

References

Avé Lallemant, H.G., 1996. Displacement partitioning and arc parallel extension in the Aleutian volcanic island arc. Tectonophysics. 256, 279-293.

Avé Lallemant, H.G., Oldow, J.S., 2000. Active displacement partitioning and arc-parallel extension of the Aleutian volcanic arc based on Global Positioning System geodesy and kinematic analysis. Geology 28, 739-742.

Atwater, T., 1970. Implications of plate tectonics for the Cenozoic tectonic evolution of western North America. Geological Society of America bulletin. Vol 81, No. 12, 3513-3535.

Bobyarchick, A.R., 1986. The eigenvalues of steady flow in Mohr space. Tectonophysics Vol. 122, 35-51.

Clifton, A.E., Schlische, R.W., 2003. Fracture populations on the Reykjanes Peninsula, Iceland: comparison with experimental clay models of oblique rifting. Journal of Geophysical Research. 108.

Clifton, A.E., Kattenhorn, S., 2006. Structural architecture of a highly oblique divergent plate boundary segment. Tectonophysics. Vol. 419, 27-40.

Cashman, S.M., Kelsey, H.M., Erdman, C.F., Cutten, H.N.C., Berryman, K.R., 1992. Strain Partitioning between structural domains in the forearc of the Hikurangi subduction zone, New Zealand. Tectonics. 11, 242-257.

DeMets, C., Gordon, R. G., Argus, D. F., Stein, S. 1994. Effect of recent revisions to the geomagnetic reversal time scale on estimates of current plate motions. Geophysical Research Letterrs. Vol. 21, 2191–2194.

De Paor, D.G. 1981. Strain analysis using deformed line distributions. Tectonophysics 73: T9-T14

Ellis, M., Watkinson, A.J., 1987. Orogen parallel extension and oblique tectonics: The relation between stretching lineations and relative plate motions. Geology, Vol. 15, 1022-1026.

Fitch, T. J., 1972. Plate convergence, transcurrent faults and internal deformation adjacent to South-East Asia and the western Pacific. Journal of Geophysical Research. 77, 4432-4460.

Fossen, H., Tikoff, B., 1993. The deformation matrix for simultaneous simple shearing, pure shearing and volume change, and its application to transpression-transtension tectonics. Journal of Structural Geology 15, 413-422.

Fournier, M. & Petit, C., 2007. Oblique rifting at oceanic ridges: Relationship between spreading and stretching directions from earthquake focal mechanisms. Journal of Structural Geology 29, 201-208.

Hreinsdottir, S., Einarsson, P., 2001. Crustal deformation at the oblique spreading Reykjanes Peninsula, SW Iceland: GPS measurements from 1993 to 1998. Journal of Geophysical Research, Vol. 106, No. B7. 13,803-13,916.

Jiang, D., Williams, P.F., 1998. High-strain zones: a unified model. Journal of Structural Geology. Vol. 20, No. 8, 1105-1120.

McCaffrey, R., 1992. Oblique plate convergence, slip vectors and forearc deformation. Journal of Geophysical Research, Vol. 97 No. B6, 8905-8915.

Means, W. D., Hobbs, B. E., Lister, B. E., Williams, P. F., 1980. Vorticity and non-coaxility in progressive deformations. Journal Structural Geology, Vol. 2, p. 371-378.

Murphy, J. J., Watkinson, A. J., Oldow, J. S., 2006. Graphical method that relates displacement fields and strain for the kinematic analysis of deforming tectonic zones: examples from the Walker Lane, western Great Basin and the Aleutian Island Arc, Alaska. Geological Society of America Abstracts with Programs. Vol. 38 No 7, p. 132.

Oldow, J.S., 2002, Active strain partitioning in the central Walker Lane, western Great Basin: Compatibility of GPS velocities and nonplane incremental strain estimated from seismicity and fault-slip inversion: Geological Society of America Abstracts with Program, v. 34, no. 5, p. A88.

Oldow, J.S., 2003. Active transtensional boundary zone between the western Great Basin and Sierra Nevada block, western U.S. Cordillera. Geology. 31, 1033–1036.

Oldow, J.S., Bally, A.W., Ave Lallemant, H.G., and Leeman, W.P., 1989, Phanerozoic evolution of the North American Cordillera (United States and Canada), in Bally, A.W., and Palmer, A.R., eds., The geology of North America: An overview: Boulder, Colorado, Geological Society of America, Geology of North America, Vol. A, 139–232.

Ramsay, J. G., 1967. Folding and Fracturing of Rock. McGraw Hill, New York.

Ramsay, J. G., Huber, M. I., 1987. The techniques of modern structural geology Volume 1: Strain Analysis. Academic Press, London.

Rogers, A.M., Harmsen, S.C., Corbett, E.J., Priestly, K., and de Polo, D., 1991, The seismicity of Nevada and some adjacent parts of the Great Basin, *in* Slemmons, D.B., et al., eds., Neotectonics of North America: Boulder, Colorado, Geological Society of America, Decade Map Volume 1, p. 153–184.

Simpson, C., De Paor, D.G., 1993. Deformation and Kinematics of High Strain Zones. Journal of Structural Geology. 15, 1-20.

Teyssier, C., Tikoff, B., 1994. Strain modeling of displacement-field partitioning in transpressional orogens. Journal of Structural Geology. 16, 1575–1588.

Thatcher, W., 1995. Microplate versus continuum descriptions of active tectonic deformation, *J. Geophys. Res., 100,* 3885-3994.

Tikoff, B., Fossen, H., 1995. Limitations of three-dimensional kinematic vorticity analyses. Journal of Structural Geology Vol. 17, 1771-1784.

Teyssier, C., Tikoff, B., 1998. Strike-slip partitioned transpression of the San Andreas fault system: a lithospheric scale approach, in: Holdsworth, R.E., Strachan, R.A., Dewey, J.F. (Eds.), Continental Transpressional and Transtensional Tectonics Geological Society of London Special Publication, 135, pp. 143–158.

Thatcher, W., Foulger, G.R., Julian, B.R., Svarc, J., Quilty, E., and Bawden, G.W., 1999. Present day deformation across the Basin and Range province, western United States. Science, Vol. 283, p. 1714–1718.

Twiss, R.J., Unruh, J.R., 1998. Analysis of fault slip inversions: Do they constrain stress or strain rate? Journal of Geophysical Research Vol. 103, No. B6. 12,205-12,222.

Unruh, J., Humphrey, J., Barron, A., 2003. Transtensional model for the Sierra Nevada frontal fault system, eastern California. Geology. 31, 327-330.

Walcott, R.I., 1978, Geodetic strains and large earthquakes in the axial tectonic belt of North Islane, New Zealand. Journal Geophysical Research. 83, 4419-4469.

Weijermars, R., Poliakov, A., 1991. Stream functions and complex potentials: implications for development of rock fabric and the continuum assumption. Tectonophysics. Vol. 220, 33-50.

Figure 4.1. Diagram illustrating the effect rotational strain has on the orientation of the finite strain axes. In pure shear, coaxial strain, the incremental and finite strain axes remain parallel throughout deformation. However, in general, or simple shear, the non-coaxial strain component results in the progressive rotation of the finite strain axes towards the boundary of the deforming zone.

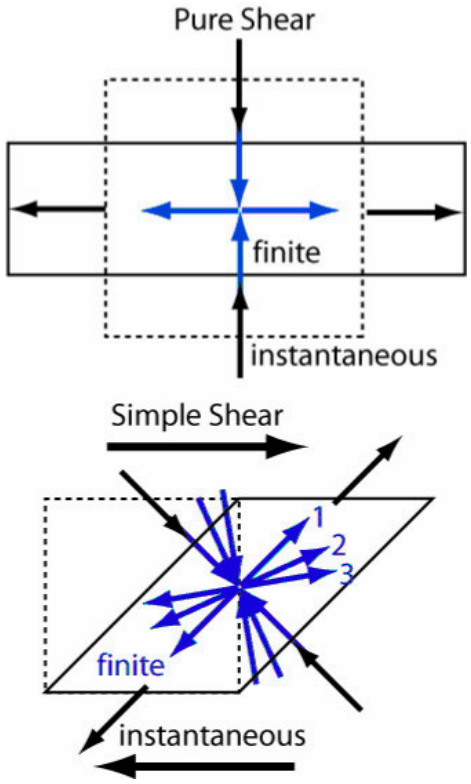

Figure 4.2. The three plate cartoon problem with side by side comparison of completed analytical and graphical techniques. The analytically based solution of Tikoff & Fossen (1995) (left) and the graphical technique of De Paor (Simpson & De Paor, 1993) (right).

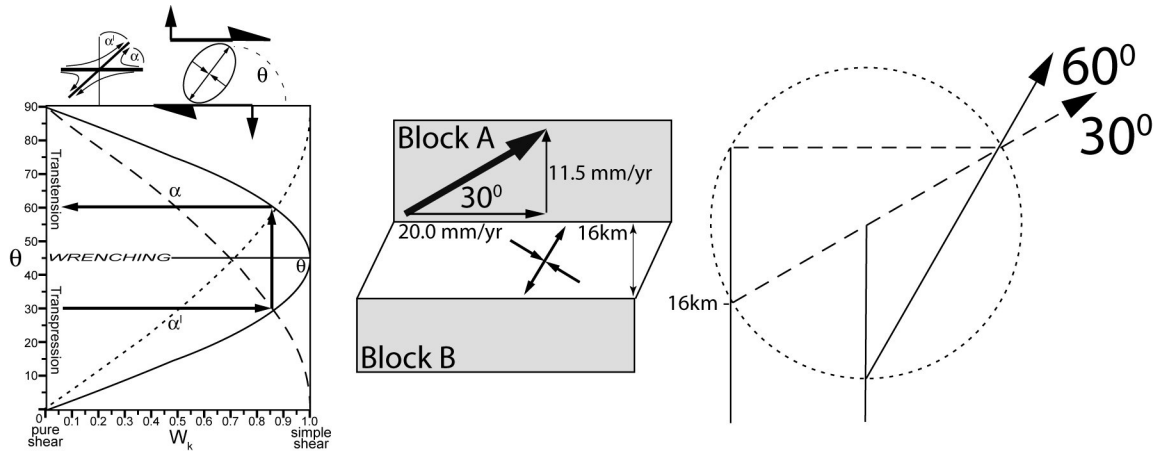

Figure 4.3. Stepwise construction of the graphical method. (A) The reference axis (vertical) and baseline (horizontal) are scaled to the width of the deforming zone being analysed. The Anchor Point (yellow dot) is translated in the direction of the velocity field an amount equal to the velocity integrated over an amount of time consistent with the geologic data. In this example the Anchor Point is translated 11.5 km perpendicular and 20 km parallel to the zone, rates integrated over one million years. (B) A line is drawn in the orientation of the velocity field (blue arrow) and parallel to the zone, which creates three points. (C) The Mohr circle is constructed to pass through these three points (yellow dots). A line drawn from the origin through the center of the circle creates two intercepts, S_1 (upper intercept) and S_2 (lower intercept), which corresponding to the greatest stretch (S_1) and least stretch (S_2). (D) A line drawn from S_2 through the Anchor Point gives the orientation of the long axis of the strain ellipse. Note the solutions are inverted through the Anchor Point.

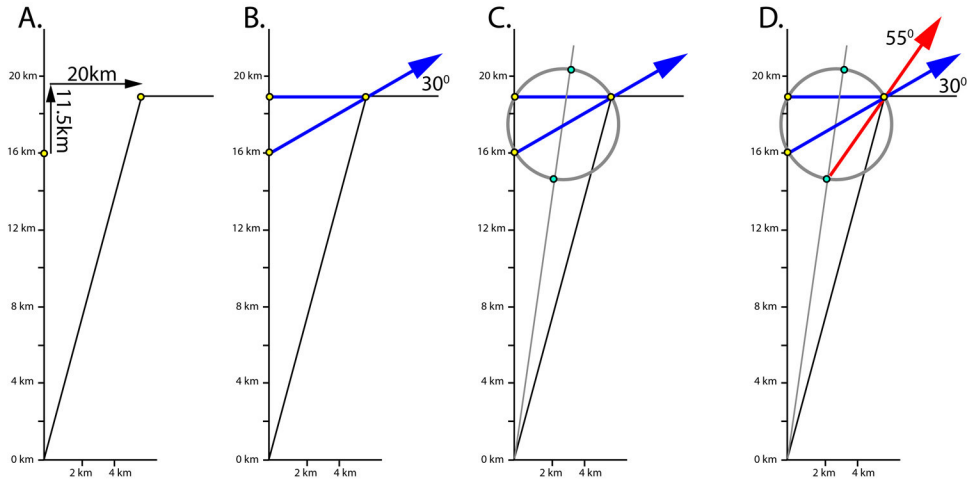

Figure 4.4. Diagram showing the Aleutian Arc discritized into approximately parallel segments, adapted from Apel et al. (2002). Pacific plate velocities are NUVEL-1A (De Mets et al., 1994). P Axes compiled from seismicity in the subducting Pacific Plate beneath the deforming margin of North America by Apel et al. (2002).

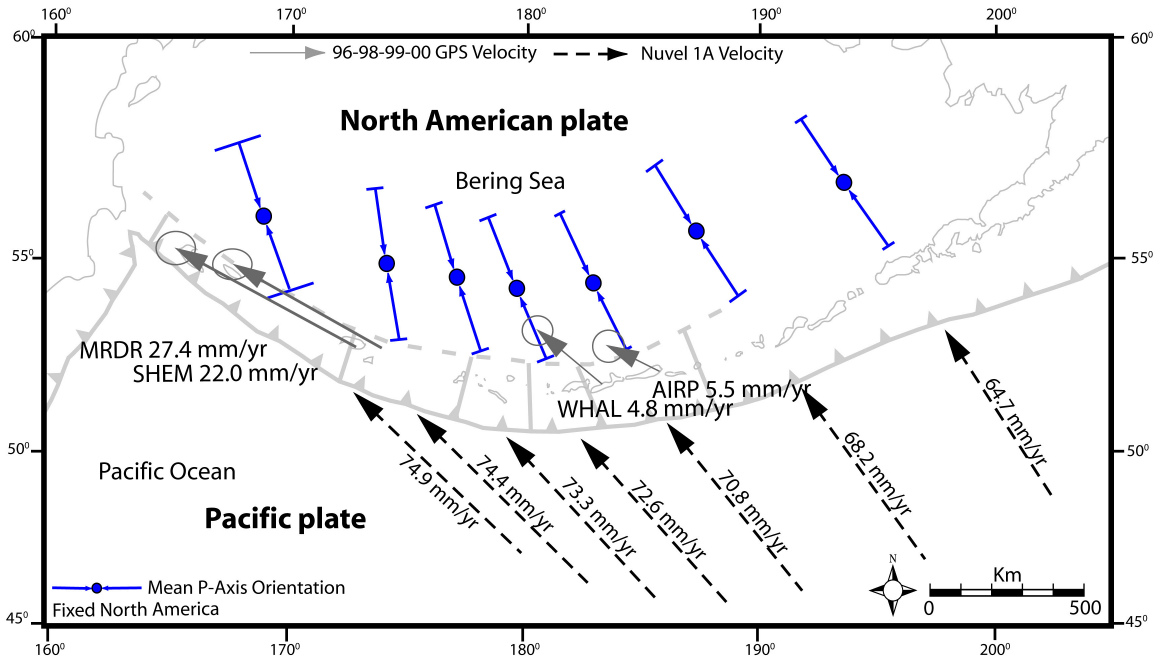

Figure 4.5. (A) Enlarged solutions from the graphical construction of De Paor (Simpson & De Paor, 1993) for the Aleutian Arc, Alaska. (B) Enlarged solutions from the graphical construction of De Paor (Simpson & De Paor, 1993) for the Wrench Dominated domain (left) and Extension Dominated domain (right) of the central Walker Lane, Nevada (Oldow, 2003).

A.

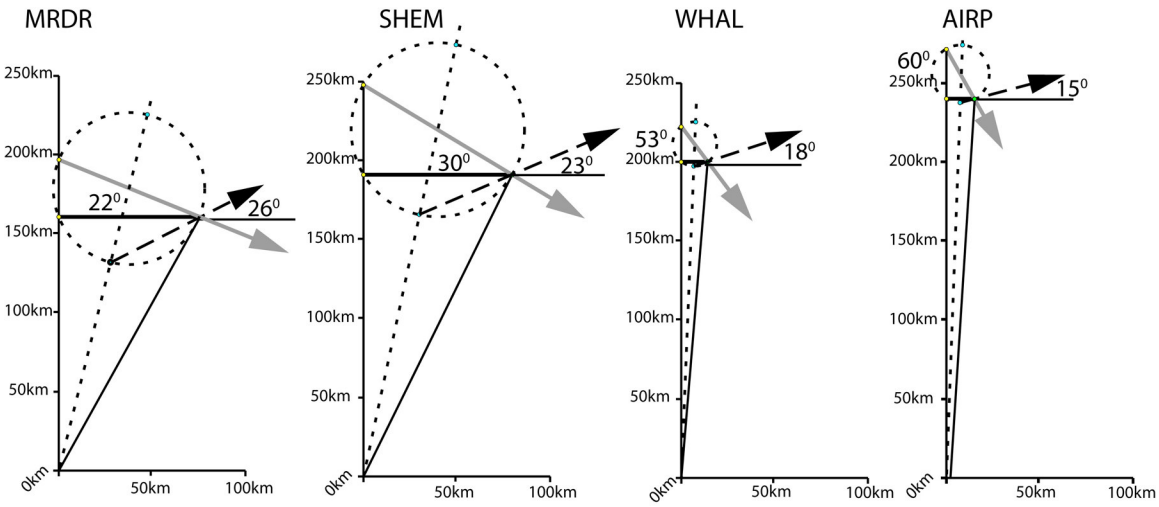

B.

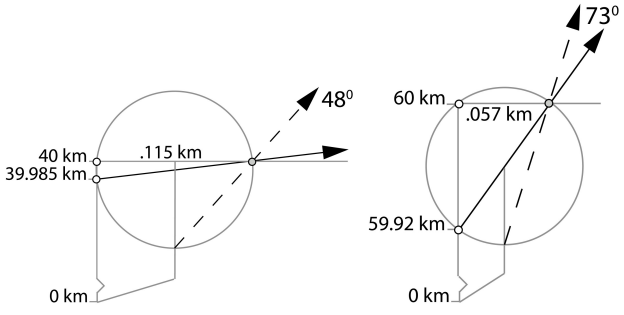

Figure 4.6. Map showing the predicted orientation of strain found using the graphical technique of De Paor. These solutions are also consistent with the predicted strain directions found using the analytical method of Tikoff & Fossen (1995).

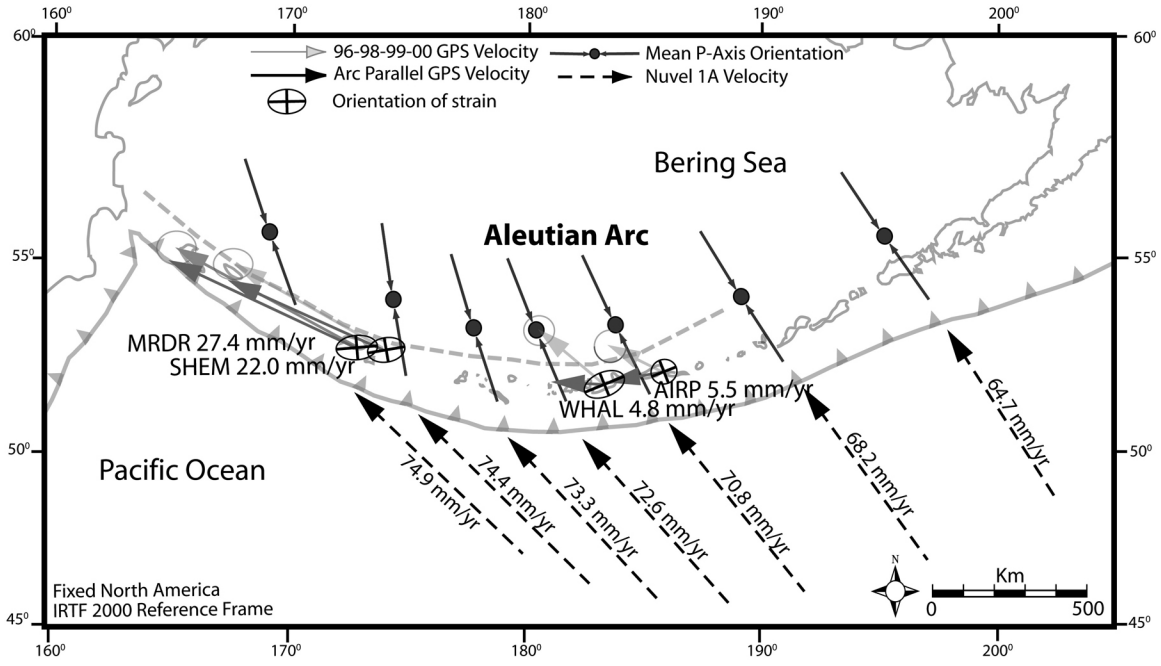

Figure 4.7. The Walker Lane acts as a zone of accommodation between the northwesterly translation of the Sierra Nevada block and the east-west extension within the Central Great Basin (after Oldow, 2003).

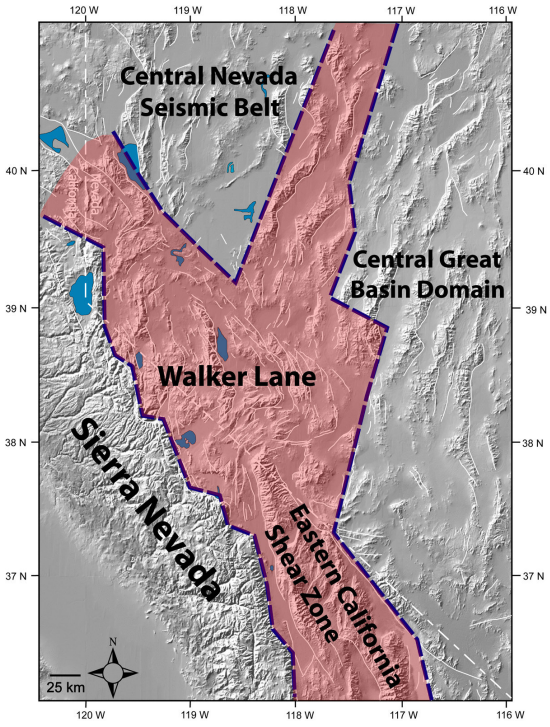

Figure 4.8. Map of the Central Walker Lane, Nevada showing the rotation and deviation of the strain trajectories (white) and GPS velocity trajectories (grey) toward the Sierra Nevada. (After Oldow, 2003).

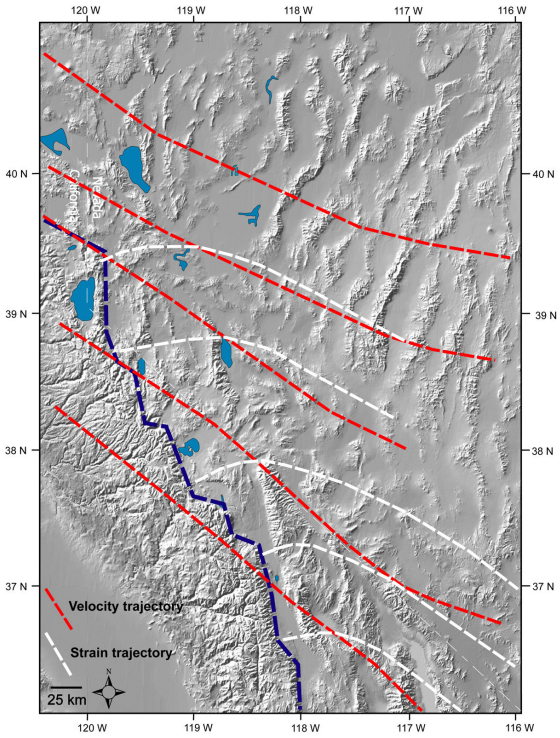

Figure 4.9. Map of the central Walker Lane showing the wrench dominated (right) and extension dominated (left) domains within the central Walker Lane, the velocity (red) and strain (white) trajectories from Oldow (2003) and the predicted orientations of strain for each domain obtained from the graphical construction of De Paor (Simpson & De Paor, 1993).